UNIVERSITÀ DEGLI STUDI DI PERUGIA

Dipartimento di Chimica, Biologia e Biotecnologie

Dottorato di ricerca in Scienze Chimiche

(XXXV ciclo)

Curriculum: Materiali e metodi per la tutela dell'ambiente e dei beni culturali

Doctorate in Chemical Sciences (XXXV cycle)

Curriculum: Materials and methods for environmental and cultural heritage protection

LEAD-CALCIUM PHOSPHATES AS A CUE FROM MULTI-TECHNICAL ANALYSES TO SCIENTIFIC COMMUNICATION IN HERITAGE SCIENCE

Doctoral Thesis

Claudio Costantino

Supervisors

Prof. Aldo Romani

Dr. Letizia Monico

Dr: Marine Cotte

Coordinator

Prof. Luigi Vaccaro

INDEX

ABSTRACT

In the last decades, unusual components, namely lead-calcium phosphates, were found in several artworks. The origin of their presence is still a matter of debate. It is not yet clear if lead-calcium phosphates (in natural or synthetic forms) were intentionally introduced by the artists or if their presence results from the transformation processes of the original artwork materials. Lead-calcium phosphates are also well known in environmental science, where hydroxyapatite [$Ca_5(PO_4)_3OH$] is used as a detoxifier in heavy-metal polluted environments. This compound spoils its property of cation exchanger, by substituting Ca^{2+} with another bivalent cation, including Pb^{2+} cations, to give rise to lead calcium phosphates as final product. Such information suggests that, under specific circumstances, similar process might have been responsible for the formation of lead-calcium phosphates in artworks.

Within this framework, the present PhD thesis addresses the study of lead-calcium phosphates in order to provide a deeper comprehension of their morphological and structural properties and of their identification in the context of cultural heritage objects.

The work is divided into two main sections: the first one concerns the study of morphological and structural properties of lead-calcium phosphate solid solutions ($Pb_xCa_{1-x})_5(PO_4)_3OH$ (Chapter 3.1-3.2) and their identification in a historical fragment from a Fresco painting (Chapter 3.3); the second one is focused on the development of an effective communication format exploitable by a non-specialist audience, through the definition of appropriate tools for the presentation of steps and final outcomes of the experimental research.

After describing the state-of-the-art for both scientific and communication fields (Chapter 1), the thesis will outline the analytical protocol employed for the synthesis and characterisation of lead-calcium phosphates solid solutions (Chapter 2), along with the description and discussion of the corresponding results (Chapter 3). The study of lead-calcium phosphates powders and related paint mock-ups was performed by means of a multi-technique approach based on the combination of vibrational spectroscopy methods, such as Fourier-Transform InfraRed (FT-IR) spectroscopy and μ-Raman (with bench-top and portable instruments), and X-ray techniques employing both conventional sources and synchrotron radiation [i.e., X-ray powder diffraction (XRPD) and X-ray absorption near edge structure (XANES) spectroscopy at Ca K- and P K-edges]. The obtained dataset was then successfully used to build up a database for the identification of lead-calcium phosphate compounds in historical cultural heritage objects; the same techniques were then applied to an historical paint fragment.

The last part of this thesis (Chapter 4) is devoted to the development of a format (a docuseries in three episodes of about 10 minutes each) specifically realized to communicate and disseminate the

context, motivation and outcomes of this research and to increase non-specialist public awareness on some challenges of heritage science field. More specifically, as a first step, a survey was created to investigate the interest of the public in scientific content, to know which media they normally use and the preferences of contents. Results obtained from the survey primed the decision to create a docuseries as the best output to communicate research results. The produced videos will be published on the web and social media. These tools will allow us to reach a remarkable number of people and to spread scientific research in an innovative and easily accessible way.

CHAPTER 1

INTRODUCTION

1.1 Lead-calcium phosphates: properties, identification, and uses

The identification and origin of lead-calcium phosphate solid solutions [$(Pb_xCa_{1-x})_5(PO_4)_3OH$] in different kind of cultural heritage objects have enliven the debate within the Heritage Science community over the past decades, leaving still unanswered a series of fundamental questions: *Can different types of lead calcium phosphates be distinguished in artworks? Were lead calcium phosphates intentionally used by the artists or they are the product of degradation processes of the constitutive materials of the artwork?*

To better understand the scenario of this debate and the approach proposed here to answer to these questions, in the following sections we present i) the structural properties, ii) identification and iii) uses of lead-calcium phosphates in heritage, life and environmental sciences.

1.1.1 Structural properties

Apatites, with general formula $M_5(ZO_4)_3X$, (where M = Ca, Sr, Pb…; Z = P, As, Si…; X = F, OH, Cl…), represent a class of materials with a variable chemical composition, being remarkably tolerant to structural distortion and chemical substitution [1–5]. Depending on the type of substitution, the compounds are classifiable in three main groups: cationic substituted, anionic substituted, and phosphate substituted. Most of studied natural and synthesised apatite-like compounds ideally belong to the $P6_3/m$ space group [6,7], although the introduction of some atoms in the crystal lattice can produce some structural variation, as reported by many authors [8–10]. These modifications produce a small deviation from the $P6_3/m$ space group to similar structures. For this reason, authors often just discuss the atomic arrangements of all apatites relative to the hexagonal unit cell and the $P6_3/m$ structure to facilitate direct comparisons among them [9–11].

In natural environments, apatites can easily exchange Ca^{2+} with other bivalent cations, such as Pb^{2+} (as for lead-calcium phosphate), Ba^{2+}, Sr^{2+}, Mn^{2+}, and Mg^{2+}, [2,12–14], and tetravalent cations, including Th^{4+} and U^{4+} [15].

Further substitutions with monovalent (e.g., Na^+, K^+, Li^+, Rb^+) and trivalent cations (e.g., Y^{3+}, Sb^{3+}, Bi^{3+}) were instead produced in laboratory [11]. The anionic substitution in the *c*-axis channels for apatites is known to occur between OH^- and F^- or Cl^- [2,6,11,16–18]. Additional substituents include other monovalent anions (e.g., Br^-, I^-, O_2^-, NO_3^-) [8,12,19,20], divalent anions (e.g., O^{2-}, CO_3^{2-}, NCN^{2-}) [21–23], and/or vacancy clusters [24]. The phosphate group in apatite-like compounds may instead

be replaced commonly by a variety of tetrahedral anionic groups, namely: AsO_4^{3-}, VO_4^{3-}, MnO_4^{3-}, CrO_4^{3-}, SO_4^{2-}, SiO_4^{4-}, and others. [11].

Regarding lead-calcium phosphate solid solutions, $(Pb_xCa_{1-x})_5(PO_4)_3OH$ (with $0 \leq x \leq 1$, hereinafter referred to as $PbHA_x$), previous electron microscopy analysis evidenced that the crystal structure and morphology are affected by the Pb/(Pb+Ca) atomic ratio [25–27]. With increasing of x, the unit cell parameters gradually increase with increasing size variation of the needle-like $PbHA_x$ crystals (Figure 1.1). Nevertheless, it is important to report that electronic microscopy also highlights that $PbHA_x$ can present irregularly shaped particles coexisting with the needle-like ones; the irregular shaped particles play a relevant role because they can contribute to the broadening of the X-Ray peaks [26].

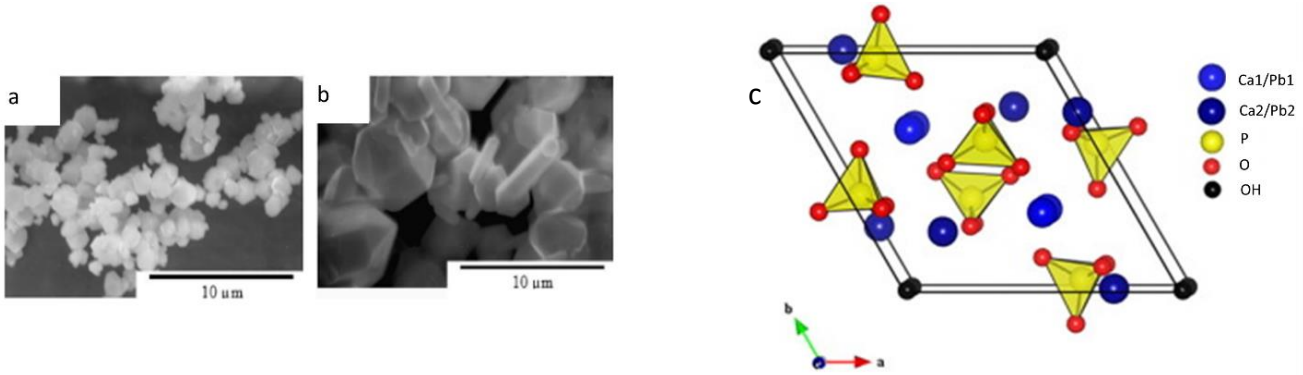

Figure 1.1 SEM images of (a) PbHA-80 (b) and HPy** (reproduced from [26]); (c) scheme of HA, $PbHA_x$ and Hpy structure and disposition into the crystal.*
**PbHA-80 is referred to $(Pb_{0.80}Ca_{0.20})_5(PO_4)_3OH$. **HPy is referred to $Pb_5(PO_4)_3OH$.*

1.1.2 Identification in cultural heritage objects

Dating back to the times of Antiquity, lead compounds have largely been employed as coloured materials, being present in several natural and synthetic pigments. They cover a wide range of colours from white [e.g. lead white, that is usually a mixture of hydrocerussite ($Pb_3(CO_3)_2(OH)_2$) and cerussite ($PbCO_3$)] [28–30], to red [e.g., islamic/red lead (Pb_3O_4)] [31], to yellow [e.g., chrome yellows ($PbCr_{1-x}S_xO_4$, with $0.0 \leq x \leq 0.8$) [32,33], lead tin antimony yellows ($Pb_2SbSnO_{6.5}$) [31,34,35], lead tin yellows (Pb_2SnO_4 and $PbSn_xSi_{1-x}O_3$, with $x \approx 1/4$)] [28,36,37], litharge and massicot (α-PbO and β-PbO respectively) [28,38–40]. Greyish galena (PbS) is also a traditional pigment, but it has been more frequently used in cosmetic (kohl) than in artistic contexts [41]. Lead was also detected in several secondary reaction products, such as anglesite ($PbSO_4$), palmierite [$K_2Pb(SO_4)_2$] and carboxylates [42–46].

In the last decades, uncommon lead-phosphate based compounds were identified in different artworks, such as papyri [47,48], wall paintings [49], paintings [50] and archaeological artifacts [51].

Table 1.1 reports an overview of the main cases found in literature where different types of lead-phosphate based compounds were found, along with the methods used for their identification.

Table 1.1 Summary of the main lead-phosphates based compounds found in cultural heritage objects reported in literature.

Material	Phase identified	Techniques	Attribution	Reference
Red ink in Islamic papyri	phosphohedyphane or unidentified Pb-Ca phosphate	μ-XRD, μ-XRF	unclear	[54]
Metallic ink in Herculaneum papyri	unidentified Pb-Cl phosphate (Pb, P, Cl seem to be strongly correlated)	XRF	unclear	[55]
Roman wall painting	hydroxypyromorphite	XRD	unclear	[56]
Japanese painting	lead phosphate [$Pb_9(PO_4)_6$]	XRD	unclear	[57]
Lead pigments and tools from Bronze Age	PbHA-81 [$Ca_{0.81}Pb_{4.19}(PO_4)_3(OH)$]	XRD	possible degradation product	[58]
Buried roman bronze inkwell	hydroxypyromorphite	EDX, FT-IR	corrosion product	[60]
Bronze Islamic dining table	pyromorphite	XRD, FT-IR	corrosion product	[61]
early Islamic wall paintings	pyromorphite	XRD, Raman	pigment	[63]
Wall paintings on ancient silk road	pyromorphite	EDX, FT-IR	pigment	[64]
Palmyra's funerary portrait	pyromorphite	XRF, EDX, FT-IR	pigment	[65]

Lead-phosphate-based compounds are usually found as a micrometric transparent film at the surface of the objects. Based on previous studies and the information of Table 1.1, [49,51–54] it is still a matter of debate to determine whether these compounds can be associated or not to either a degradation process of an originally employed lead-based pigment (e.g., *via* reaction with environmental P-containing compounds or from an apatite-based compound, e.g., white bone or ivory commonly used as pigments) or to a peculiar formulation of the pigments or inks used.

In some Roman wall paintings, [55] it has been suggested that the presence of hydroxypyromorphite [$Pb_5(PO_4)_3OH$ hereinafter referred to as HPy, a lead-calcium phosphate with the 100% substitution of Ca^{2+} with Pb^{2+}], detected along with red ochre, is linked to the intentional use of pyromorphite [$Pb_5(PO_4)_3Cl$]. This compound, that shares a structure like that of lead-calcium phosphates, could have been employed as a mineral for the preparation of the pigment *sandyx*, as described by Pliny the Elder [28] (*ca*. 77-78 CE).

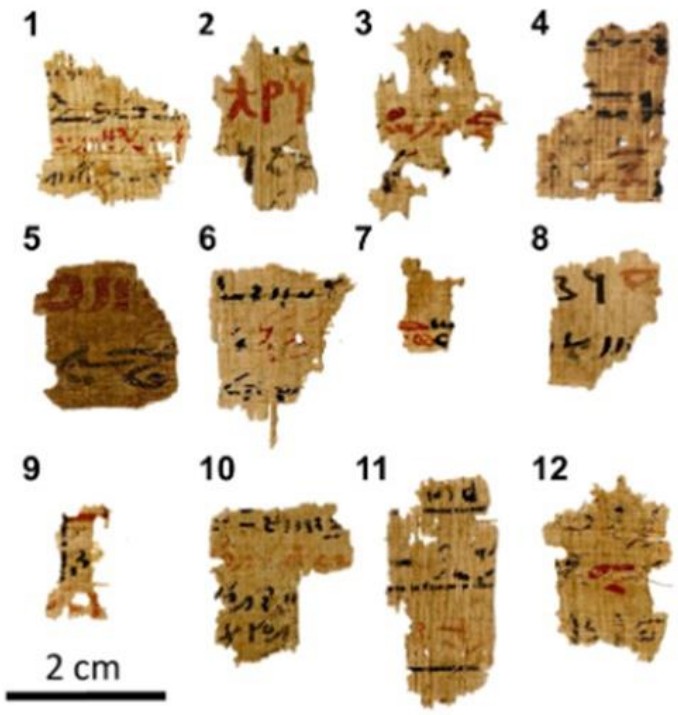

Figure 1.2 Example of a cultural heritage object where $PbHA_x$ compounds was found: an Egyptian Papyri from Christiansen et al. [20].

The presence of pyromorphite has also been reported in Early Islamic pigments at Nishapur (north-eastern Iran); since no geological records shows the presence of neither $PbHA_x$ nor other apatitic minerals around Nishapur area, authors have hypothesized the importation of those materials [56]. Lead phosphate ($Pb_9[PO_4]_6$), found in a 14th century Japanese Buddhist painting on silk, was instead thought to have been used as original white pigment [50].

In a number of artistic and archaeological contexts, the detection of lead-calcium phosphates was instead associated to a degradation process of the originally employed materials, namely: the result of specific interactions between the metallic alloy of a buried Roman bronze inkwell and residues from agricultural fertilizers and soil amendments [53]; the interaction of Pb^{2+} from bronze with contiguous Ca_3PO_4-based material (bone or ivory) of a dining table of the Han dynasty [54]; the reaction of hydroxyapatite [$Ca_5(PO_4)_3(OH)$ or HA] with litharge (tetragonal PbO), cerussite or other lead oxides in tools employed for the preparation or use of lead pigments at Akrotirion (Thera, Greece) during the Early, Middle and Late Cycladic Bronze Age (*ca.* 3000–1600 BCE) [51]; the interaction between black bone (burnt hydroxyapatite) of the preparation and lead white, as hypothesized in the case of Oranjezaal, an oil paint from the XVII century [52]. Furthermore, pyromorphite was revealed on an ancient bronze from the Han dynasty (*ca.* 175 BCE) as a corrosion product [54]. Its presence was more frequently reported as a pigment in different kinds of objects,

namely: ancient Silk Road, early Islamic wall paintings (*ca.* IX-XII century CE) [56], Kizil grottoes' wall paintings (*ca.* III-VIII century CE) [57], and polychrome funerary sculptures (*ca.* 150-250 CE) [58].

Pyromorphite molecular structure is close to HPy [a lead-calcium phosphate ($Pb_xCa_{1-x})_5(PO_4)_3OH$ where x=1], where the OH^- group is substituted with Cl^-. This further structural modification could probably happen as a second-step modification after the formation of HPy, even though the literature mainly reports the presence of this material as an original material.

1.1.3 Uses and applications of calcium-phosphate based compounds in heritage, life, and environmental sciences

In the context of artistic materials, apatite-based compounds have found extensive applications not only as white pigments and fillers [for details see for example *Il Libro dell'arte* by Cennino Cennini (1437 CE)] but also as consolidating agents [59]. For a number of carbonate substrates affected by rain dissolution and thermally induced micro-cracking, such as marbles, [60] or by ice and salt crystallization in pores causing stress, like limestones, [61] HA is formed using as precursors mostly diammonium hydrogen phosphate [$(NH_4)_2HPO_4$, DAP], ammonium dihydrogen phosphate ($NH_4H_2PO_4$, ADP) or triammonium phosphate [$(NH_4)_3PO_4$, TAP]. The newly-formed calcium phosphates have been found to effectively restore the mechanical properties of weathered marbles and limestones and significantly increase their resistance towards dissolution in acidic solutions (because of the lower solubility of HA with respect to that of calcite).
Already-formed HA nanoparticles were also used for the restoration/conservation of ancient paper, which is mainly composed of cellulose fibres, hemicellulose, lignin, and other components (e.g., binding materials, fillers, dyes, pigments, metal ions). [62]. This complex substrate degrades through yellowing and depolymerisation of the fibres (promoted by an acid environment), and the application of a hydroalcoholic solution containing a nano-HA suspension was found to decrease the efficiency of these ageing processes. Notably, the treatment promoted the covering of microscopic surface imperfections, improved the lightfastness of substrate, favoured the increasing of local pH and the decreasing of yellowing phenomena [62].

Beyond the field of cultural heritage, HA is crucial in other fields of study, such as medical and biomaterial applications, since it is the main biomaterial component in hard body tissues, including bones and teeth. These materials are subject to deterioration mainly because of decomposition of collagen, chemical deterioration of the mineral phases and biodeterioration, resulting in pulverization and cracking [61,63]. In this context, nano-HA can be exploited as a remedy in orthopaedic and dental implants, due to its excellent biocompatibility and bone integration ability [64], or in bone defect treatments [35,36].

Due to their high cationic substitution capacity, HA-like compounds have found a wide range of applications also in the field of environmental sciences. For example, in the UK, HA was used to treat lead polluted in tap water. The objective is to add phosphate into drinking water to minimise the release of soluble lead ions arising from the corrosion of lead water pipes, so as to favour the formation of insoluble $PbHA_x$ [65]. Instead, this study highlights how in this environment there is the formation of a range of different $PbHA_x$ (Figure 1.3). Considering the general apatite formula $M_5(PO_4)_3X$, the synthetic apatites that most closely resembled the unit cell dimensions of the apatites on lead water pipes were shown to be: $Pb_{3.4}Ca_{1.3}(PO_4)_3Cl_{0.03}OH_{0.97}$, $Pb_{3.6}Ca_{1.2}(PO_4)_3Cl_{0.07}OH_{0.93}$, and $Pb_{3.6}Ca_{1.2}(PO_4)_3Cl_{0.27}OH_{0.73}$ [65].

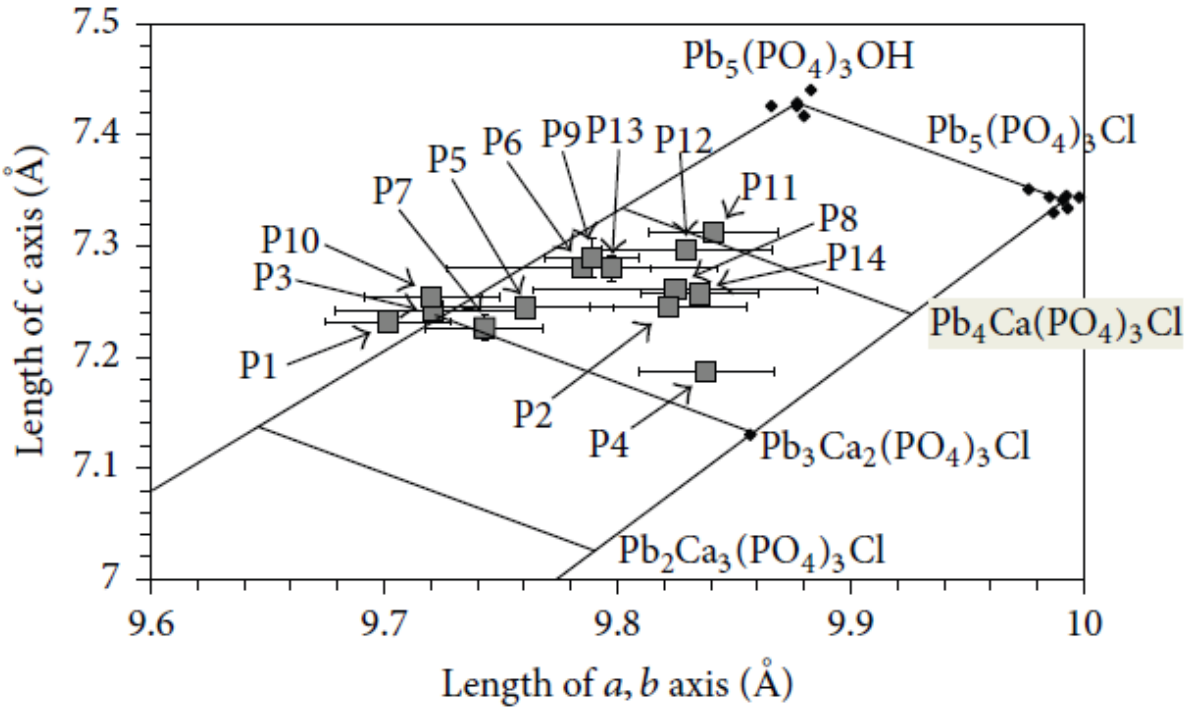

Figure 1.3 Unit cell graph for apatites from lead water pipes where it is highlighted the formation of lead apatites compounds (reproduced from Hopwood et. al [65]).

The worldwide pollution of soils and waters by lead is a worldwide threat to ecosystem functioning and human health [66–68]. The source of a 1000-fold increase in environmental levels of lead is mainly anthropogenic over the past years. The use of lead in paintings, pigments, inks (but also gasoline) is now forbidden, but its presence in other daily materials (storage batteries, glazed ceramics, bearings, ammunition, motor vehicle and other transportation equipment, electrical and electronic equipment, nuclear and X-ray protection devices, pesticides, joint soldering, etc…) and its release from active and decommissioned mines still raises concerns with respect to its impact to the environment.

Extensive lead ore mining, tailings and smelting has caused high levels of soil environment contamination, particularly in developing countries [69,70]. As such, high levels of lead have been detected in plants and soils [71–73]. Furthermore, several pesticides containing substantial amount of lead, like lead arsenate, are widely used in horticulture and agriculture. In this context it was exploited HA high cationic substitution capacity [74] for the decontamination of heavy metals, such as Pb^{2+}, in polluted soil environments. Laperche et al. [72] report that Pb^{2+} totally substitutes Ca^{2+} within hydroxyapatite crystal, thus leading to the precipitation of HPy, which is a pH dependent reaction (Hpy formation is higher at pH 5 than 6 or 7). It is also important to evidence that HPy was identified but not $PbHA_x$ compounds.

Based on what above-mentioned, HA, $PbHA_x$ and HPy are extensively naturally present and intentionally used in our daily life. In the context of heritage science, despite there are still many questions about their formation, the exchange property of bivalent cations (Pb^{2+} with Ca^{2+}) contained in HA crystals can provide a reasonable hypothesis for the presence of $PbHA_x$ and/or HPy as secondary compounds resulting from the reaction between original Pb-compounds and apatite in some artworks.

Being on this subject or on any scientific matter, it is highly relevant to keep non-specialist public aware of on-going scientific research. Moreover, the infodemic and the spread of fake news in the COVID-19-era have further highlighted the urgent need of developing tools that allow performing an efficient dissemination and communication of scientific contents in the full respect of ethical principles but, at same time, easily understandable by the non-expert persons. Several different details have emerged over the last three years, such as that population is interested in scientific topics, and as never before in human history, people believe in science and its work. On the other hand, scientists need to clearly explain scientific research and its processes as well as how the scientific community reaches results. The COVID-19 pandemic also evidences that when there is a lack of correct and ethical communication with the non-specialist public, fake news can more easily grow. The fake news issue that we experienced during the COVID-19 pandemic has pushed the scientific community to open a lively debate on the role and relevance of scientific communication in our society. All such aspects point out why it is significant that researchers implement a communication strategy for their work. In this context, the close collaboration among researchers and science communicators provides the most effective strategy to spread a concept effectively without trivialising it.

The following paragraphs will describe why the attention to science communication is growing over the last two decades and how it can successfully contribute to share scientific content and to increase the relative level of information and awareness among stakeholders and the general public.

1.2 Different ways to communicate science

1.2.1 How to explain research on $PbHA_x$ to a non-specialist user?

Communicating science is among the main goals that every researcher would include in their career and it has two main objectives: 1) sharing tough contents with as large as possible audiences regardless of their background; 2) growing the visibility of their research within the expert scientific community.

But if in peer-to-peer communication this commonly takes place, the communication addressed to a non-specialistic public often does not. Why this happens is beyond the aims of this thesis, that is focused on finding an efficient way to help a non-specialist audience to comprehend a scientific issue, how to approach it, and how the scientific process is developed.

Public communication of the progress and results of one's research activities also serve to broaden and increase consensus, by stimulating public debate on topics of societal interest, while raising public awareness. The communication of scientific advances, with global perception and awareness, has been strongly emphasized and studied during the COVID-19 pandemic; apart from the interaction between the scientific community and the world population, there was also a more rapid increase and spread of false news [75–78]. These aspects highlight how researchers cannot underestimate scientific communication, which is one of the most important tools against misinformation and to raise scientific awareness and perception.

Furthermore, an element to be considered when evaluating the communication strategy is the chance of expanding its own network, with new collaborations or fundings, that can enlarge the research group with new personnel and upgrading the facilities may arise; all these aspects can help to improve and push the research further.

Tools available to spread scientific content to the audience are multiple nowadays; each channel of communication has different characteristics and peculiarities, that require different communication strategies. These strategies depend on whether the researcher's work is published in journals addressed to a specialised audience or whether it is disseminated to the general public *via* generalist audience through magazines (e.g., Wired, Sapere, Le Scienze, etc…,) websites, blogs, social networks, or forums. Therefore, the major task is to plan the correct communication strategy to make researchers' activity dissemination effective and to pursue the two above-mentioned objectives.

Concerning the research activities developed in this thesis, communication focuses on the following multiple goals:

- sharing new knowledge about the study and use of $PbHA_x$ materials in the context of heritage science;

- helping the public to understand how research is structured and which steps were followed to develop it;
- promoting research groups and facilities that are international excellences;
- improving the awareness and the importance of heritage science, a not well-known field of study outside the expert community.

The afore-mentioned goals, despite related to the communication of a very specific research, should be seen and considered appliable in a wider context. The main issue is to show the population in a convincing way why this specific study is important, even though, at a glance, some research may appear superfluous. Moreover, another important function of communication is the simplification of the research's information without trivialising the research itself.

My scientific background and my interest in the medium of film and social media communication put me in a privileged position to understand these issues and try to provide possible solutions for efficiently communicating this scientific research.

1.2.2 Europe and open science

At the end of 2013, the European Commission set out how to access both the publications of research results and the research data itself. The European Commission aimed at promoting and disseminating open science and foster greater collaboration and sharing of results and methodologies between researchers.

To this end, the European Commission made it mandatory that the beneficiaries of the funding from Horizon 2020 and Horizon Europe programmes [79,80] are obliged to publish the results of their research activity through one of two methodologies [81,82]:

- The *green* open access, which consists of depositing the publication in an open archive chosen by the researcher, often after an embargo period.
- The *gold* open access, which consists of publication in peer-reviewed journals with open access, immediately once the results of the research activities have been obtained.

The second step towards promoting open science was in 2016, when it was introduced the EOSC project (European Open Science Cloud Initiative) [83], a set of procedures for the implementation of a network infrastructure that allows researchers an easier sharing of research data.

Subsequently, since 2017, researchers benefiting from Horizon 2020 fundings are also obliged to make research data available in public repositories and publicly accessible according to the principles of traceability, accessibility, interoperability, and reusability (known as FAIR: Findable, Accessible, Interoperable, Reusable).

In recent years, individual European countries have independently equipped themselves with national services to support the dissemination of research data and results. These services are mainly aimed at researchers, public institutions and their staff.

1.2.3 Horizon programmes guidelines

As part of both Horizon funding programmes (Horizon 2020 and Horizon Europe), the European Commission has made some informative videos on YouTube [84] to disseminate guidelines for an effective science communication strategy to non-specialist audiences.

Rhonda Smith, director of Minerva Communication in the UK, states that researchers today are confused about what science communication is and what it is about, asserting that scientific communication is mainly addressed to an audience of non-experts nowadays, so it is no longer possible, as it used to be, to stay in one's own 'ivory tower' and communicate only between specialists within one's area of interest. This means that specialist communication must be integrated with a communication addressed to a broader and non-specialistic public of stakeholders. Again, according to Smith, researchers must communicate the results of their work, especially to those who pay taxes and thus receive financing and investing in the research projects promoted by the European Commission.

Alexandra Ruete, Communication Officer at the Directorate-General for Research and Innovation of the European Commission, states that researchers need to 'sell' what they are working on, in the same way as a product or service. In order to increase the probability of the project being founded, Ruete suggests implementing an effective science communication strategy early in the project. The importance of undertaking a communication strategy from the earliest stages of research activity is also emphasised by Smith, to get out of the closed laboratories and the peer-review circle and have an impact on society. Researchers must think strategically in terms of communication, to decide which communication channel to use and the message they want to convey.

The example of *Horizon magazine* is interesting, because it discloses success stories based on interviews with project coordinators, as well as organising annual events open to the public in Brussels, it produces audio-visual material, such as maps and infographics on how the European Commission finances research and spends citizens' money, and it is present on social media, including Twitter and Facebook [85]. Kevin Mitchell of Trinity College Dublin states that any topic can become interesting if you package it in a certain way according to the situation and the context that leads the audience to be interested in it. Smith advises not only to look at the results of one's research activity but also at the process that led to the achievement of those results throughout the life of a project, thus creating a narrative that engages the audience.

The focus of researchers should not be to communicate every single detail of their research activity, but to give clues to stimulate the curiosity in the audience. Derrick Williams, journalist at Deutsche

Welle, addressing researchers, suggests that they should ask themselves why they started their research to study and understand the emotions and passion that initially drove researchers towards science, so that they may in turn enthuse the audience and share the same feelings.

Williams also affirmed that, for the public, most researchers are "opaque', that is, they do not arouse any interest in their audience target because the message they want to communicate is about explaining their work and their research activity, not creating emotions and connections, with the result of arousing disinterest in the audience. The public wants a story, not simply an explanation of what has been done and the results achieved. Every researcher should answer this question: "why should the public be interested in my work?". The language must consequently be simple, not overly technical, such as explaining to a teenager the results achieved with one's activity.

For this reason, creating a story helps the audience understand why they should be interested in the research. In this narrative, images and videos represent a crucial element. In magazines, images take on the same importance as the article. On TV and the internet, audio-visual communication took on added importance. Improved visual presentation makes science more user-friendly and allows a story to be told more interestingly than a text article. Engaging the public thus becomes one of the cornerstones of science communication.

1.2.4 Communication, dissemination, and exploitation

The EC Research & Innovation Participant Portal Glossary/Reference Terms [86] define project communication as ‘a strategically planned process that starts at the beginning of the action and continues through the entire life cycle, to promote the communication action and results’. It requires strategic measures aimed at communicating the research activity and its results to the public, including the media, and possibly interacting with mutual exchanges. In what follows and in Figure 4, the definition, objectives, and targets of the three main ways to communicate research activities are summarized.

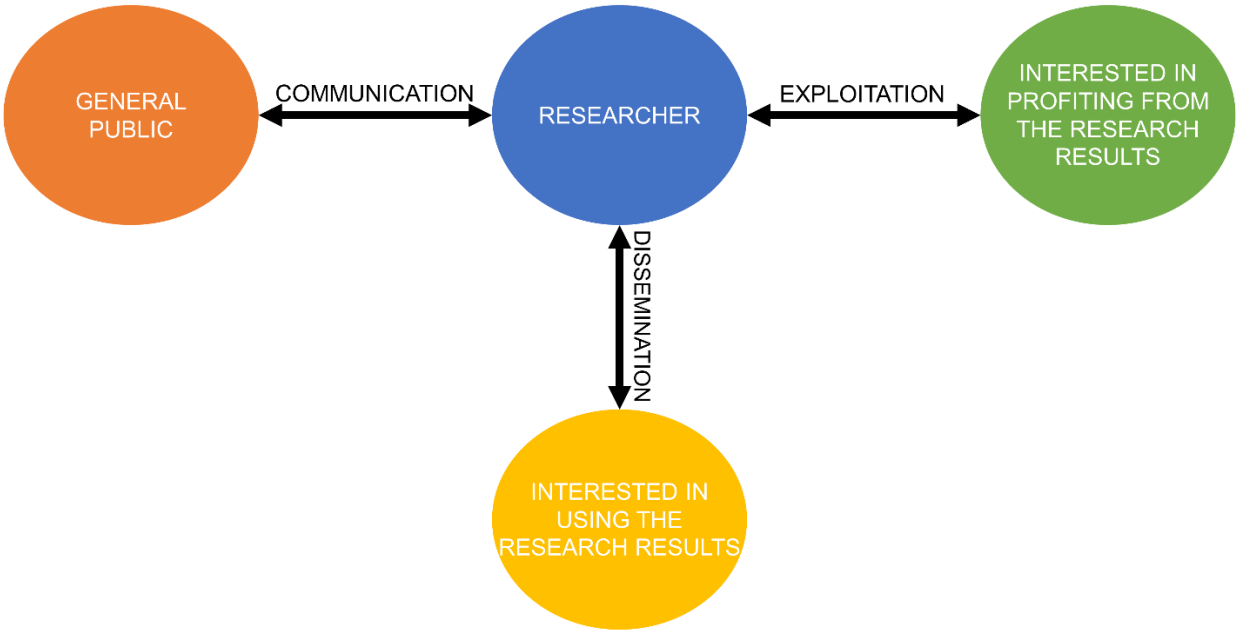

Figure 1.4 Scheme summarizing the differences among communication, dissemination, and exploitation through their targets.

a. *Communication:* its objective is to reach out to society to maximise the impact and benefits of the results achieved through the research, while also providing solutions to the challenges faced by society, informing, and promoting the project and its results. The target audience is diverse and goes beyond the scientific community, including the media and the general public [87];

b. *Dissemination:* it is defined as 'The public dissemination of results through any appropriate medium (except those resulting from the protection and exploitation of the results themselves), including scientific publications by any medium' [88]. The objective of dissemination is to transfer knowledge and results to enable their use by third parties, by maximising the impact of the research carried out. The target audience consists of anyone interested in using the research results;

c. *Exploitation:* it refers to 'the use of results in further research activities other than those covered by the action concerned, or in the development, creation and marketing of a product or process, or the creation and provision of a service, or in the standardisation of activities' [86]. The objective of the exploitation is the effective use of the results of the project to bring concrete added value to society through the utilisation of research results in the scientific, economic, or political sphere. Therefore, the target audience to which the exploitation must

be addressed consists of people and organisations that are potentially interested in profiting from the research results.

In the present thesis, dissemination is considered by the publication of papers in scientific journals, while the communication is carried out through the creation of docuseries for the general public. On the other hand, currently this research does not have any evident aspects that can be identified as exploitation. However, not always the boundaries among communication, dissemination and exploitation activities are clearly defined in this thesis, making it difficult to place some activities under a precise category. For instance, the publication of initial research activities in a specialised journal might attract new stakeholders to the research project, thus turning communication into dissemination.
Nonetheless, the connection among communication, dissemination, and exploitation is therefore maximising the impact of research results in society. The difference among the three activities lies in the objectives and the target audience to which they are addressed.

1.2.5 Communication approaches

Over the past decades, scientific communication opened to an increasingly wider public, stimulating researchers to adapt to the new context and use new tools and a more accessible language to share with a broader public the results of their research work.

Different use of communication channels has been observed by science, with a focus from a paradigm anchored only on traditional mass media (TV, radio, museums, newspapers and specialised journals) to the exploitation of the opportunities that Internet has made available. Until the 1990s, the scientific community used a communication model characterised by a top-down approach (Public Understanding Science, PUS). The scientific community and the public were distinct units and the flow of information was uniquely top-down, namely: from the scientific community to the mass public. It was, therefore, necessary to simplify the concepts so that as many people could benefit from the dissemination of science.

Because of the spread of new media *via* Internet, this paradigm has been overturned, making it possible to realise a model no longer based on unidirectionality but on continuous exchange of information, feedback, and interaction (Public Engagement with Science, PEST). According to the PEST approach, the public is no longer seen as a passive actor in the process of communication of scientific activities but is part of it, by influencing each other. Decisive for this is the feedback received by researchers from the public itself.

Furthermore, each communication product must be designed to achieve the best possible outcomes. Some aspects should be considered in the defined areas:

- Define the objective: to help clarify the purpose of the communication and to ensure that the message is transmitted effectively to the intended audience;

- clear and concise information: a good design of scientific communication should present the information in a clear and concise manner, free of jargon or complex technical terms that may hinder understanding;

- visual content: the use of appropriate graphics, diagrams, illustrations, and videos are essential in scientific communication as they help to present complex data in a visually appealing way, by assisting the audience to quickly understand the message;

- target audience: the communication product must be tailored to the target audience. Whether the product is intended for use by scientists, policy makers or the general public, it must be presented in a way that is accessible and understandable to the intended audience;

- engaging design: scientific communication products must be designed to be visually appealing, engaging and interesting, to capture the attention of the audience and keep them interested in the content;

- accurate and credible content: information must be accurate and based on sound scientific principles. Avoid speculative or dubious claims as they can undermine the credibility of the product.

1.2.6 Why social media and why video?

The annual digital report issued by We Are Social in collaboration with Hootsuite (updated to July 2022) [89], particularly after the COVID-19 pandemic, highlighted the need for an Internet connection. For example, from January 2020 (pre-COVID-19 pandemic) to July 2022, there was an increase in internet users to 4.1% and active social media users up to + 10%. Just these few data give an overview of how the pandemic accelerated the trend of the usage and relevance of internet in our contemporary society. We can also understand how social media are the most used and powerful media nowadays.

In July 2022 there were 4.7 billion active users (59% of the global population) that daily spend an average time of 2h and 29min only on social media (36.4% of the average total time spent on the internet) and +4.9% of the time compared to January 2020. If we focus on the primary reason people use the internet, we can see how 40.9% of internet users employ it for educational and study-related purposes. The report also shows that 92.6% of internet users watch video content via the internet

each week (+2.6% compared to January 2020), and related data is that Youtube.com, a social based uniquely on videos, is the second most used social platform in the world with 3.62 billion unique monthly visitors, with an average time per visit of 27min (74min/day). Other social media have a high average time per day spent on the platform, such as TikTok (95 min/day), Instagram (51 min/day) and Facebook (49 min/day), and their common denominator is that they all are focus (or they are increasing their focus) on video content.

If we focus more on video content, we can understand that 44.9% of the global average use online videos as a source of learning each week (educational, how-to videos, tutorials). Figure 1.5 reports how this percentage is age-composed, with the younger generation more interested in this kind of content. Nevertheless, the minimum percentage of interest in video as a source of learning is still more than 1/3 of the interviewees.

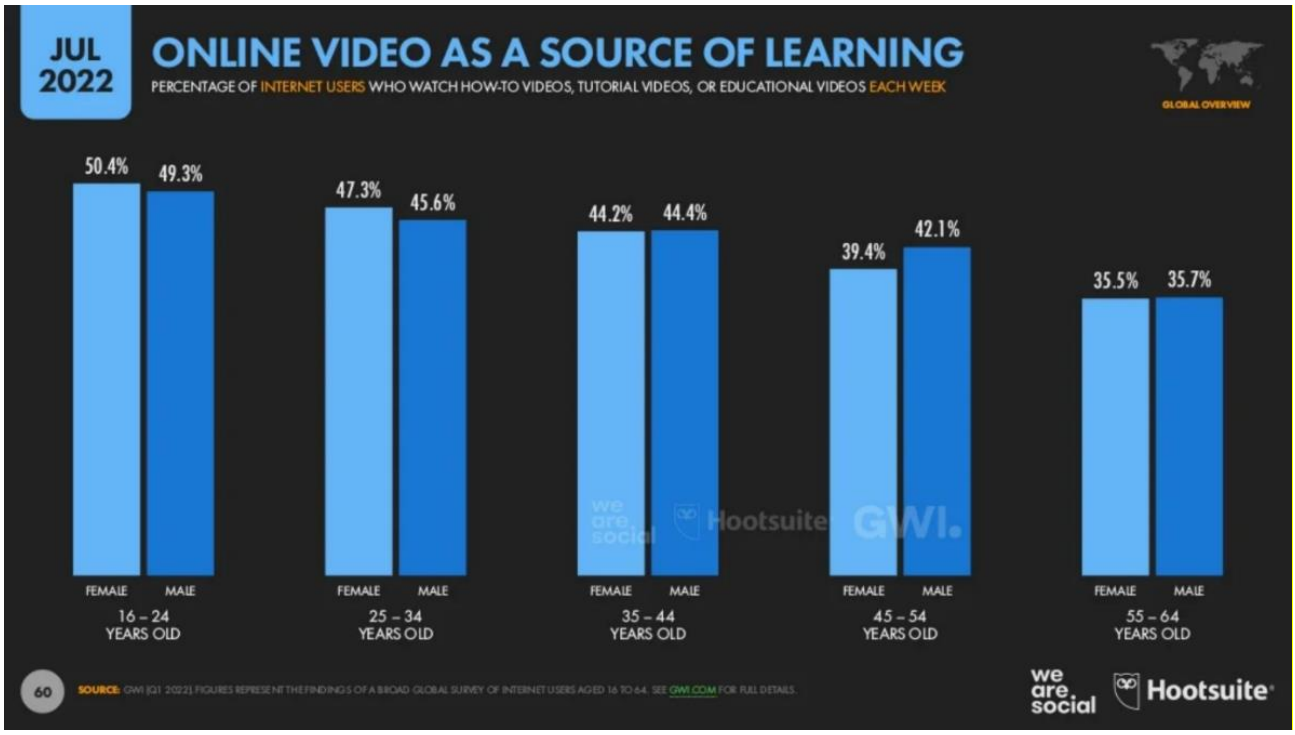

Figure 1.5 Percentage of internet users who watch educational videos each week divided by age and gender, from July 2022 Annual Digital Report.

In summary, thanks to this brief analysis on the uses of internet by the global population, it is possible to conclude that videos can be a helpful and incisive tool to create scientific content for a general audience. Nevertheless, this does not mean that every content must be a video. The type of media (video, podcast, article, etc..,) must be decided case by case to emphasise and help the scientific message be conveyed at its best.

REFERENCES

[1] B.O. Fowler, Infrared studies of apatites. I. Vibrational assignments for calcium, strontium, and barium hydroxyapatites utilizing isotopic substitution, Inorg Chem. 13 (1974) 194–207. https://doi.org/10.1021/ic50131a039.

[2] W.E. Klee, G. Engel, IR spectra of the phosphate ions in various apatites, Journal of Inorganic and Nuclear Chemistry. 32 (1970) 1837–1843. https://doi.org/10.1016/0022-1902(70)80590-5.

[3] H. Liu, X. Cui, X. Lu, X. Liu, L. Zhang, T.S. Chan, Mechanism of Mn incorporation into hydroxyapatite: Insights from SR-XRD, Raman, XAS, and DFT calculation, Chem Geol. 579 (2021) 120354. https://doi.org/10.1016/j.chemgeo.2021.120354.

[4] V.M. Bhatnagar, The preparation, X-ray and infrared spectra of lead apatites, Arch Oral Biol. 15 (1970) 469–480. https://doi.org/10.1016/0003-9969(70)90099-3.

[5] D. Laurencin, N. Almora-Barrios, N.H. de Leeuw, C. Gervais, C. Bonhomme, F. Mauri, W. Chrzanowski, J.C. Knowles, R.J. Newport, A. Wong, Z. Gan, M.E. Smith, Magnesium incorporation into hydroxyapatite, Biomaterials. 32 (2011) 1826–1837. https://doi.org/10.1016/j.biomaterials.2010.11.017.

[6] J.M. Hughes, M. Cameron, K.D. Crowley, Structural variations in natural F, OH, and Cl apatites, American Mineralogist. 74 (1989) 870–876.

[7] K. Sudarsanan, P.E. Mackie, R.A. Young, Comparison of synthetic and mineral fuorapatite, Cas (PO4)s F, in cristallographic detail, Mat. Res. Bull. 7 (1972) 1331–1338.

[8] J. Huang, A.W. Sleight, The Apatite Structure without an Inversion Center in a New Bismuth Calcium Vanadium Oxide: $BiCa_4V_3O_{13}$, J Solid State Chem. 104 (1993) 52–58. https://doi.org/https://doi.org/10.1006/jssc.1993.1140.

[9] M.E. Fleet, X. Liu, Y. Pan, Rare-earth elements in chlorapatite [$Ca_{10}(PO_4)_6Cl_2$]: Uptake, site preference, and degradation of monoclinic structure, American Mineralogist. 85 (2000) 1437–1446. https://doi.org/10.2138/am-2000-1012.

[10] M.E. Fleet, X. Liu, Y. Pan, Site preference of rare earth elements in hydroxyapatite [$Ca_{10}(PO_4)_6(OH)_2$], J Solid State Chem. 149 (2000) 391–398. https://doi.org/10.1006/jssc.1999.8563.

[11] Y. Pan, M.E. Fleet, Compositions of the apatite-group minerals: Substitution mechanisms and controlling factors, in: Phosphates: Geochemical, Geobiological and Materials Importance, De Gruyter Mouton, 2019: pp. 13–50. https://doi.org/10.2138/rmg.2002.48.2.

[12] B. Fowler, Infrared studied apatites I. Vibrational assignment for calcium, strontium and barium Hydroxyapatites utilizing isotopic substitution, 13 (1974) 194–207.

[13] J.M. Hughes, M. Cameron, K.D. Crowley, Ordering of divalent cations in the apatite structure: Crystal structure refinements of natural Mn- and Sr-bearing apatite, American Mineralogist. 76 (1991) 1857–1862.

[14] P.N. Patel, Magnesium and Calcium Hydroxyapatite solid solutions preparation, IR and lattice constant measurements, Journal of Inorganic and Nuclear Chemistry. 42 (1980) 112–1132.

[15] R. Oberti, L. Ottolini, G. Della Ventura, G.C. Parodi, On the symmetry and crystal chemistry of britholite: New structural and microanalytical data, American Mineralogist. 86 (2001) 1066–1075. https://doi.org/10.2138/am-2001-8-913.

[16] J.S. Prener, The Growth and Crystallographic Properties of Calcium Fluor-and Chlorapatite Crystals Solution Growth of Apatite Crystals, J Electrochem Soc. 114 (1967) 77–83.

[17] F. Ruszala, E. Kostiner, Preparation and characterization of single crystals in the apatite system $Ca_{10}(PO_4)_6(Cl, OH)_2$, J Cryst Growth. 30 (1975) 93–95. https://doi.org/https://doi.org/10.1016/0022-0248(75)90204-3.

[18] S.J. Gadaleta, R. Mendelsohn, E.L. Paschalis, N.P. Camacho, F. Betts, A.L. Boskey, Fourier Transform Infrared Spectroscopy of Synthetic and Biological Apatites, Inorg Chem. 13 (1974) 194–207. https://doi.org/10.1007/978-1-4899-1400-2_23.

[19] S.Y. O'Reilly, W.L. Griffin, Apatite in the mantle: implications for metasomatic processes and high heat production in Phanerozoic mantle, 2000. www.elsevier.nlrlocaterlithos.

[20] G. Penel, G. Leroy, C. Rey, B. Sombret, J.P. Huvenne, E. Bres, Infrared and Raman microspectrometry study of fluor-fluor-hydroxy and hydroxy-apatite powders, J Mater Sci Mater Med. 8 (1997) 271–276. https://doi.org/10.1023/A:1018504126866.

[21] G. Buvaneswari, U. V Varadaraju, Synthesis and Characterization of New Apatite-Related Phosphates New phosphates of the formula, J Solid State Chem. 149 (2000) 133–136. http://www.idealibrary.comon.

[22] Y. Suetsugu, Y. Takahashi, F.P. Okamura, J. Tanaka, Structure analysis of A-type carbonate apatite by a single-crystal X-ray diffraction method, J Solid State Chem. 155 (2000) 292–297. https://doi.org/10.1006/jssc.2000.8887.

[23] S.E.P. Dowker, J.C. Elliott, Infrared Study of the Formation, Loss, and Location of Cyanate and Cyanamide in Thermally Treated Apatites, J Solid State Chem. 49 (1983) 334–340.

[24] Hata M, Marumo F, Iwai S-I, Aoki H, Structure of a lead Apatite $Pb_9(PO_4)_6$, Acta Crystallographica Section B. B36 (1980) 2128–2130.

[25] K. Zhu, K. Yanagisawa, R. Shimanouchi, A. Onda, K. Kajiyoshi, Preferential occupancy of metal ions in the hydroxyapatite solid solutions synthesized by hydrothermal method, J Eur Ceram Soc. 26 (2006) 509–513. https://doi.org/10.1016/j.jeurceramsoc.2005.07.019.

[26] K. Zhu, J. Qiu, H. Ji, K. Yanagisawa, R. Shimanouchi, A. Onda, K. Kajiyoshi, Crystallographic study of lead-substituted hydroxyapatite synthesized by high-temperature mixing method under hydrothermal conditions, Inorganica Chim Acta. 363 (2010) 1785–1790. https://doi.org/10.1016/j.ica.2010.02.031.

[27] Y. Zhu, Z. Zhu, F. Yang, Y. Huang, X. Zhao, Synthesis of the lead-calcium HAP solid solutions, Russian Journal of Applied Chemistry. 88 (2015) 178–183. https://doi.org/10.1134/S1070427215010255.

[28] A. Roy, Artists' pigments. A handbook of their history and characteristics, 2, Washington, DC: National Gallery of Art. (1993).

[29] V. Gonzalez, G. Wallez, T. Calligaro, M. Cotte, W. De Nolf, M. Eveno, E. Ravaud, M. Menu, Synchrotron-Based High Angle Resolution and High Lateral Resolution X-ray Diffraction: Revealing Lead White Pigment Qualities in Old Masters Paintings, Anal Chem. 89 (2017) 13203–13211. https://doi.org/10.1021/acs.analchem.7b02949.

[30] S. De Meyer, F. Vanmeert, R. Vertongen, A. Van Loon, V. Gonzalez, J. Delaney, K. Dooley, J. Dik, G. Van der Snickt, A. Vandivere, K. Janssens, Macroscopic x-ray powder diffraction imaging reveals Vermeer's discriminating use of lead white pigments in Girl with a Pearl Earring, Sci Adv. 5 (2019). https://doi.org/10.1126/sciadv.aax1975.

[31] R.L. Feller, Artist's pigments: a handbook of their history and characteristics. Vol. 1, 1986.

[32] L. Monico, L. Sorace, M. Cotte, W. De Nolf, K. Janssens, A. Romani, C. Miliani, Disclosing the Binding Medium Effects and the Pigment Solubility in the (Photo)reduction Process of Chrome Yellows ($PbCrO_4$ /$PbCr_{1-x}S_xO_4$), ACS Omega. 4 (2019) 6607–6619. https://doi.org/10.1021/acsomega.8b03669.

[33] L. Monico, K. Janssens, C. Miliani, B.G. Brunetti, M. Vagnini, F. Vanmeert, G. Falkenberg, A. Abakumov, Y. Lu, H. Tian, J. Verbeeck, M. Radepont, M. Cotte, E. Hendriks, M. Geldof, L. Van Der Loeff, J. Salvant, M. Menu, Degradation process of lead chromate in paintings by vincent van gogh studied by means of spectromicroscopic methods. 3. Synthesis, characterization, and detection of different crystal forms of the chrome yellow pigment, Anal Chem. 85 (2013) 851–859. https://doi.org/10.1021/ac302158b.

[34] F. Rosi, V. Manuali, C. Miliani, B.G. Brunetti, A. Sgamellotti, T. Grygar, D. Hradil, Raman scattering features of lead pyroantimonate compounds. Part I: XRD and Raman characterization of $Pb_2Sb_2O_7$ doped with tin and zinc, Journal of Raman Spectroscopy. 40 (2009) 107–111. https://doi.org/10.1002/jrs.2092.

[35] C. Sandalinas, S. Ruiz-moreno, Lead – Tin – Antimony Yellow AND IDENTIFICATION IN SEVENTEENTH-CENTURY, 9 (2003) 41–52.

[36] R.J.H. Clark, L. Cridland, B.M. Kariuki, K.D.M. Harris, R. Withnall, Synthesis, structural characterisation and Raman spectroscopy of the inorganic pigments lead tin yellow types I and II and lead antimonate yellow: Their identification on medieval paintings and manuscripts, Journal of the Chemical Society, Dalton Transactions. (1995) 2577–2582. https://doi.org/10.1039/DT9950002577.

[37] G. Agresti, P. Baraldi, C. Pelosi, U. Santamaria, Yellow pigments based on lead, tin, and antimony: Ancient recipes, synthesis, characterization, and hue choice in artworks, Color Res Appl. 41 (2016) 226–231. https://doi.org/10.1002/col.22026.

[38] E. Gliozzo, C. Ionescu, Pigments-Lead-based whites, reds, yellows and oranges and their alteration phases, Archaeol Anthropol Sci. 17 (2022) 1–66. https://doi.org/10.1007/s12520-021-01407-z/Published.

[39] J. Morales, J.M. Tirado Macias, A. Ortega, INFLUENCE OF CRYSTALLINITY ON THE KINETICS OF THE LITHARGE-MASSICOT PHASE TRANSITION, 1985.

[40] L. Burgio, R.J.H. Clark, P.J. Gibbs, Pigment identification studies in situ of Javanese, Thai, Korean, Chinese and Uighur manuscripts by Raman microscopy, Journal of Raman Spectroscopy. 30 (1999) 181–184. https://doi.org/10.1002/(SICI)1097-4555(199903)30:3<181::AID-JRS356>3.0.CO;2-8.

[41] T. Ungár, P. Martinetto, G. Ribárik, E. Dooryhée, P. Walter, M. Anne, Revealing the powdering methods of black makeup in Ancient Egypt by fitting microstructure based Fourier coefficients to the whole x-ray diffraction profiles of galena, J Appl Phys. 91 (2002) 2455–2465. https://doi.org/10.1063/1.1429792.

[42] M. Cotte, E. Checroun, W. De Nolf, Y. Taniguchi, L. De Viguerie, M. Burghammer, P. Walter, C. Rivard, M. Salomé, K. Janssens, J. Susini, Lead soaps in paintings: Friends or

foes?, Studies in Conservation. 62 (2017) 2–23. https://doi.org/10.1080/00393630.2016.1232529.

[43] S.W.T. Price, A. Van Loon, K. Keune, A.D. Parsons, C. Murray, A.M. Beale, J.F.W. Mosselmans, Unravelling the spatial dependency of the complex solid-state chemistry of Pb in a paint micro-sample from Rembrandt's Homer using XRD-CT, Chemical Communications. 55 (2019) 1931–1934. https://doi.org/10.1039/c8cc09705d.

[44] V. Gonzalez, A. Van Loon, S. Wt Price, P. Noble, K. Keune, Synchrotron micro-XRD and micro-XRD-CT reveal newly formed lead-sulfur compounds in Old Master paintings, J Anal At Spectrom. 35 (2020) 2267–2273. https://doi.org/10.1039/d0ja00169d.

[45] C. Higgitt, M. Spring, D. Saunders, Pigment-medium interactions in oil paint films containing red lead or lead-tin yellow, National Gallery Technical Bulletin. 24 (2003) 75–95.

[46] L. Monico, K. Janssens, M. Cotte, L. Sorace, F. Vanmeert, B.G. Brunetti, C. Miliani, Chromium speciation methods and infrared spectroscopy for studying the chemical reactivity of lead chromate-based pigments in oil medium, Microchemical Journal. 124 (2016) 272–282. https://doi.org/10.1016/j.microc.2015.08.028.

[47] T. Christiansen, M. Cotte, W. de Nolf, E. Mouro, J. Reyes-Herrera, S. de Meyer, F. Vanmeert, N. Salvadó, V. Gonzalez, P.E. Lindelof, K. Mortensen, K. Ryholt, K. Janssens, S. Larsen, Insights into the composition of ancient Egyptian red and black inks on papyri achieved by synchrotron-based microanalyses, Proc Natl Acad Sci U S A. 117 (2020) 27825–27835. https://doi.org/10.1073/pnas.2004534117.

[48] E. Brun, M. Cotte, J. Wright, M. Ruat, P. Tack, L. Vincze, C. Ferrero, D. Delattre, V. Mocella, Revealing metallic ink in Herculaneum papyri, Proc Natl Acad Sci U S A. 113 (2016) 3751–3754. https://doi.org/10.1073/pnas.1519958113.

[49] H. Béarat, Les pigments à base de plomb en peinture murale romaine, in: Preservation and Restoration of Cultural Heritage: Proceedings of the 1995 LCP Congress, Montreux, 24-29 September 1995= Conservation et Restauration Des Biens Culturels: Actes Du CongresLCP 1995, Montreux, 24-29 Septembre 1995, 1996: pp. 547–555.

[50] J. Winter, 'Lead white' in japanese paintings, Studies in Conservation. 26 (1981) 89–101. https://doi.org/10.1179/sic.1981.26.3.89.

[51] S. Sotiropoulou, V. Perdikatsis, C. Apostolaki, A.G. Karydas, A. Devetzi, K. Birtacha, Lead pigments and related tools at Akrotiri, Thera, Greece. Provenance and application techniques, J Archaeol Sci. 37 (2010) 1830–1840. https://doi.org/10.1016/j.jas.2010.02.001.

[52] A. Van Loon, J.J. Boon, Characterization of the deterioration of bone black in the 17th century oranjezaal paintings using electron-microscopic and micro-spectroscopic imaging techniques, in: Spectrochim Acta Part B At Spectrosc, 2004: pp. 1601–1609. https://doi.org/10.1016/j.sab.2004.03.021.

[53] C. Rémazeilles, E. Conforto, A buried Roman bronze inkwell: Chemical interactions with agricultural fertilizers, Studies in Conservation. 53 (2008) 110–117. https://doi.org/10.1179/sic.2008.53.2.110.

[54] X. Zhang, An unusual corrosion product, pyromorphite, from a bronze an: A technical note, Studies in Conservation. 47 (2002) 76–79. https://doi.org/10.1179/sic.2002.47.1.76.

[55] Pliny the Elder, Naturalis Historia, libro XXXV, par 23, 77AD.

[56] P. Holakooei, J.F. de Lapérouse, M. Rugiadi, F. Carò, Early Islamic pigments at Nishapur, north-eastern Iran: studies on the painted fragments preserved at The Metropolitan Museum of Art, Archaeol Anthropol Sci. 10 (2018) 175–195. https://doi.org/10.1007/s12520-016-0347-7.

[57] S. Aoki, Y. Taniguchi, S. Rickerby, M. Mori, T. Kijima, S. Bomin, Fumiyoshi, K. Editors, Conservation and Painting Techniques of Wall Paintings on the Ancient Silk Road, 2021. http://www.springer.com/series/13104.

[58] C. Brøns, J. Stenger, J. Bredal-Jørgensen, F. Di Gianvincenzo, L.Ø. Brandt, Palmyrene Polychromy: Investigations of Funerary Portraits from Palmyra in the Collections of the Ny Carlsberg Glyptotek, Copenhagen, Heritage. 5 (2022) 1199–1239. https://doi.org/10.3390/heritage5020063.

[59] E. Sassoni, Hydroxyapatite And Other calcium phosphates for the conservation of cultural heritage: A review, Materials. 11 (2018). https://doi.org/10.3390/ma11040557.

[60] P.F. Schuster, M.M. Reddy, Effects of Acid Rain and Sulfur Dioxide on Marble Dissolution, Mater Perform. 33 (1994) 76–90.

[61] A. North, M. Balonis, I. Kakoulli, Biomimetic hydroxyapatite as a new consolidating agent for archaeological bone, Studies in Conservation. 61 (2016) 146–161. https://doi.org/10.1179/2047058415Y.0000000020.

[62] R.M. Ion, S.M. Doncea, M.L. Ion, V. Rădiţoiu, V. Amăriuţei, Surface investigations of old book paper treated with hydroxyapatite nanoparticles, Appl Surf Sci. 285 (2013) 27–32. https://doi.org/10.1016/j.apsusc.2013.07.159.

[63] F. Yang, D. He, Y. Liu, N. Li, Z. Wang, Q. Ma, G. Dong, Conservation of bone relics using hydroxyapatite as protective material, Appl Phys A Mater Sci Process. 122 (2016). https://doi.org/10.1007/s00339-016-0015-x.

[64] H. Zhou, J. Lee, Nanoscale hydroxyapatite particles for bone tissue engineering, Acta Biomater. 7 (2011) 2769–2781. https://doi.org/10.1016/j.actbio.2011.03.019.

[65] J.D. Hopwood, G.R. Derrick, D.R. Brown, C.D. Newman, J. Haley, R. Kershaw, M. Collinge, The identification and synthesis of lead apatite minerals formed in lead water pipes, J Chem. 2016 (2016). https://doi.org/10.1155/2016/9074062.

[66] D.L. Sparks, Toxic Metals in the Environment: The Role of Surfaces, Elements. 1 (2005) 193–197. https://doi.org/https://doi.org/10.2113/gselements.1.4.193.

[67] A. Kushwaha, N. Hans, S. Kumar, R. Rani, A critical review on speciation, mobilization and toxicity of lead in soil-microbe-plant system and bioremediation strategies, Ecotoxicol Environ Saf. 147 (2018) 1035–1045. https://doi.org/https://doi.org/10.1016/j.ecoenv.2017.09.049.

[68] Y. Su, A.S. Adeleye, X. Zhou, C. Dai, W. Zhang, A.A. Keller, Y. Zhang, Effects of nitrate on the treatment of lead contaminated groundwater by nanoscale zerovalent iron, Journal of Hazardous Material. 280 (2018) 504–513. https://doi.org/https://doi.org/10.1016/j.jhazmat.2014.08.040.

[69] J. Yabe, S.M.M. Nakayama, Y. Ikenaka, Y.B. Yohannes, N. Bortey-Sam, B. Oroszlany, K. Muzandu, K. Choongo, A.N. Kabalo, J. Ntapisha, A. Mweene, T. Umemura, M. Ishizuka, Lead poisoning in children from townships in the vicinity of a lead-zinc mine in Kabwe, Zambia, Chemosphere. 119 (2015) 941–947. https://doi.org/10.1016/j.chemosphere.2014.09.028.

[70] Z. Li, Z. Ma, T. van der Kuijp, Z. Tuan, L. Huang, A review of soil heavy metal pollution from mines in China: Pollution and health risk assessment, Science of The Total Environment. 468–469 (2014) 843–853. https://doi.org/https://doi.org/10.1016/j.scitotenv.2013.08.090.

[71] E. Mavropoulos, N.C.C. Rocha, J.C. Moreira, A.M. Rossi, G.A. Soares, Characterization of phase evolution during lead immobilization by synthetic hydroxyapatite, Mater Charact. 53 (2004) 71–78. https://doi.org/10.1016/j.matchar.2004.08.002.

[72] V. Laperche, S.J. Traina, P. Gaddam, T.J. Logan, Chemical and mineralogical characterizations of Pb in a contaminated sail: Reactions with synthetic apatite, Environ Sci Technol. 30 (1996) 3321–3326. https://doi.org/10.1021/es960141u.

[73] Y. Zhu, B. Huang, Z. Zhu, H. Liu, Y. Huang, X. Zhao, M. Liang, Characterization, dissolution and solubility of the hydroxypyromorphite-hydroxyapatite solid solution [(PbxCa1-x)5(PO4)3OH] at 25 °C and pH 2-9, Geochem Trans. 17 (2016) 1–18. https://doi.org/10.1186/s12932-016-0034-8.

[74] E. Mavropoulos, A.M. Rossi, A.M. Costa, C.A.C. Perez, J.C. Moreira, M. Saldanha, Studies on the mechanisms of lead immobilization by hydroxyapatite, Environ Sci Technol. 36 (2002) 1625–1629. https://doi.org/10.1021/es0155938.

[75] K.M.C. Malecki, J.A. Keating, N. Safdar, Crisis Communication and Public Perception of COVID-19 Risk in the Era of Social Media, Clinical Infectious Diseases. 72 (2021) 697–702. https://doi.org/10.1093/cid/ciaa758.

[76] O.D. Apuke, B. Omar, Fake news and COVID-19: modelling the predictors of fake news sharing among social media users, Telematics and Informatics. 56 (2021). https://doi.org/10.1016/j.tele.2020.101475.

[77] Y.M. Rocha, G.A. de Moura, G.A. Desidério, C.H. de Oliveira, F.D. Lourenço, L.D. de Figueiredo Nicolete, The impact of fake news on social media and its influence on health during the COVID-19 pandemic: a systematic review, Journal of Public Health (Germany). (2021). https://doi.org/10.1007/s10389-021-01658-z.

[78] I. Hromatko, M. Tonković, A. Vranic, Trust in Science, Perceived Vulnerability to Disease, and Adherence to Pharmacological and Non-pharmacological COVID-19 Recommendations, Front Psychol. 12 (2021). https://doi.org/10.3389/fpsyg.2021.664554.

[79] European Commission, Horizon 2020, (2013). https://research-and-innovation.ec.europa.eu/funding/funding-opportunities/funding-programmes-and-open-calls/horizon-2020_en.

[80] European Commission, Horizon Europe, (2021). https://research-and-innovation.ec.europa.eu/funding/funding-opportunities/funding-programmes-and-open-calls/horizon-europe_en.

[81] European Commission, Horizon 2020 manual, (2013). https://ec.europa.eu/research/participants/docs/h2020-funding-guide/index_en.htm.

[82] European Commission, Horizon Europe manual, (2021). https://webgate.ec.europa.eu/funding-tenders-opportunities/display/OM/Online+Manual.

[83] European Commission, European Open Science Cloud (EOSC), (2016). https://ec.europa.eu/info/research-and-innovation_en?pg=open-science-cloud.

[84] European Commission, The EU guide to Science Communication, (2017). https://www.youtube.com/playlist?list=PLvpwljZTs-Lhe0wu6uy8gr7JFfmv8EZuH.

[85] European Commission, Horizon Magazine social media accounts, (n.d.). https://www.facebook.com/horizon.magazine.eu (accessed January 18, 2023).

[86] The European IPR Helpdesk, Making the Most of Your Horizon 2020 Project, (2013). https://www.iprhelpdesk.eu/.

[87] A. Campos, L. Codina, Communication, dissemination and exploitation strategy analysis in Horizon 2020, Prisma Social Journal. 32 (2021) 294–319.

[88] L. and S.N. and G.I. Lettieri E. and Marone, Exploitation, Dissemination, and Communication: An Integrated Framework in EU Research, in: C. Andreoni Giuseppe and Mambretti (Ed.), Digital Health Technology for Better Aging: A Multidisciplinary Approach, Springer International Publishing, Cham, 2021: pp. 273–297. https://doi.org/10.1007/978-3-030-72663-8_17.

[89] We are social, Hootsuite, Digital 2022 Report (July update), (2022). https://datareportal.com/reports/digital-2022-july-global-statshot (accessed August 10, 2022).

CHAPTER 2

MATERIALS AND METHODS

2.1 Analytical approach

The series of $(Pb_xCa_{1-x})_5(PO_4)_3OH$ solid solutions is a class of materials that has been widely studied, especially its end-members HA and HPy (for further details see Chapter 1, par. 1.1). The literature describes a wide range of possibilities both for the synthesis methods and characterisation of these compounds, usually based on the exploitation of different techniques, such as XRPD, Scanning Electron Microscopy with Energy Dispersive X-ray Spectroscopy (SEM-EDX), and vibrational spectroscopies (especially FT-IR) [1–7].

The study of literature has prompted the development of a systematic multi-technique and multi-scale analytical approach, significant for increasing knowledge on the morphological and structural properties of $(Pb_xCa_{1-x})_5(PO_4)_3OH$ solid solutions and their identification in different types of samples, especially cultural heritage objects. Notably, in the framework of this thesis, a combination of complementary techniques, including microscopy (SEM-EDS), X-ray based methods with conventional and synchrotron sources (XRPD, XRF, and XANES), and vibrational spectroscopies (FTIR and Raman), were employed.

First, such multi-technique approach was applied for the characterisation of a series of commercial and in-house synthesised $PbHA_x$ compounds. Second, paint mock-ups were prepared by mixing $PbHA_x$ powders with either linseed oil or arabic gum, and then, after drying, they were characterised by non-invasive vibrational spectroscopies with portable devices. In a last step, the outcomes arising from the study of $PbHA_x$ powders and paint mock-ups were exploited for studying a historical fresco fragment, where the presence of lead-calcium phosphate based compounds has been hypothesised but never proved.

2.2 Samples preparation

2.2.1 Synthesis of $PbHA_x$ solid solutions

$PbHA_x$ solid solutions were synthesized according to earlier literature [8] based on the following reaction:

$$5M^{2+} + 3PO_4^- + OH^- \rightarrow M_5(PO_4)_3OH$$

where M = (Pb^{2+}_x + Ca^{2+}_{1-x}) for the solid solution (with 0<x<1), and M = Ca^{2+} or Pb^{2+} for the end-members (hydroxyapatite and hydroxypyromorphite, respectively).

The synthesis was performed by following the steps listed here below:

i) a series of solutions with a variable Pb/(Pb+Ca) molar ratio (equal to 0.1 and 1, in PbHA-10 and HPy, respectively) were prepared by dissolving different amounts of $Pb(CH_3COO)_2$, $Ca(CH_3COO)_2{\cdot}3H_2O$ and CH_3COONH_4 (as a buffer) into distilled water;

ii) a 0.12 mol/L solution of $NH_4H_2PO_4$ was quickly added to the previous solution under stirring and the pH was adjusted to *ca.* 7.5 with a NH_4OH 30% (w/w) solution;

iii) after the pH adjustment, the resulting solution was left under stirring for 10 min at room temperature, thus aged at 100°C for 48h; the obtained precipitate was then filtered and carefully washed with distilled water and dried in the oven at 70 °C overnight.

HA was provided from Sigma-Aldrich and used as a reference for the in-house synthesised compounds.

The complete list of HA, $PbHA_x$, and HPy compounds along with volumes of precursor used for their synthesis is summarized in Table 2.1.

Table 2.1. List of in-house synthesised $(Pb_xCa_{1-x})_5(PO_4)_3OH$ compounds (with 0≤ x≤1), along with volumes of precursor used for their synthesis; the obtained $PbHA_x$ weight is also reported. Note that only HA is a commercial powder (Sigma-Aldrich).

Sample	***Volumes of precursor (mL)***				**Product weight (g)**
	0.4 M $Pb(CH_3COO)_2$	***0.4 M*** $Ca(CH_3COO)_2{\cdot}3H_2O$	***4.4 M*** CH_3COONH_4	***0.12 M*** $NH_4H_2PO_4$	
HA	-	-	-	-	-
PbHA-10	12.5	112.5	125	250	11.69
PbHA-20	25	100	125	250	11.65
PbHA-40	50	75	125	250	11.70
PbHA-50	62.5	62.5	125	250	11.63
PbHA-70	87.5	37.5	125	250	11.76
PbHA-80	100	25	125	250	11.79
HPy	125	0	125	250	12.00

2.2.2 Preparation of paint mock-ups

The following two different sets of paint mock-ups were prepared:

1. the first one was obtained by mixing HA, $PbHA_x$ and HPy with cold-pressed linseed oil (by Zecchi).
2. The second one was prepared by mixing HA, $PbHA_x$ and HPy with arabic gum (by Zecchi).

All mixtures so obtained were then applied on the surface of polycarbonate slices and left to dry for about two months at environmental temperature (ca. 35 °C) and relative humidity percentage (RH ~35-40%) before being analyzed. Mock-ups were prepared with a variable pigment to binder weight ratio to consent the application of a homogeneous and spreadable layer on the polycarbonate support (for details see Table 2.2 and 2.3).

Table 2.2 List of analyzed linseed oil paint mock-ups.

Composition	Ratio $PbHA_x$: binder (w/w)
HA : linseed oil	1 : 1
PbHA-10 : linseed oil	1.4 : 1
PbHA-20 : linseed oil	2.6 : 1
PbHA-40 : linseed oil	1.3 : 1
PbHA-50 : linseed oil	1.3 : 1
PbHA-70 : linseed oil	1.5 : 1
PbHA-80 : linseed oil	1.8 : 1
HPy : linseed oil	4 : 1

Table 2.3 Arabic gum paint mock-ups.

Composition	Ratio $PbHA_x$ / binder (w/w)
HA : arabic gum	0.7 : 1
PbHA-10 : arabic gum	0.8 : 1
PbHA-20 : arabic gum	0.9 : 1
PbHA-40 : arabic gum	0.9 : 1
PbHA-50 : arabic gum	0.9 : 1
PbHA-70 : arabic gum	1 : 1
PbHA-80 : arabic gum	1.4 : 1
HPy : arabic gum	1.8 : 1

2.3 Scanning Electron microscope with an Energy Dispersive Spectrometry (SEM-EDS)

Morphological information (i.e., particle shapes and sizes) of HA, $PbHA_x$ and HPy powder were obtained by SEM-EDS imaging investigations. Morphological images were recorded by the Field Emission Gun – Scanning Electron Microscope (FEG-SEM) LEO 1525 (ZEISS) based on the third generation GEMINI column. The microscope can operate with 0.1-30 kV acceleration voltage and a 4 pA - 10 nA probe current with a nominal resolution of 1.5 nm at 20 kV. All the secondary electron images were acquired by a high-efficiency in-lens detector. The Energy Dispersive X-ray Spectroscopy system (EDS, by Bruker) annexed to the microscope, allows the identification of the elemental composition of the powdered samples to be performed.

2.4 X-ray techniques

Diffraction and spectroscopy X-ray techniques were exploited for the study of HA, $PbHA_x$ and HPy powders and the historical Fresco fragment NJH-18 (for details cf. Chapter 3, par. 3.3).
X-Ray powder diffraction (XRPD) measurements were performed using three different set-ups: a laboratory device equipped with a conventional source, owned by the University of Perugia; the High angular resolution X-ray powder diffraction (HR-XRPD) and a High lateral resolution X-ray powder diffraction (μ-XRD) set-ups of beamlines ID22 and ID13 respectively at the European Synchrotron Radiation Facility (ESRF, in Grenoble France). X-ray absorption near edge structure (XANES) and X-ray fluorescence spectroscopy *(*XRF) were performed instead at beamline ID21 of ESRF and beamline PHOENIX of the Swiss Light Source (SLS) of the Paul Scherrer Institute (PSI).

2.4.1 Basic principles of XRPD and of the three used configurations

The X-Ray diffraction techniques allows studying periodically ordered structures at atomic scales, by obtaining structural information, such as the material composition, its degree of crystallinity, and lattice parameters. The wavelengths of X-rays are in the same order of magnitude as the distance between lattice planes in crystalline materials. When X-rays enter the material, they will be scattered by the electron clouds around the atoms. The periodicity of the lattice planes gives rise to constructive interference of the X-rays and the intensity of the scattered X-rays is plotted against the angle 2θ. From the plotted peaks the lattice distance can be calculated using Bragg's law [$n\lambda = 2d\sin(\theta)$].
The main differences between the three selected XRPD set-ups are in the type and energy of source: the lab XRPD diffractometer is equipped with a traditional Cu Kα anode (ca. 8 keV); the HR-XRPD and μ-XRD set-ups are instead furnished with a monochromatic X-ray source (35 keV and 13 keV, respectively), produced by a synchrotron radiation. Advantages of HR-XRPD measurements relies on the possibility to provide small changes in the lattice parameter which may result from strain,

doping elements into the host lattice, or other effects; on the other hand, no spatial information about the distribution of different phases are achievable by this kind of analysis. On its turn µ-XRD uses X-ray optics to focus the excitation beam to a small spot on the sample surface, so that small features on the sample can be analysed by obtaining a bi-dimensional (2D) map of the phase distribution present on the sample. This technique can be extremely useful to analyse historical samples, usually characterised by a compositional heterogeneity that is of the order of the micrometre scale length. .

2.4.2 Laboratory X-ray powder diffraction (XRPD)

XRPD patterns were collected with a PanalyticalX'Pert PRO diffractometer and PW3050 goniometer equipped with an X'Celerator detector using the Cu-Kα radiation source, with a 2θ step size of 0.0170° and step scan of 100 s. The LFF ceramic tube operated at 40kV, 40mA. To minimize preferred orientations, powder samples were carefully side loaded onto an aluminium sample holder.

2.4.3 High angular resolution X-ray powder diffraction (HR-XRPD)

HR-XRPD measurements in transmission mode were performed at the beamline ID22 of ESRF, fitted with a 9-channel Si (111) multi analyser stage [9]. The incident beam was set to 1 mm^2 at 35 keV (0.354205 Å). The 300-500 µm glass capillaries, filled with powder, were spun at 12 rps during the experiment to avoid preferential orientation effects. Data were collected in the 0.002°-41.912° 2θ range and combined into 0.002° bins for further treatments.

2.4.4 High lateral resolution X-ray powder diffraction (µ-XRD)

Micro-X-ray powder diffraction (µ-XRD) maps were collected at the ID13 "microbranch" beamline of ESRF [10]. Powders were spread as a thin layer on Kapton tape covered with Ultralene film. Samples were mounted vertically, perpendicular to the micro-beam. The energy of the incident beam was 13.0 keV (0.953734 Å). The beam was focused down to ~2×2 µm² using compound refractive lenses mounted in a transfocator. µ-XRD maps were obtained by raster scanning the samples and collecting XRD 2D patterns, in transmission mode, with a Dectris Eiger 4M single photon counting detector that provides frames with 2070 × 2167 pixels (75 × 75 µm² pixel size) at a rate up to 750 Hz. µ-XRD maps were acquired with a dwell time of 25 ms/pixel on reference powders and of 60 ms/pixel on the historical sample (prepared as a thin section of ca. 20 µm thickness) . µ-XRF was collected simultaneously to µ-XRD using a Vortex-EM silicon drift detector (Hitachi, USA), positioned on the rear of the sample.
2D XRD patterns were azimuthally integrated using the PyFAI software package [11] through dedicated Jupyter notebooks [12]. This creates .h5 files with an integrated XRD pattern of each pixel of the 2D maps. µ-XRD maps were analysed with the PyMca ROI imaging software package [13]. XRF spectra were batch fitted using the PyMca software [14].

2.4.5 Rietveld refinement

All XRD patterns were processed by Rietveld refinement. The refinement allows the lattice parameters to be calculated using the GSAS-EXPGUI software package [15]. For the measurement with laboratory set-up and HR-XRPD, internal standard calibration with powdered cubic (Fd-3m) silicon (λ = 5.43008 Å) was performed to correct the sample displacement errors. The refinement involved the scale factor, background, unit cell, peak profile parameters, atomic positions, and isotropic displacement factors. Site occupancy factors of Ca and Pb atoms, which share the same crystallographic sites, were also refined. At the end of the refinement procedure the calculated shifts of all refined parameters were less than their estimated standard deviations and were lower than $3x10^{-4}$ (by error propagation).

2.4.6 XANES at P K- and Ca K- edges

Ca K-edge and P K-edge XANES analyses were performed at the beamline ID21 of the ESRF. [16] Analysis of HA, HPy and $PbHA_x$ powders, spread on S-free tape, covered with Ultralene, were carried out in unfocused mode with a beam of 0.2-0.3 mm^2; those of the historical NJH-18 thin section were performed instead in focused mode by means of a beam focused to 0.7 µm ver.×0.8 µm hor. using Kirkpatrick Baez mirrors system. Samples were mounted vertically, with an angle of 62° with respect to the incident beam. The beam intensity was monitored continuously using a photodiode placed upstream of the sample. For the powders, the absorption was measured in transmission, thanks to a photodiode place downstream of the sample. For the historical paint sample, absorption was measured indirectly through the collection of XRF signal done with a large area (80 mm^2 collimated active area) Silicon Drift Diode (Bruker, Karlsruhe, Germany). A first µ-XRF map (at 4.3 keV) was acquired over a 2D region and points of interest (POI) were selected in the graphical user interface, Daiquiri [17]. For the measurement of XANES spectra in XRF mode, a region of interest was defined over Ca and P Kα emission lines. X-ray energy of the incoming beam was selected and tuned by means of a horizontal deflecting double-mirror system (Si coating for harmonics rejection) and a Si (111) monochromator ($\Delta E/E \sim 2.10^{-4}$). XANES spectra were acquired by scanning the energy from 2120.45 to 2498.42 eV, with steps of 0.2 eV at the P K-edge and from 4020.23 to 4115.75 eV, with steps of 0.24 eV at the Ca K-edge. The monochromator was calibrated with the HA reference powder, with a maximum of absorption at 2152.7 eV at the P K-edge and at 4060.50 eV at the Ca K-edge. Averages of XANES spectra were calculated from different acquisition per point, on different points. XANES analysis was performed using the Orange software package [18]. Briefly, data were pre-processed by (i) calculating the second derivative of the spectra, (ii) selecting regions of interest for each element (here 2150 – 2180 eV for P and 1755 – 455 keV for Ca), vector normalization and smoothing by Savitzky-Golay filter. Principal component analyses (PCA) were performed to visualize the data (from both the reference powders and the historical sample) in a new coordinate space optimized for detection of differences between groups.

2.4.7 High energy resolution fluorescence detection (HERFD)-XANES at P K-edge

HERFD-XANES spectra at the P K-edge were collected on the X-ray micro-spectroscopy beamline PHOENIX of the Swiss Light Source (SLS) of the Paul Scherrer Institute (PSI). X-rays are produced with an undulator, their energy is defined with a Si (111) monochromator and the beam is focused in vertical and horizontal planes (100 µm 240 µm) using Kirkpatrick-Baez mirrors positioned downstream of the monochromator. HERFD-XANES spectra are collected with a compact Von Hamos spectrometer. The Von Hamos spectrometer uses a cylindrically bent Si (111) crystal of 7 cm and a position sensitive detector (MÖNCH) to resolve the emission signal [19]. The effective energy resolution, which was obtained by the convolution of the total instrumental energy bandwidth (spreads of the incident and emitted rays) and the 3p core−hole width from the Kα1 line was about 3.0 eV, compared to about 6.1 eV in conventional fluorescence yield measurement with a solid-state detector.

The scanned energy range is between 2100 and 2240 eV, and its Kα1 emission was continuously measured. The inelastically scattered X-ray signal and P K-edge fluorescence were acquired in the RIXS plane. The P K-edge HERFD-XANES) was extracted from the RIXS plane at fixed emission energy 2014.40 eV. For these measurement, HA, HPy and $PbHA_x$ powders were pressed into 7mm pellets.

2.5 Vibrational Spectroscopies

Vibrational spectroscopies, namely FT-IR and Raman spectroscopy, were complementary exploited to investigate the molecular structure of HA, HPy and $PbHA_x$ powders and paint mock-ups as well as the historical sample NJH-18. Investigations were performed by employing both bench-top and portable devices. Transmission mode measurements were carried out for the FT-IR study of powders, while reflection mode analysis were performed for that of paint mock-ups and the historical paint fragment

2.5.1 Mid and Near Fourier Transform Infrared Spectroscopy

Mid FT-IR spectra were recorded through the portable ALPHA spectrometer by Bruker Optics. The instrument is equipped with a Global source, a DLaTGS detector and a modified Michelson interferometer (RockSolid^{TM}).

Measurements were performed in transmission and reflection mode, using different dedicated modules:

- A transmission sample compartment with its 2x3” standard sample holder was employed to analyse the HA, HPy and $PbHA_x$ powders previously pressed in KBr pellets, that were

prepared by mixing few mg of each sample in ca. 120 mg of KBr powder. Data were recorded in the 4000–320 cm^{-1} spectral range, with 2 cm^{-1} spectral resolution and with 200 scans;

- A dedicated reflection module was employed to non-invasively acquire reflection spectra (shown in pseudo-absorbance A'=log(1/R, with R=reflectance) directly at the surface of paint mock-ups. Profiles were recorded from areas of 5 mm diameter and ca. 1cm to the probe, in the 7000–320 cm^{-1} range, with 4 cm^{-1} spectral resolution and with 800 scans, reflection mode analysis do not need sample preparation;

Deconvolution of transmission mode FT-IR spectra was performed by means of the Origin 2018 software, using a Gaussian curve fitting. The curve-fit results were characterized by squared regression coefficient values $R^2 \geq 0.992$.

Non-invasive reflectance near FT-IR measurements were performed on paint mock-ups using a portable JASCO VIR-9600 spectrophotometer equipped with a near-infrared fibre optic sampling probe. The optical bench top consists of a halogen lamp as the source, a Michelson interferometer equipped with a CaF_2 beam splitter, and a room temperature InGaAs detector. Pseudo-absorbance spectra were recorded in the 15000–4000 cm^{-1} spectral range, with an energy resolution of 4 cm^{-1} and with 800-1000 scans. During measurements, the fibre optic probe was kept perpendicular to the sample surface, by allowing the reflection with a spatial resolution of about 10 mm^2 to be measured. Correction for background absorption was carried out by measuring a metal mirror plate as reference.

2.5.2 μ-FT-IR

μ-FT-IR mapping of historical NJH-18 thin section (thickness of ca. 20 μm) was performed by employing a Hyperion 3000 FTIR microscope coupled to a Tensor 27 spectrometer (Bruker GmbH). A liquid nitrogen cooled 64 × 64-pixel focal plane array (FPA), which has a field of view of 132 × 132 μm^2, was used for the simultaneous acquisition of FT-IR spectral dataset. FPA images were taken in reflection mode with a 20× objective at the nominal lateral resolution of about 2-3 μm, averaging 1000 scans at 6 cm^{-1} spectral resolution in the 900–5000 cm^{-1} spectral range. Correction for background absorption was performed by analysing a gold mirror plate as a reference.

2.5.3 μ-Raman

μ-Raman measurements of powders and historical NJH-18 thin section were performed with a laboratory JASCO NRS-3100 spectrophotometer equipped with an Ar^+ ion laser (emitting at 488 and 514 nm), a laser diode emitting at 785 nm, two gratings (1200 l/mm for the green and blue lines and 800 l/mm for the red laser), an optical microscope with four objectives (5x, 20x, 50x, and 100x) and a charge-coupled device detector (CCD) cooled by Peltier effect down to -50°C. Spectra were recorded with the 100x objective, in the range of 200-2000 cm^{-1} by setting different values of

exposure time (from 1 s to 40 s) and number of accumulation (from 3 to 30). The laser power at the sample ranged from 0.3 to a maximum of 5.0 mW for the Ar^+ ion laser and from 0.6 to a maximum of 10 mW for the laser diode. The curve-fit of the spectra was performed via the Origin 2018 software using Lorentzian functions and employing the minimum number of components ($R^2 \geq 0.973$)

2.5.4 Portable Raman

Raman measurements were performed using B&W Tek portable Raman, a high spectral resolution fibre optic portable Raman system equipped with laser excitations at 532 and 785 nm, an optical microscope with four objectives (4x, 20x, 40x and 80x) and a high quantum efficiency CCD array detector with cooling to -25°C. Spectra were recorded both with the probe (BAC102) which allows it to work directly on the analysed surface and this can be useful during in situ analysis. The probe offers a laser spot diameter at the focal plane of 85 µm for both the laser excitations at 532 nm and 785 nm with a working distance of 5.4 mm and 5.5 mm, respectively, and with microscope objectives giving rise to a spot size ranging from 15-400 µm in accordance with the selected objective. Spectra were collected in the range of 200-2000 cm^{-1} on variation of exposure time (1s to 20 s), and number of accumulations (3 to 15). The power of the laser at the sample were ranged from 6.89 to 257 mW (for the 785 nm laser), and 10 to 40 mW (for the 532 nm laser); this device has a spectral resolution of *ca.* 6-10 cm^{-1}.

REFERENCES

[1] M. Andres-Verges, F.J. Higes-Rolando, P.F. Gonzalez-Diaz, Infrared spectra of calcium-strontium phosphate apatites, J Solid State Chem. 43 (1982) 237–243. https://doi.org/https://doi.org/10.1016/0022-4596(82)90235-3.

[2] A. Bigi, A. Ripamonti, S. Brückner, M. Gazzano, N. Roveri, S.A. Thomas, Structure refinements of lead-substituted calcium hydroxyapatite by X-ray powder fitting, Acta Crystallographica Section B. 45 (1989) 247–251. https://doi.org/10.1107/S0108768189001928.

[3] A. Benmoussa, M. Mikou, J.L. Lacout, A.M. Siouffi, Lead phosphate hydroxyapatite high-performance liquid chromatography, J Chromatogr A. 694 (1995) 486–491. https://doi.org/10.1016/0021-9673(94)01204-R.

[4] J.D. Hopwood, G.R. Derrick, D.R. Brown, C.D. Newman, J. Haley, R. Kershaw, M. Collinge, The identification and synthesis of lead apatite minerals formed in lead water pipes, J Chem. 2016 (2016). https://doi.org/10.1155/2016/9074062.

[5] T.A. Olds, A.R. Kampf, J.F. Rakovan, P.C. Burns, O.P. Mills, C. Laughlin-Yurs, Hydroxylpyromorphite, a mineral important to lead remediation: Modern description and characterization, American Mineralogist. 106 (2021) 922–929. https://doi.org/10.2138/am-2021-7516.

[6] J. Winter, 'Lead white' in japanese paintings, Studies in Conservation. 26 (1981) 89–101. https://doi.org/10.1179/sic.1981.26.3.89.

[7] F.J. Higes-Rolando, M. Andres-Verges, P.F. González-Díaz, Infrared spectra of heterocationic and heteroanionic apatites, Spectrochim Acta A. 38 (1982) 197–203. https://doi.org/https://doi.org/10.1016/0584-8539(82)80196-7.

[8] Y. Zhu, B. Huang, Z. Zhu, H. Liu, Y. Huang, X. Zhao, M. Liang, Characterization, dissolution and solubility of the hydroxypyromorphite-hydroxyapatite solid solution [$(Pb_xCa_{1-x})_5(PO_4)_3OH$] at 25 °C and pH 2-9, Geochem Trans. 17 (2016) 1–18. https://doi.org/10.1186/s12932-016-0034-8.

[9] C. Dejoie, M. Coduri, S. Petitdemange, C. Giacobbe, E. Covacci, O. Grimaldi, P.O. Autran, M.W. Mogodi, D.Š. Jung, A.N. Fitch, Combining a nine-crystal multi-analyser stage with a two-dimensional detector for high-resolution powder X-ray diffraction, J Appl Crystallogr. 51 (2018) 1721–1733. https://doi.org/10.1107/S1600576718014589.

[10] C. Riekel, M. Burghammer, R. Davies, Progress in micro- and nano-diffraction at the ESRF ID13 beamline, IOP Conf Ser Mater Sci Eng. 14 (2010) 012013. https://doi.org/10.1088/1757-899x/14/1/012013.

[11] G. Ashiotis, A. Deschildre, Z. Nawaz, J.P. Wright, D. Karkoulis, F.E. Picca, J. Kieffer, The fast azimuthal integration Python library: PyFAI, J Appl Crystallogr. 48 (2015) 510–519. https://doi.org/10.1107/S1600576715004306.

[12] L. Huder, Jupyter notebooks for azimuthal integration, (2021). https://gitlab.esrf.fr/loic.huder/juno.

[13] M. Cotte, T. Fabris, G. Agostini, D. Motta Meira, L. de Viguerie, V.A. Solé, Watching Kinetic Studies as Chemical Maps Using Open-Source Software, Anal Chem. 88 (2016) 6154–6160. https://doi.org/10.1021/acs.analchem.5b04819.

[14] V.A. Solé, E. Papillon, M. Cotte, P. Walter, J. Susini, A multiplatform code for the analysis of energy-dispersive X-ray fluorescence spectra, Spectrochim Acta Part B At Spectrosc. 62 (2007) 63–68. https://doi.org/10.1016/j.sab.2006.12.002.

[15] B.H. Toby, EXPGUI, a graphical user interface for GSAS, Applied Cristallogrhy. (2001) 210–213.

[16] M. Cotte, E. Pouyet, M. Salomé, C. Rivard, W. de Nolf, H. Castillo-Michel, T. Fabris, L. Monico, K. Janssens, T. Wang, P. Sciau, L. Verger, L. Cormier, O. Dargaud, E. Brun, D. Bugnazet, B. Fayard, B. Hesse, A.E. Pradas Del Real, G. Veronesi, J. Langlois, N. Balcar, Y. Vandenberghe, V.A. Solé, J. Kieffer, R. Barrett, C. Cohen, C. Cornu, R. Baker, E. Gagliardini, E. Papillon, J. Susini, The ID21 X-ray and infrared microscopy beamline at the ESRF: Status and recent applications to artistic materials, J Anal At Spectrom. 32 (2017) 477–493. https://doi.org/10.1039/c6ja00356g.

[17] S. Fisher, M. Oscarsson, W. de Nolf, M. Cotte, J. Meyer, Daiquiri: a web-based user interface framework for beamline control and data acquisition, J Synchrotron Radiat. 28 (2021) 1996–2002. https://doi.org/https://doi.org/10.1107/S1600577521009851.

[18] J. Demšar, A. Erjavec, T. Hočevar, M. Milutinovič, M. Možina, M. Toplak, L. Umek, J. Zbontar, B. Zupan, Orange: Data Mining Toolbox in Python Tomaž Curk Matija Polajnar Laň Zagar, 2013.

[19] A. Bergamaschi, M. Andrä, R. Barten, C. Borca, M. Brückner, S. Chiriotti, R. Dinapoli, E. Fröjdh, D. Greiffenberg, T. Huthwelker, A. Kleibert, M. Langer, M. Lebugle, C. Lopez-Cuenca, D. Mezza, A. Mozzanica, J. Raabe, S. Redford, C. Ruder, V. Scagnoli, B. Schmitt, X. Shi, U. Staub, D. Thattil, G. Tinti, C.F. Vaz, S. Vetter, J. Vila-Comamala, J. Zhang, The MÖNCH Detector for Soft X-ray, High-Resolution, and Energy Resolved Applications, Synchrotron Radiat News. 31 (2018) 11–15. https://doi.org/10.1080/08940886.2018.1528428.

CHAPTER 3

RESULTS AND DISCUSSION

3.1 Characterisation of $PbHA_x$ reference powders

Based on the synthesis method described in chapter 2 (par 2.1) [1], Table 3.1 shows the percentage yield of the precipitation reaction along with the theoretical Pb content (arising from the starting molar ratio between Ca- and Pb-containing reactants) and the one experimentally obtained by Rietveld refinement of the XRPD patterns of the synthesized and commercial powder.

Table 3.1 $PbHA_x$ reaction yield and [(a)] X_{Pb} = mol Pb^{2+}/(mol Pb^{2+} + mol Ca^{2+}); [(b)] calculated by Rietveld refinement of the XRPD patterns (see Figure 3 chapter 3.2.2).

Sample	***Yield %***	***Theorical x*** [(a)]	***Experimental x*** [(b)]
HA*	-	0	0
PbHA-10	97.42	0.1	0.125 ±0.001
PbHA-20	97.10	0.2	0.288±0.002
PbHA-40	97.53	0.4	0.463±0.003
PbHA-50	96.97	0.5	0.505±0.002
PbHA-70	98.01	0.7	0.728±0.004
PbHA-80	98.32	0.8	0.816±0.004
HPy	100	1	1

*HA was purchased from Sigma-Aldrich and it is used as commercial reference.

The high reaction yield can be reasonably explained by a considerable decrease of the solubility in water K_{sp} of $PbHA_x$ solid solution (in standard condition), from the $K_{sp}(NH_4H_2PO_4)=428$ to $K_{sp}(HA)=10^{-58.38}$. $PbHA_x$ solid solution water solubility is also inversely proportional to X_{Pb}, with a minimum of $K_{sp}(HPy)=10^{-80.77}$ [1]. From the obtained yield, it is also possible to affirm that the reaction is quantitative because all the Ca^{2+} and Pb^{2+} present in the solution contribute to the formation of $PbHA_x$ as is also shown by the experimentally determined stoichiometries.

The experimental X_{Pb} obtained by Rietveld refinement of the XRPD patterns does not exactly correspond to the theoretical X_{Pb}. This can be justified considering that, in the starting solutions, the lead molar amount which have really reacted was always a little bit greater than the calcium one. Such aspect might be related, for example, to a different purity grade of the reactants: in the

hypothesis that the calcium acetate was less pure with respect to the lead acetate, the obtained compound might have a lead molar fraction larger than the theoretical one; this would be also in agreement with the reaction yield values which increase with the increasing lead molar ratio.

The $PbHA_x$ synthesised powders (Figure 3.1) were analysed using the multi-technique and multi-scale approach described in Chapter 2, with the aim of identifying: (i) specific markers to discriminate $(Pb_xCa_{1-x})_5(PO_4)_3OH$ compounds in historical artworks ($0 \leq x \leq 1$); (ii) pros and cons of each employed analytical method.

In a first step, morphological and structural measurements were performed by a combination of SEM and X-Ray techniques (i.e., XRPD and XANES at Ca and P K-edges) in order to understand the effects of Pb content on microstructure and local atomic structure of $PbHA_x$ powders. In a second step, vibrational spectroscopy was carried out to obtain further molecular information about the solid solutions.

Figure 3.1 Photograph of the complete set of the synthesised $PbHA_x$ compounds. From top left: HA, PbHA-10, PbHA-20, PbHA-40, PbHA-50, PbHA-70, PbHA-80 and HPy.

3.1.1 Morphological, microstructure and local atomic structure investigations

SEM images collected from $(Pb_xCa_{1-x})_5(PO_4)_3OH$ compounds (Figure 3.2) show that all samples' crystallites have homogeneous shapes and sizes, approximately in the 20-110 nm range. The shape of the crystallites is rather isotropic for all powders, except for HA and PbHA-20 for which dimension appears somewhat longer than the others. Such visual observations were better determined via calculation of Dv (crystallite size) and ε (percentage of isotropic microstrain) parameters by Rietveld refinement (Table 3.2). Calculations were performed by adopting both isotropic and uniaxial models. Only when the adoption of the uniaxial model, either for crystallite size or microstrain, produced a relevant improvement in the statistical agreement factors (Rp and Rwp), it was considered acceptable, otherwise, the isotropic model was kept. Notably, the use of an anisotropic size model was effective for HA, PbHA-10, PbHA-20 and HPy, while the remaining samples were better described by isotropic models. For what concerns microstrain, for all samples the introduction of anisotropic effects did not significantly improve the refinement, therefore an isotropic model was adopted.

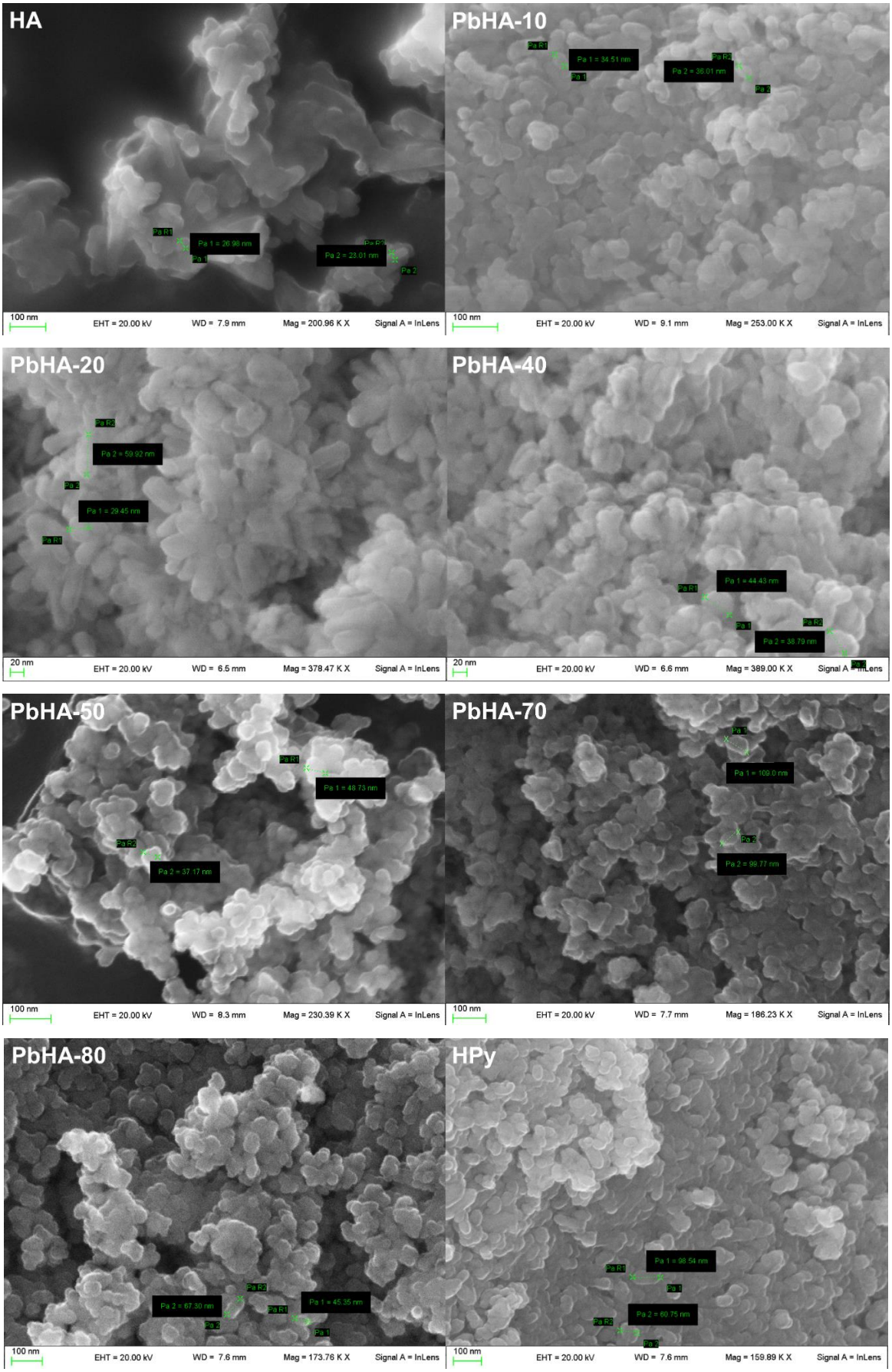

Figure 3.2 SEM images of HA, PbHA$_x$ and HPy powders.

Rietveld refinements of the ID22 HR-XRPD data recorded from the same powders (Figure 3.3 and Table 3.2) allowed obtaining accurate information on a variety of structural parameters, namely: unit cell and atomic positions; compositional parameters, *via* refinement of atomic site occupancy factors; microstructural features, such as crystallite sizes and microstrain (ε), through accurate refinement of peak profile functions.

Table 3.2 Composition, refined unit cell parameters, crystallite sizes (Dv) and % isotropic microstrain (ε) values for $(Pb_xCa_{1-x})_5(PO_4)_3OH$ (with 0≤x≤1) samples.

Sample	*Theorical x*	*Experimental x*[a]	*a* (Å)	*c* (Å)	Dv^ (nm)	Dv|| (nm)	*ε* (%)
HA[b]	0	0	9.4261	6.8699	25	118	0.31
PbHA-10[b]	0.10	0.112	9.4776	6.9115	26	83	0.36
PbHA-20[b]	0.20	0.286	9.5654	6.9730	22	65	0.83
PbHA-40[c]	0.40	0.453	9.6356	7.0434	38	-	2.2
PbHA-50[c]	0.50	0.530	9.6813	7.0981	31	-	2.0
PbHA-70[c]	0.70	0.733	9.7610	7.2443	46	-	2.0
PbHA-80[c]	0.80	0.769	9.7935	7.3067	54	-	1.3
HPy[b]	1.00	1	9.8797	7.4148	32	103	0.58

[a] Calculated by Rietveld refinement of ID22 HR-XRPD data (see Figure 3.3).
Dv: [b] isotropic; [c] perpendicular and parallel to the (0 0 1) crystallographic axis.

Experimental results on HA, $PbHA_x$ and HPy are in agreement with those reported in literature [2], showing that all samples are well described using a structural model derived from that of pure HA hexagonal symmetry (space group P63/m). Generally, their crystallinity grade is lower than the calcium-strontium apatitic solid solution [3] and decreases with increasing of the lead content in the solid solution [4]. $PbHA_x$ samples were considered as solid solutions, in which Pb atoms isomorphously replace Ca atoms in their two crystallographically independent positions in HA structure [4–6]. Therefore, Ca1 and Pb1 occupy a 4*f* Wickhoff position, with a coordination number of 9 which corresponds to an estimated ionic radius of 1.18 and 1.35 Å, respectively, while Ca2 and Pb2 occupy a 6*h* position, with a coordination number of 7 and ionic radius of 1.06 and 1.23 Å, respectively [7]. In both configurations, the difference in the estimated Ca and Pb ionic radii is 0.17 Å. When Pb replaces Ca, this difference induces a linear increase with the exchanged fraction of average unit cell parameters (Vegard's law) [4,5]. However, as early reported [7], Pb has a strong preference for the 6*h* position, probably because it is less hindered than 4*f*, with the consequence that the 4*f* position starts to be massively exchanged only when the other position is almost fully occupied, and this occurs for about a 50% global exchange. Notably, in the samples described in this work, for a global replacement of 53%, the 6*h* position is 79% exchanged, while the 4*f* position is only 14% exchanged.

The replacement of Ca with Pb in 4*f* position induces a larger increase in the *c* lattice parameter than the same replacement in 6*h*, because their reciprocal distances are shorter along the *c* axis (~3.43 Å) than other directions (~3.95 Å) and other crystallographic sites (~4.16 Å). For these reasons the

plot of the *c* axis *vs* X_{Pb} shows two distinct linear trends (Figure 3.4A, red): the range $0 < X_{Pb} < 0.5$ is referred to the exchange of the 6*h* position, while the range $0.5 < x < 1$ is referred to the exchange of the 4*f* position. The plot of *a* axis *vs* X_{Pb} is instead described only by one linear regression equation (Figure 3.4A, black). Such results highlight that the composition of a specific $(Pb_xCa_{1-x})_5(PO_4)_3OH$ compound in heterogeneous and complex samples (from example from artworks or soils), is in principle feasible only based on the position of a few diffraction peaks.

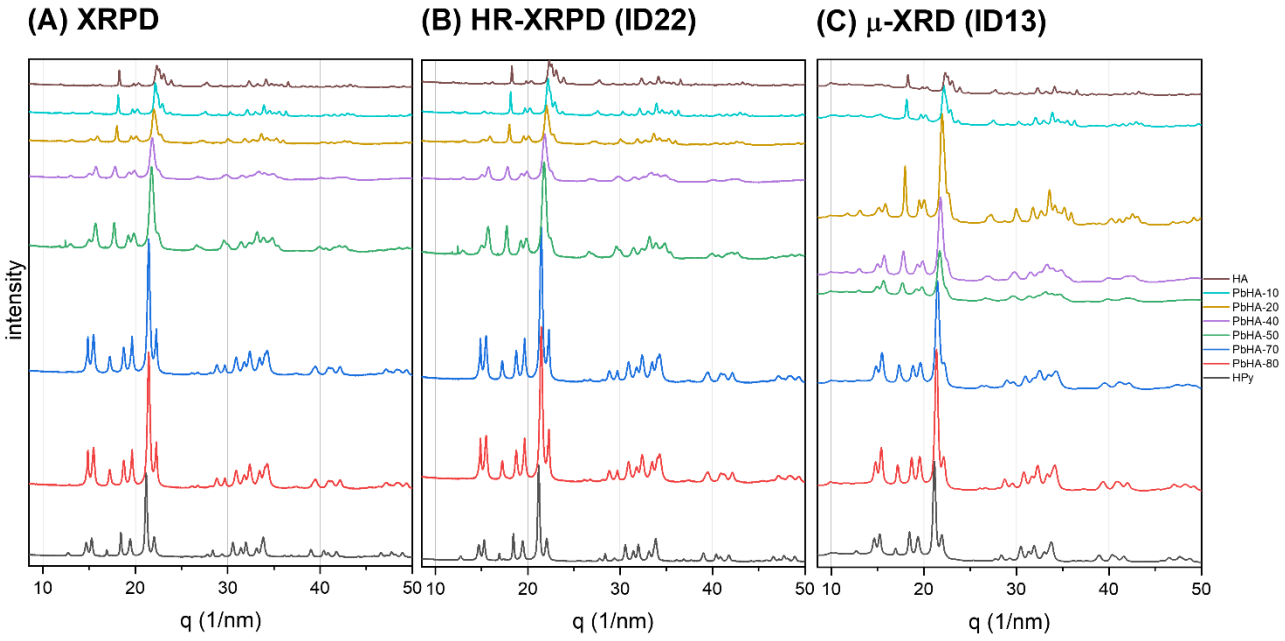

Figure 3.3 Comparison of (a) Lab XRPD, (b) HR-XRPD, and (c) μ-XRD patterns of the $(Pb_xCa_{1-x})_5(PO_4)_3OH$ powders.

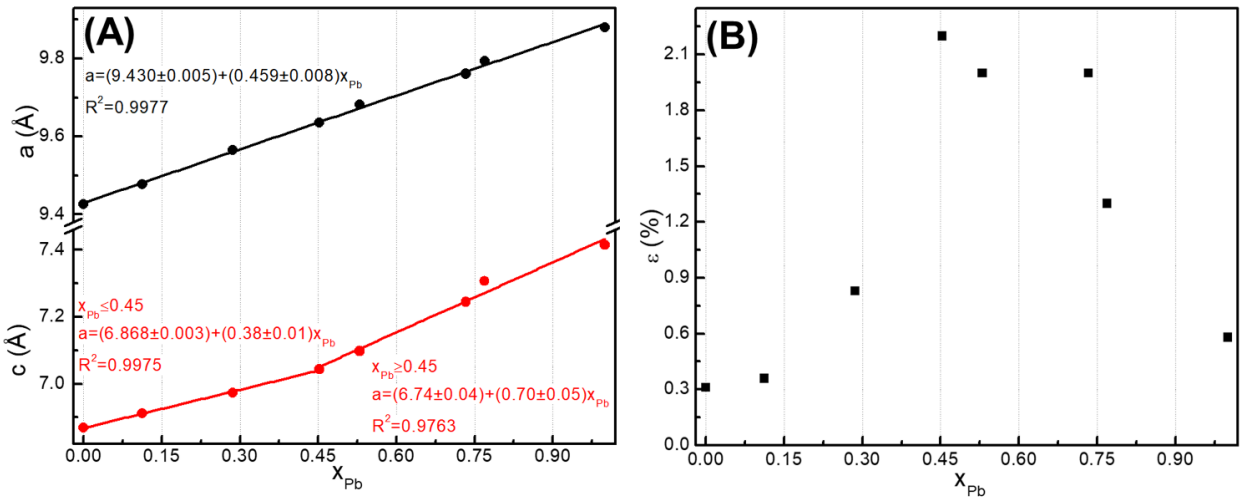

Figure 3.4 (A) Unit cell parameters and (B) % microstrain as a function of x for $(Pb_xCa_{1-x})_5(PO_4)_3OH$ samples. Data were obtained by Rietveld refinements of ID22 HR-XRPD data.

Furthermore, the replacement of Ca with Pb induces a local distortion (or microstrain) of the crystal lattice, which can be estimated by the analysis of XRPD patterns (Figures 3.3 and 3.4). Crystallite size and microstrain are the most relevant factors that usually contribute to the broadening of diffraction peak profiles. By the refinement of the peak profiles as a function of 2θ in a wide enough spectral region, it is possible to separate and estimate the size and microstrain of the sample, since the peak broadening depends on size effects with 1/cosθ, while microstrain contribution depends on tanθ. In some cases, it is possible to estimate also the anisotropic size and microstrain, because they affect to a different extent distinct classes of diffraction peaks.

As reported in Table 3.2, results obtained about size usually agree with SEM analysis (Figure 3.2), while the microstrain level shows a characteristic dependence on X_{Pb}, being more pronounced for intermediate values (~0.45) when the massive occupation of 6*h* positions by the Pb ions starts to occur (Figure 3.4B). This suggests that, for low degrees of substitution of Ca with Pb (lower X_{Pb} values) or Pb with Ca (higher X_{Pb} values), the parent structure is poorly distorted, whereas, when 4*h* positions are almost completely occupied by Pb, the introduction of further Pb in 6*h* positions generate the greatest structural distortions.

It should be noted that, due to relatively small particle sizes and high microstrain levels, the broadening of $PbHA_x$ samples is rather high (Figure 3.5). It follows that μ-XRD measurements performed at ID13 beamline, which is characterized by a lower instrumental resolution than ID22 (at ID13 the average FWHM of the peaks is 0.0544° 2θ, while at ID22 is equal to 0.0025° 2θ), provided similar results because the instrumental contribution to the broadening is still much lower than that coming from the sample (Figure 3.3). Similar considerations can be done for laboratory XRPD data, that are characterised by an instrumental profile similar to that of ID13.

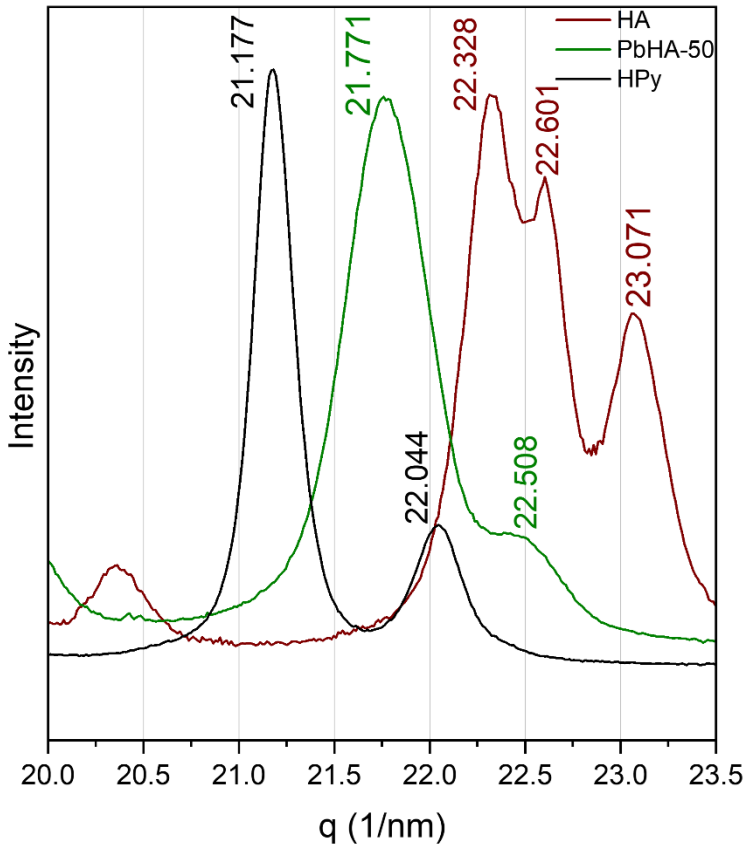

Figure 3.5 Example of peak broadening and shift of HR-XRPD patterns (acquired at ID22) depending on the variation of Pb content in the $(Pb_xCa_{1-x})_5(PO_4)_3OH$ compounds: HA (dark red), PbHA-50 (green) and HPy (black). The selected peaks are respectively (1 2 1) and (1 1 2); the peaks position is reported in Å.

As already mentioned in Chapter 1.1.2, Hopwood et al. [8] studied the presence of apatites compounds in some lead water pipes from Yorkshire (UK), and the determination of different lead-calcium phosphate solid solution was carried out by XRD analysis. The authors plotted similar apatites compounds latter parameter *a, b* versus *c* [HA, HPy, $Ca_5(PO_4)_3Cl$, and $Pb_5(PO_4)_3Cl$ as references]. These references form a square within, the authors suggested, that is useful for the recognition of unknown samples. By plotting the samples' latter parameters, it should be possible to identify if samples are part of the selected solid solutions, and have an idea about their composition.

Therefore, the same plot was reproduced (using standards reported in the literature) for the characterisation of the obtained synthesised $PbHA_x$ powders. Figure 3.6 shows the deviation from the hypothesised linear correlation between the end-terms $Ca_5(PO_4)_3OH$ and $Pb_5(PO_4)_3OH$, probably because the deviation of *c* parameter from Vegard's law (cf. Figure 3.4A) was not considered.

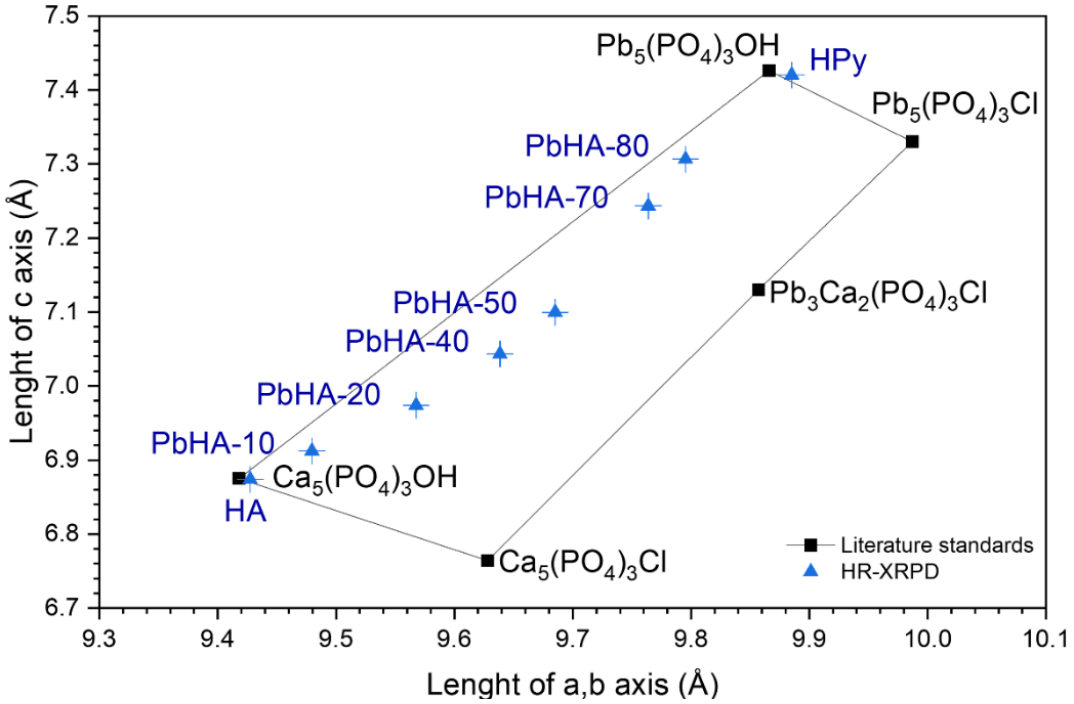

Figure 3.6 unit cell graph (a,b versus c parameters) taken from ref. [8] (black) and modified by including the HR-XRPD results of PbHAx powders analyzed in this thesis (blue).

The P K-edge XANES spectra for HA, $PbHA_x$ and HPy samples are shown in Figure 3.7A. The energy of the absorption edge range from ~2152 to 2153 eV and is attributed to the transition of a 1s core electron to the 3p lowest unoccupied antibonding molecular orbital. Across the samples, the intensity of the white line peak increases with increasing lead content; its energy position follows a similar trend by shifting from 2154 to 2155.54 eV. The spectra with high Pb content show a distinct pre-edge feature in the energy range 2148–2151 eV, consistent with the results of Ingall et al.[9] for mineral. Closer inspection (Figure 3.7B) reveals that the pre-edge signal is only present in samples with above 40% substitution of Ca by Pb. The characteristic post-edge shoulder of calcium phosphates at 2156 eV [9,10] is evident in samples with up to 50% substitution of Ca by Pb, and disappears with increasing substitution of Ca by Pb (Figure 3.7C). The position of the post-edge peak at 2164 eV in HA, decreases with increasing substitution of Ca by Pb.

Ca K-edge XANES spectra from the same set of lead phosphate samples are shown in Figure 3.7D. In the case of Ca, the XANES spectra results from the excitation of Ca 1s electrons to empty molecular orbitals localized on the calcium atom. The absorption edge energies for all samples range from ~4050 to 4070 eV at the edge is attributed to the transition of a 1s core electron to the 3d molecular orbital, which may include both quadrupole (1s → 3d) and dipole allowed (1s → 3d + np) transitions [11]. In the case of Ca K-edge XANES, the position white line peak increases with increasing Pb content from ~4049 to 4051 eV, while the intensity decreases. Furthermore, the intensity of the pre-edge of the Ca XANES spectra, which is routinely used to assess the Ca

coordination environment [11], decreases with increasing Pb content (Figure 3.7E). The post-edge features of the Ca XANES spectra, also show a slight increase with increasing Pb content (Figure 3.7F).

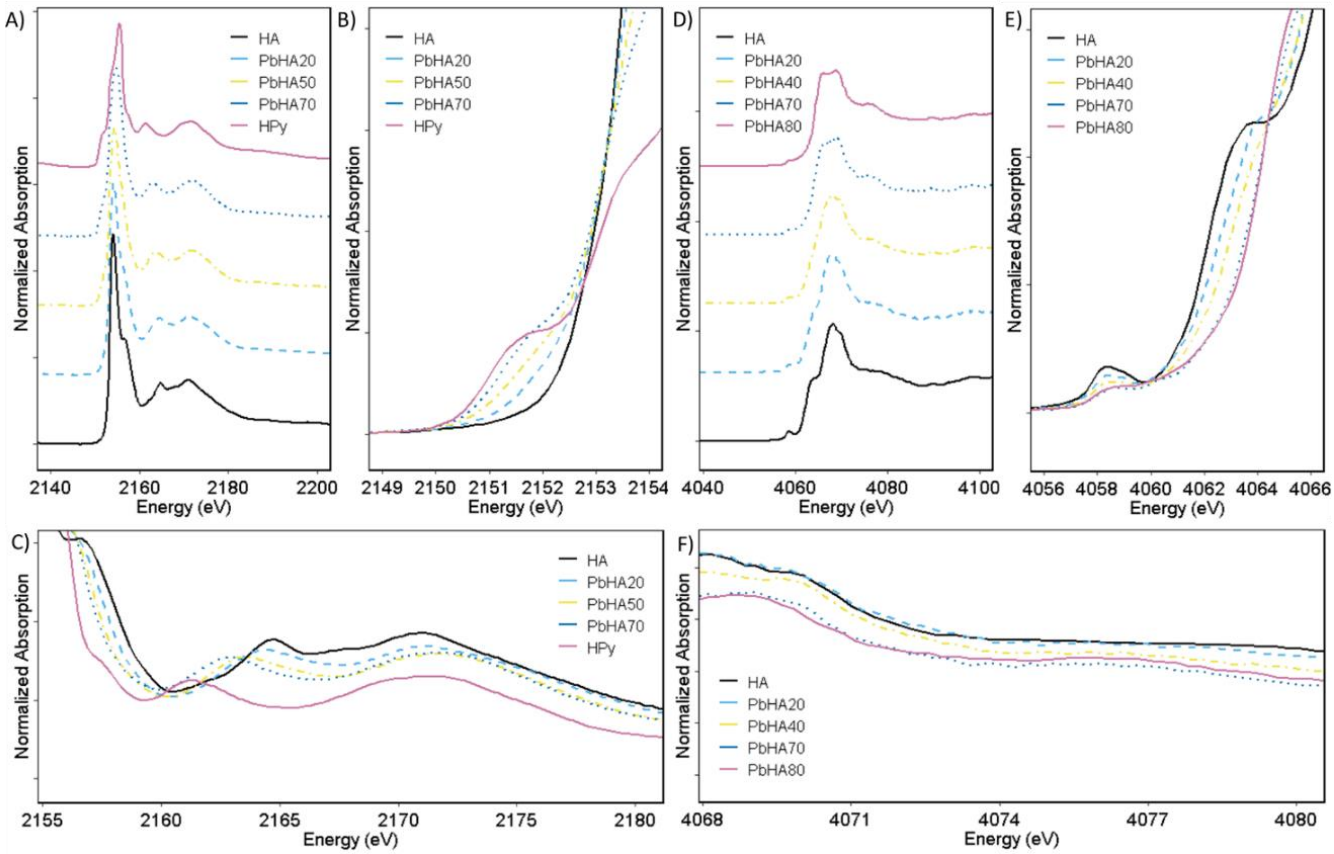

Figure 3.7 (A) P K-edge XANES spectra of hydroxyapatite (HA), with increasing Ca by Pb substitution and Hydroxyyromorphite (HPy). (B) Close-up view of pre-edge region. (C) Close-up view of post-edge region. (D) Ca K-edge XANES spectra of hydroxyapatite (HA), with increasing Ca by Pb subsitution (E) Close-up view of pre-edge region. (F) Close-up view of post-edge region. Here are reported only five selected spectra to highligh differences.

We also investigated the informational gain of performing HERFD XANES spectroscopy, at the Kα1 emission, in comparison to conventional XANES spectroscopy (Figure 3.8). While HERFD XANES spectra have a lower background than conventional XANES spectra, there was little informational gain. This could be attributed to the fact that the Kα line probes the 3p final states, which are not bonding for P. Similar results have been achieved for As, and Se in a previous study, [12] where their HERFD-XANES spectra yield little gain in comparison to conventional XANES spectroscopy due to their electronic structure. A possibility that remains unexploited is to probe the Kβ emission, as this probes the 3d final states [13]. The 3d orbitals are bonding, implying that one is sensitive to the chemical bonds of P, however the weak cross section of the Kβ emission may limit its application in diluted samples [13].

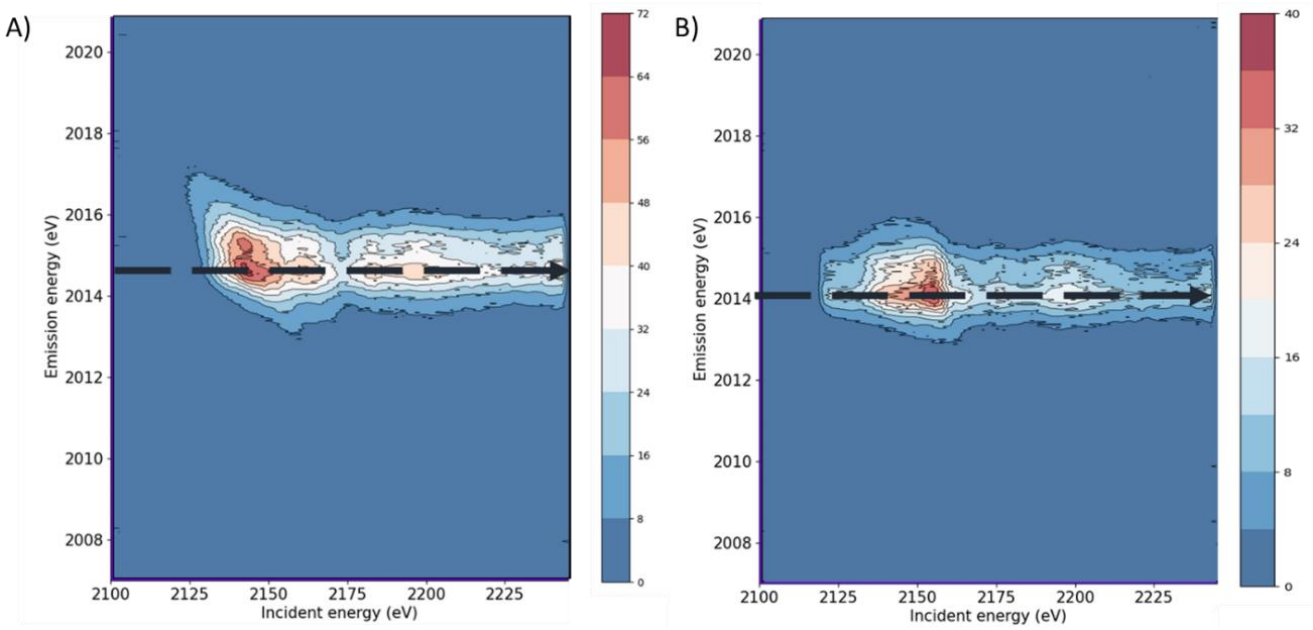

Figure 3.8 (A) P Kα-edge Resonant Inelastic Scattering (RIXS) plane of hydroxyapatite (HA), and (B) hydroxypyromorphite (HPy). The dashed line corresponds to the cut plane extracted for HERFD-XANES.

In summary, the composition of a specific $(Pb_xCa_{1-x})_5(PO_4)_3OH$ compound (with $0 \leq x \leq 1$) in heterogeneous and complex cultural heritage samples, can be successfully determined only based on the position of a few diffraction peaks, even when performing an accurate Rietveld analysis and the refinement of site occupancy factors, as for data XRPD collected at ID13 or by diffractometer using traditional X-ray sources, is not feasible. An accurate and more reliable microstructural determination of HA, $PbHA_x$, and HPy compounds were possible only by analysis of the ID22 HR-XRPD dataset due to the neglectable instrumental contribution to the peak broadening. The local atomic structure analysis does not allow for precisely determining the $PbHA_x$ stoichiometry: P K-edge XANES permit the discrimination of higher or lower X_{Pb} in the solid solution ($X_{Pb} \approx 0.4$) , whereas Ca K-edge is more sensitive to X_{Pb} variation in the $PbHA_x$ lattice environment; for this reason, XANES is a valuable technique for a qualitative and semi-quantitative $PbHA_x$ identification.

3.1.2 Molecular structural investigations

The transmission mode FT-IR and μ-Raman spectra (λ_{exc}=785 nm) of HA, $PbHA_x$ and HPy powders are reported in Figure 3.9.

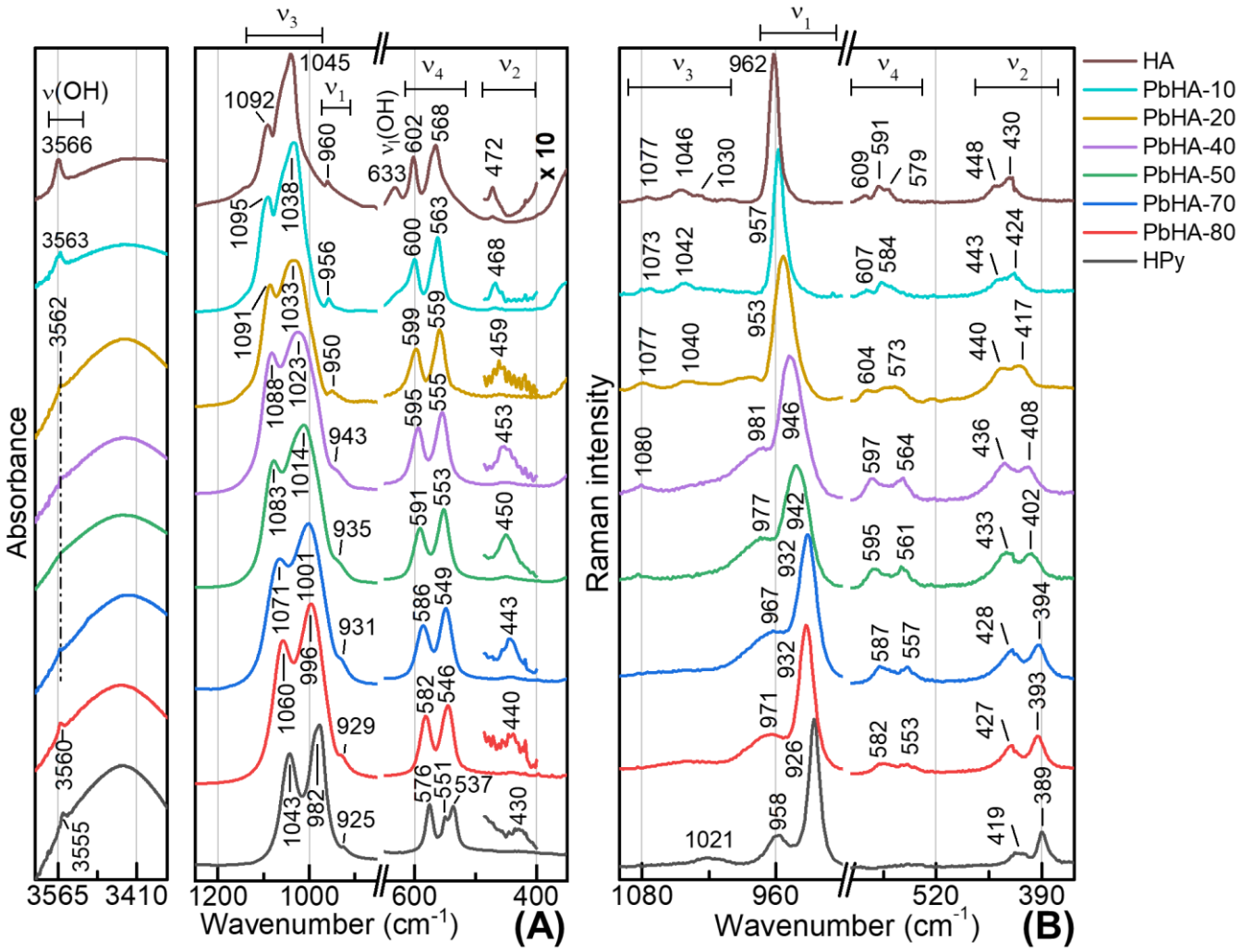

Figure 3.9 (A) Transmission mode FT-IR and (B) μ-Raman spectra of powders of HA, PbHAx solid solutions and HPy (λ_{exc}=785 nm).

As widely described in the literature [14–20], the ν_3 vibrational modes of HA (brown line) are detectable at 1092 and 1045 cm^{-1} in the FT-IR spectrum, whereas they are located at 1077, 1046 and 1030 cm^{-1} in the Raman one.

The tetrahedral PO_4^{3-} group can be recognised by the assignment of two main different regions: stretching modes (symmetric: ν_1 and asymmetric: ν_3) and bending modes (symmetric: ν_2 and asymmetric: ν_4) [21].

The ν_1 mode is recognizable at 960 and 962 cm^{-1} in the FT-IR and Raman spectra, respectively [14,15,20,22–25]. The FT-IR ν_4 and ν_2 bending modes are present at 602, 568, and 472 cm^{-1}, while the corresponding Raman bands are detectable at 609, 591, 579, 448, and 430 cm^{-1} [14,16,22–24,26]. Bands of the hydroxyl group are located at 3566 and 633 cm^{-1} and are assigned to the stretching [ν(OH)] and librational modes [ν_l(OH)], respectively [23,24]. As earlier reported for a series of synthetic substituted hydroxyapatite compounds [1,27–30], the position and band-shape of all the

previously described signals depend on the nature of the incorporated cation and the extent of substitution. Vibrational spectra of $PbHA_x$ solid solutions and HPy (Figure 3.9) clearly show a shift towards lower wavenumber of all PO_4^{3-} peaks and a change of their band-shape with increasing lead amount. A lower wavenumber shift is observed also for the ν(OH) mode, whose intensity is altogether lower when Pb^{2+} cations are present in the apatite lattice.

A further analysis on FT-IR transmission mode and μ-Raman spectra was performed using a mathematical treatment with the aim of finding reliable spectral markers for distinguishing different $(Pb_xCa_{1-x})_5(PO_4)_3OH$ compounds (Figure 3.10). It was decided to investigate the P-O stretching and bending regions since are here located the most intense bands of the vibrational spectra. After a baseline subtraction pre-treatment, the deconvolution process was performed using the minimum number of Gaussian and Lorentzian components, for the FT-IR and Raman spectra, respectively. The results were characterized by satisfying squared regression coefficient values $0.973<R^2<0.999$.

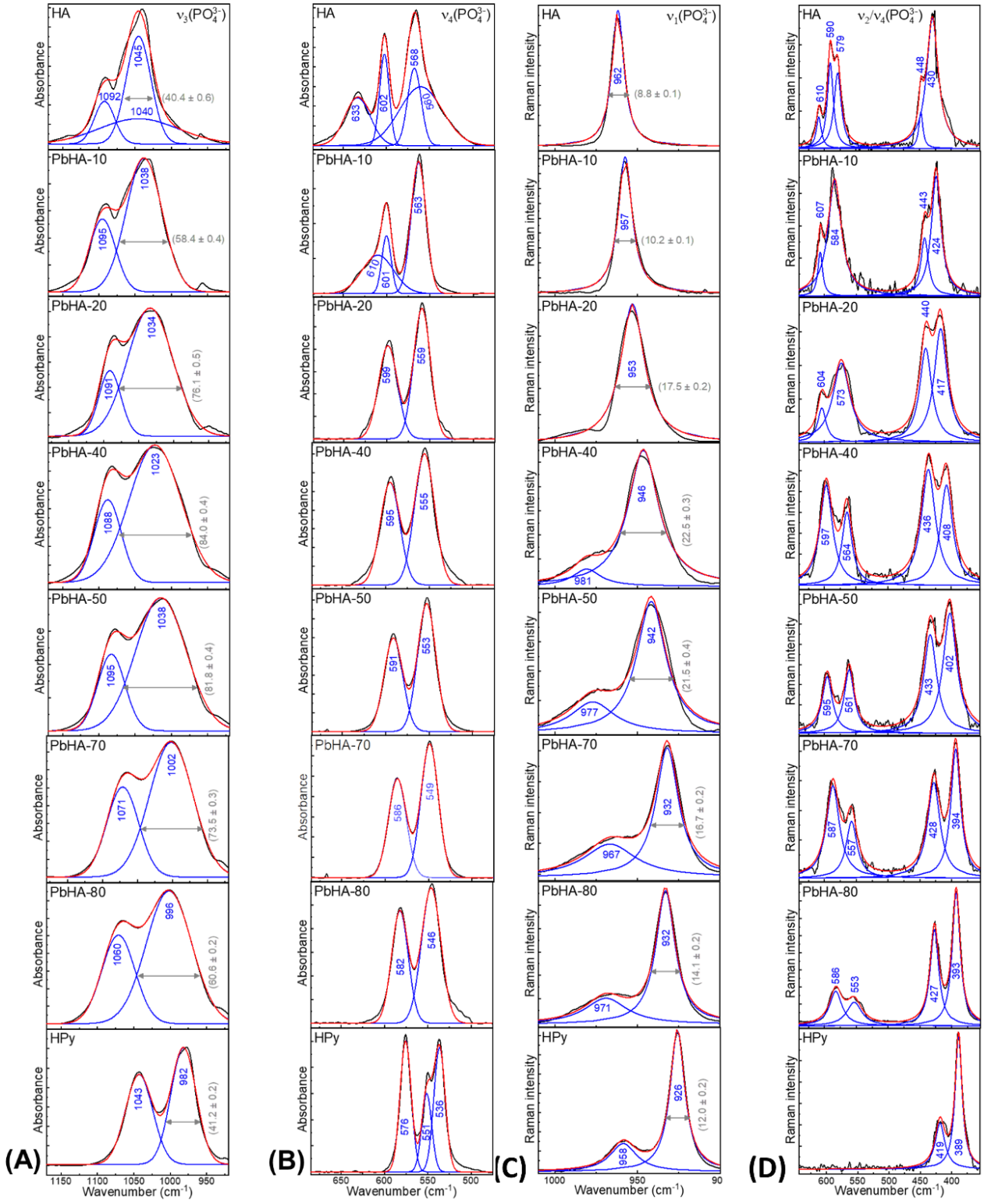

Figure 3.10 Phosphate stretching and bending modes regions of (A, B) transmission mode FT-IR spectra and (C, D) μ-Raman spectra acquired from HA, PbHAx and HPy powders and corresponding curve fit results (blue: Gaussian or Lorentzian components; red: total fit; black: data). Blue labels indicate the wavenumber positions of each component, while in grey the full width at half maximum (FWHM) values for the bands at 982–1045 cm^{-1} and at 982–1045 cm^{-1} are shown.

The deconvolution treatments of the peaks (Figure 3.10) permit to assign the wavenumber positions of the most intense IR [ν_3 and ν_4] and Raman [ν_1 and ν_2] modes and their characteristic full width at

half maximum (FWHM) values more precisely; in addition, they gave the possibility to highlight how IR and Raman modes monotonically decrease with increasing lead content (Figure 3.11 A, B). Consistent with the XRPD data (*cf.* Figures 3.3, 3.5 and Table 3.2), the observed shifts can be explained considering the apatite lattice expansion effect due to substitution of smaller Ca^{2+} ions with larger Pb^{2+} ions. The FWHM values of both ν_3 and ν_1 component (Figure 3.11 C, D) show a discontinuous trend, by reaching a maximum value at X_{Pb} of ca. 0.4-0.5 and then progressively decreasing again until the Ca^{2+} substitution with Pb^{2+} is complete (i.e., X_{Pb}=1). Such discontinuity reflects changes in both the crystal structure disorder and crystallite size induced by the Ca^{2+}/Pb^{2+} substitution, as shown by XRPD analysis (Figure 3.3).

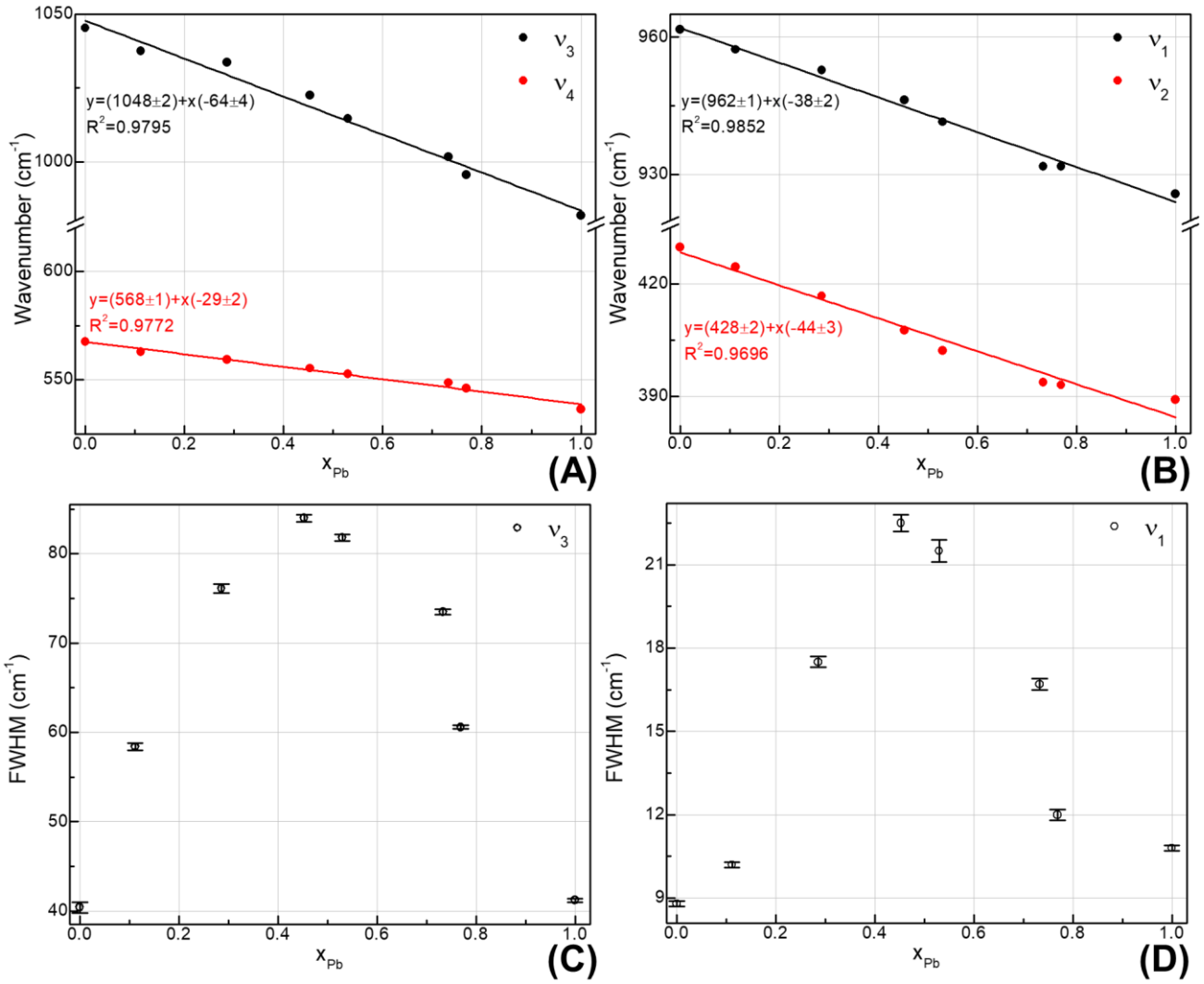

Figure 3.61 Plots of the frequencies of (A) $\nu_3(PO_4^{3-})$ (black) and $\nu_4(PO_4^{3-})$ (red) IR modes and (B) $\nu_1(PO_4^{3-})$ (black) and $\nu_2(PO_4^{3-})$ (red) Raman modes versus the lead content obtained via Rietveld refinement of XRPD patterns and corresponding results of the linear fit. Plots of the full width at half maximum (FWHM) values of (C) $\nu_3(PO_4^{3-})$ and (D) $\nu_1(PO_4^{3-})$ bands versus the amount of lead.

To evaluate the effects of excitation wavelength on the efficiency of Raman scattering of HA, $PbHA_x$, and HPy compounds, μ-Raman measurements were also performed at 488 and 514 nm. As illustrated in Figure 3.12, compounds are still distinguishable based on the position of the most intense modes ν_1 and ν_2, but spectra are generally affected by a higher fluorescence background. Such result makes 785.0 nm excitation as the most appropriate wavelength for the Raman detection and discrimination of $PbHA_x$ compounds.

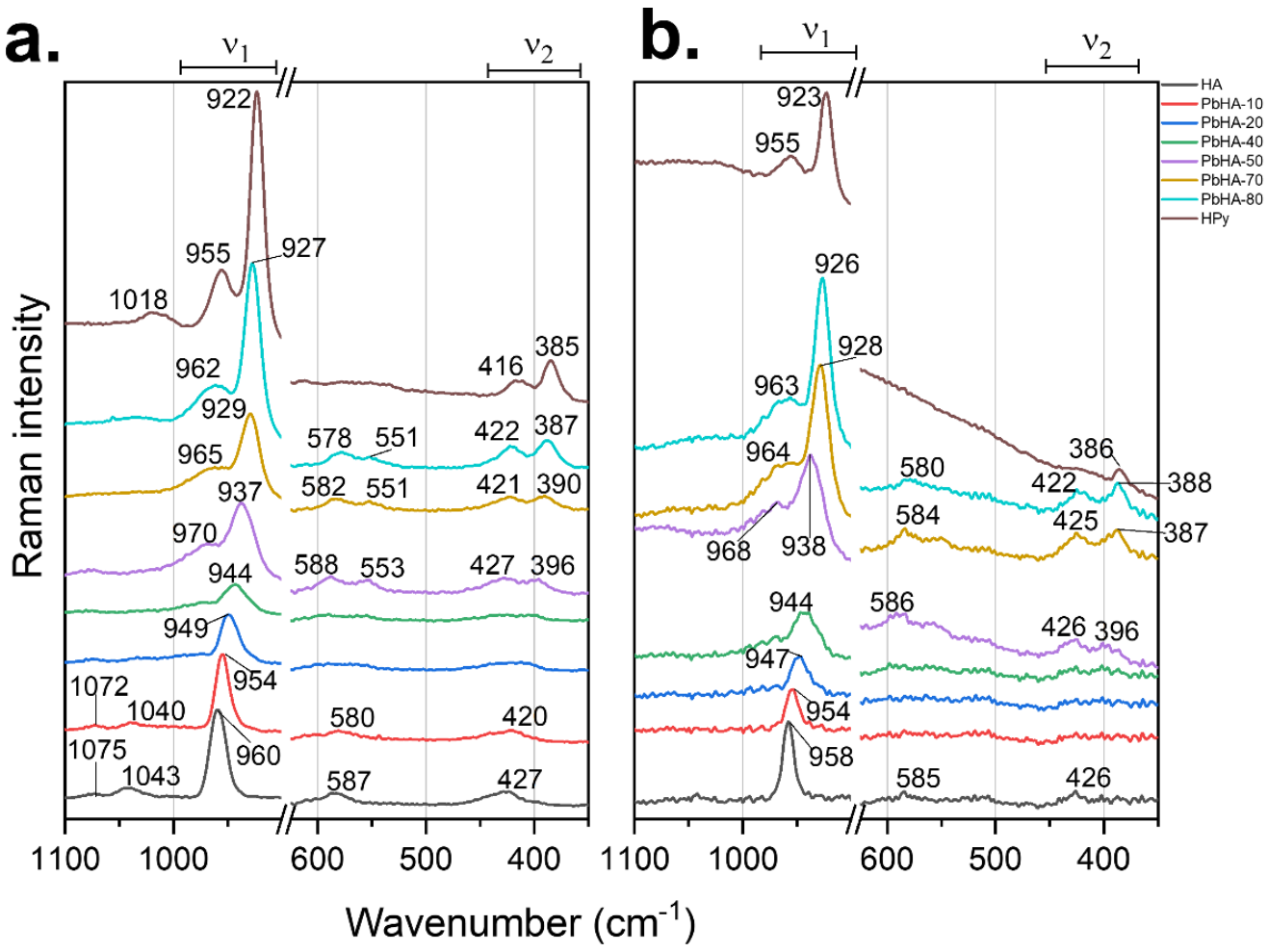

Figure 3.12 μ-Raman spectra recorded with t excitation λ at 488 nm (a.) and 514 nm (b.) of HA, $PbHA_x$ solid solutions and HPy powders.

3.2 Non-invasive characterisation of $PbHA_x$ paint mock-ups by vibrational spectroscopies

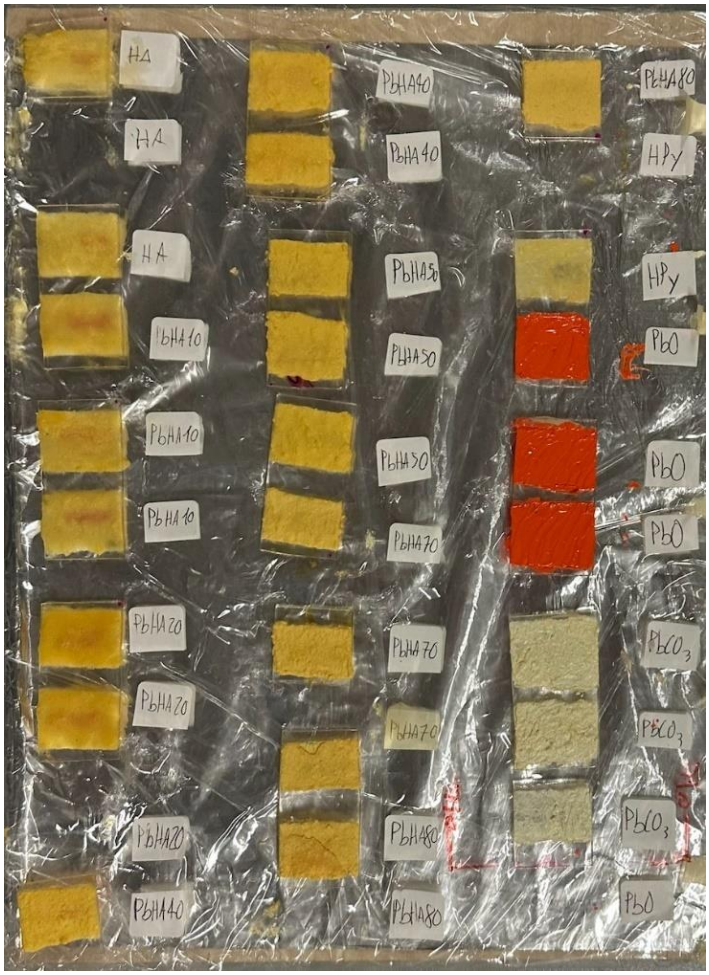

Figure 3.13 Photographs of HA, $PbHA_x$ and HPy paint mock-ups.

To establish whether it is possible to detect differences among $(Pb_xCa_{1-x})_5(PO_4)_3OH$ compounds on historical cultural heritage painted objects non-invasively, arabic gum and linseed oil paint mock-ups (Figure 3.13) were also examined by reflection near-/mid-FT-IR and Raman spectroscopy. Since it is known that lasers may induce damages to the paint surfaces during measurements [31,32], Raman tests were performed in advance to find the safest condition of analysis.

Reflection mode spectra in the near infrared (NIR) 7200–6500 cm^{-1} range are shown in Figure 3.14A. The strong feature located in this range is due to the first overtones of the fundamental hydroxyl stretching modes [2ν(OH)] [33], observed in the mid- IR region of the powders spectra at 3566-3555 cm^{-1} (Figure 3.9A).

For both arabic gum and oil paint mock-ups, the band shift remains within the uncertain of the spectral resolution (i.e., 6 cm^{-1}) from HA (6973 cm^{-1}) to PbHA-50 (6979 cm^{-1}), while it becomes

significant for X_{Pb}>0.5, undergoing a progressive red-shift up to about 20 cm^{-1} for HPy (6954 cm^{-1}). A decrease of the intensity and a broadening of the 2ν(OH) mode is observed going from HA to PbHA-50; for X_{Pb}>0.5 an opposite trend is instead detected. It is important to note that for the arabic gum mock-ups, the 2ν(OH) band is not visible in PbHA-40 and PbHA-50 samples due to the contribution of a binder band (*cf.* light grey line in Figure 3.14A). This leads to conclude that the accurate discrimination among different $(Pb_xCa_{1-x})_5(PO_4)_3OH$ compounds based on the 2ν(OH) band position depends on the nature of the binder and its NIR spectral properties [34,35], becoming more difficult in the presence of arabic gum rather than linseed oil.

Reflection mode mid-FTIR spectra of all paint mock-ups (Figure 3.14B) show the presence of spectral distortions, with significant changes occurring in the maximum position, shape, and relative intensity of bands. These modifications are related to the properties of the paint, both in terms of surface morphology and intrinsic infrared optical and reflection physical processes [36]. Notably, the most intense $\nu_3(PO_4^{3-})$ modes are inverted by the Reststrahlen effect, while the weaker $\nu_4(PO_4^{3-})$ bands, amplified by the volume diffusion effect, show a derivative shape. Despite these distortions, a consistent similarity with transmission mode mid-FTIR results is present (*cf.* Figure 3.9A): the progressive shift towards lower energy is still observable in the minima and inflexions points of $\nu_3/\nu_4(PO_4^{3-})$ peaks with increasing Pb amount, thus allowing a reliable distinction among different $(Pb_xCa_{1-x})_5(PO_4)_3OH$ materials to be performed. The minor visible differences in the band-shape and relative intensity of $\nu_3(PO_4^{3-})$ modes of the spectra recorded from oil and gum paint mock-ups are ascribable to the variable contribution of the two different binding media in this spectral region [37].

As done for FT-IR spectroscopy, data from paint mock-ups were collected by a portable Raman spectrometer suitable for *in-situ* analyses (Figure 3.14C). Concerning the equivalent spectra recorded from powders with the bench-top instrument (Figure 3.9B), the high fluorescence background due to the presence of the binding medium (even more significant for oil paint mock-ups) makes difficult, sometimes impossible, the detection of ν_2 and $\nu_4(PO_4^{3-})$ modes. Nevertheless, analogous systematic differences to those of powders can be observed in the position of the $\nu_1(PO_4^{3})$ band as a function of the Pb content. It follows that this signal can be used as a reliable marker for the non-invasive discrimination of different $(Pb_xCa_{1-x})_5(PO_4)_3OH$ compounds and their lead content in cultural heritage objects. Regarding measurements performed at 532 nm, Raman signals were all completely masked by a strong fluorescence background, therefore indicating again 785 nm excitation as the most appropriate wavelength for the non-invasive Raman detection and discrimination of $(Pb_xCa_{1-x})_5(PO_4)_3OH$ compounds in historical artworks.

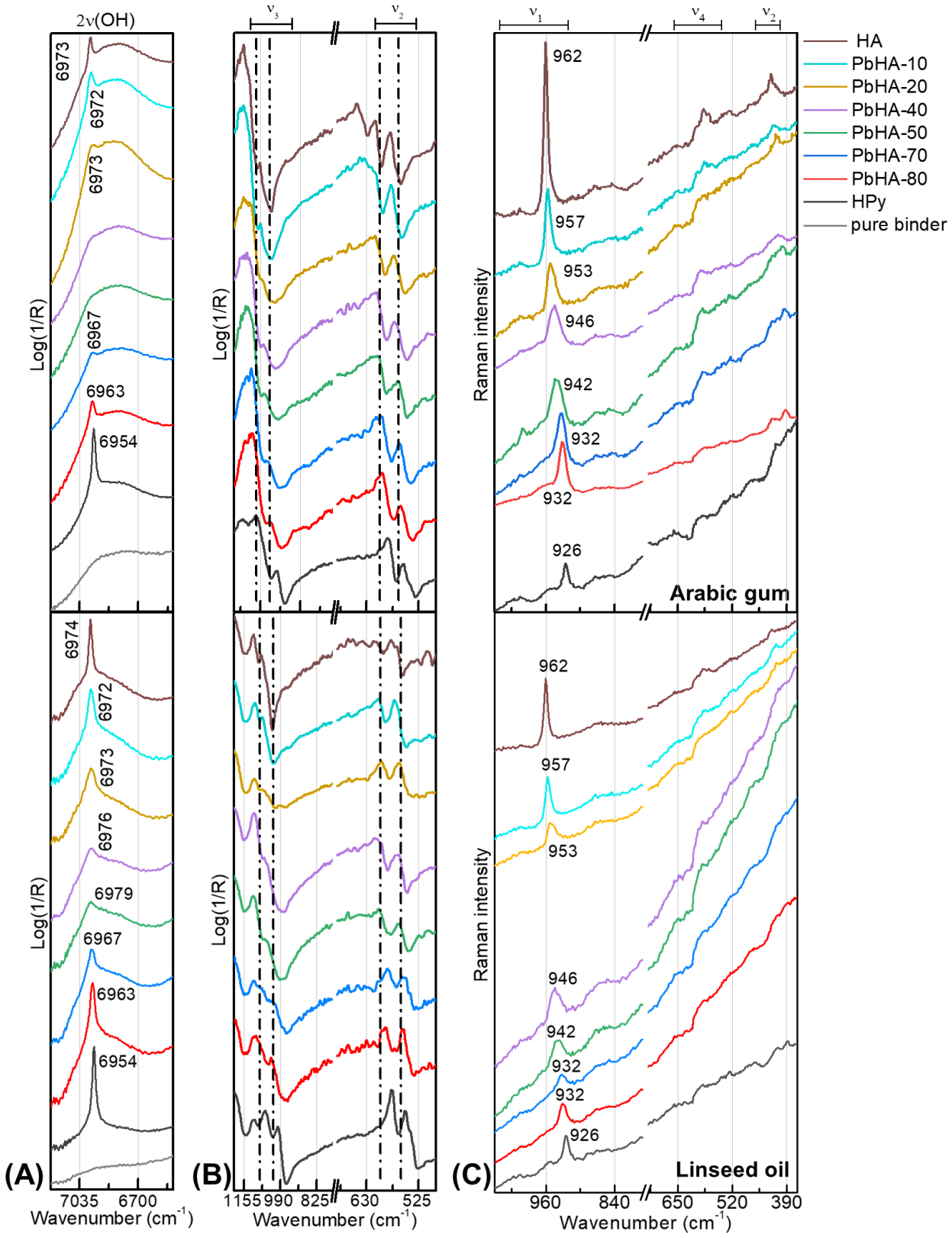

Figure 3.74 Non-invasive vibrational spectroscopy analysis of HA, PbHAx solid solutions and HPy arabic gum (top) and linseed oil (bottom) paint mock-ups: (A) reflection mode near FT-IR spectra, (B) reflection mode mid FT-IR spectra and (C) μ-Raman spectra (λ_{exc}=785.0 nm).

Before performing Raman measurements to historical objects, tests on mock-up samples are usually required for finding the safest conditions of analysis that allow avoiding any laser-induced damage to the sample. To this aim, a series of laser damage tests were performed on selected $PbHA_x$ oil and arabic gum paint mock-ups, namely: HA, PbHA-50, and HPy. Samples were left under the maximum power of both lasers (257 mW for the 785 nm laser, and 40 mW for the 532 nm laser) for 1 hour. To assess the presence of any damage, visual examinations of the paint surface were carried out using the optical camera of the Raman microscope, before and after laser exposure; potential changes on the spectra were instead evaluated by comparing the spectral profile collected at the maximum power of the laser after one hour of exposure and the one recorded at the minimum laser power (6.89 mW for 785 nm laser, and 10 mW for 532 nm laser), for 1s, and 3 accumulations.

As an example, Figure 3.15 shows the 785 nm laser damage tests obtained from the HA, PbHA-50, and HPy arabic paint mock-ups. No visible damages were observed at the paint surface of all samples under the optical microscope. In line with the visual observation, no changes have occurred in the spectra before and after prolonged exposure to laser. Comparable results were obtained for the tests carried out at 532 nm and for the oil paint mock-ups, even if Raman spectra were dominated by a strong fluorescence background.

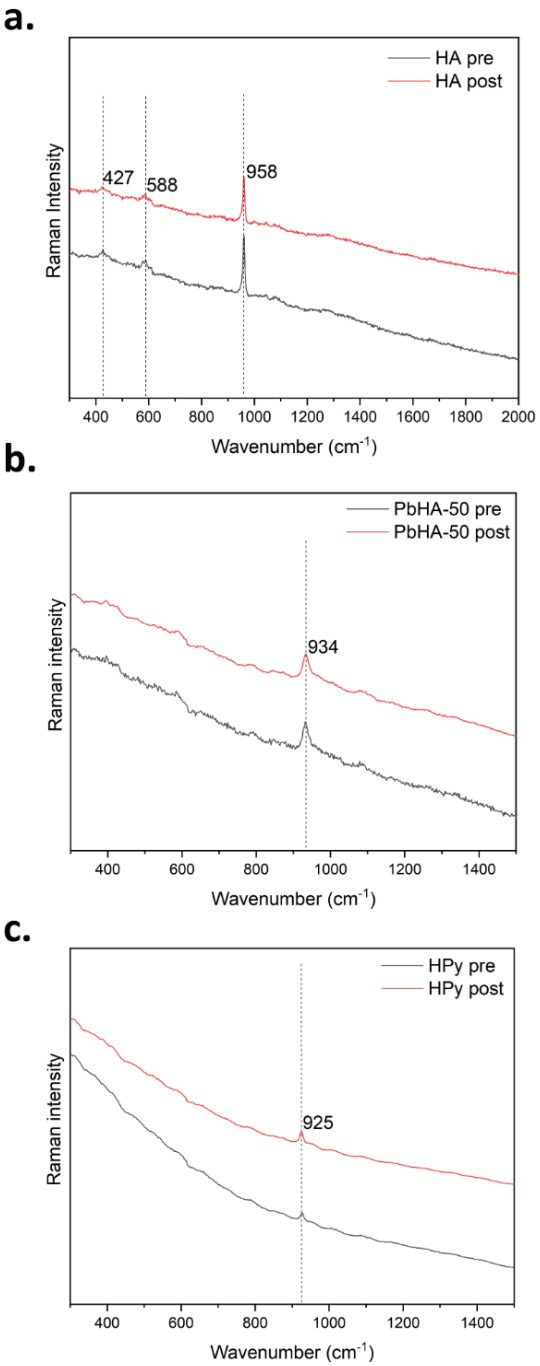

Figure 3.15 Raman spectra collected after 3 s (black) and 1 hour (red) of 785 nm laser exposure from (a) HA, (b) PbHA-50, and (c) HPy arabic gum paint mock-ups.

Based on the obtained results, it is possible to conclude that under the employed conditions, Raman measurements did not induce any damage

Nevertheless, since working on historical artworks at high laser power is not advisable, the experimental conditions of analysis were optimised by finding the following compromise in terms of lower power value, number of accumulations, and time exposure: 25 mW power, 1-15 accumulations, and 1-10 s time exposure.

3.3 Dataset application

3.3.1 Description of the historical painting

The characterization of powders and paint mock-ups allow us to create a solid database that can be helpful for the recognition of $(Pb_xCa_{1-x})_5(PO_4)_3OH$ with variable Pb content in a more heterogeneous and complex system, such as cultural heritage objects/samples.

The knowledge acquired from powders and paint mock-ups was therefore exploited to obtain a detailed characterization of the historical sample NJH-18 taken from a Roman fresco (I century CE) located in Nijmegen (Netherlands). The paint fragment was embedded in polyester and polished as a cross-section for standard observation with optical microscopy. For the µXRD analyses, a 20 µm thin section was prepared, using a microtome, slicing one of the sides of the cross-section and collecting the section on a piece of tape. The complete protocol is described in previous literature [38] .

3.3.2 Analytical results obtained on a fragment from the historical painting

As shown in Figures 3.16 and 3.17, the paint fragment is mainly composed of an orange-brown layer, mainly composed of P, Ca, Pb and Cl, and with a Ca-rich layer below the Pb layer, and a Fe-rich layer above (in Figures 3.16 P and Ca XRF maps are reported). Points of interest (POIs) were selected in both the P-rich and the Ca-rich layers for the acquisition of P K- and Ca K-edges µ-XANES spectra. Combining µ-XRF and µ-XANES spectroscopy revealed the presence of at least 2 major phases of Ca and phosphate containing compounds (Figure 3.16A). The PCA analysis of the series of synthesized Pb/Ca phosphates, shows a linear gradient (both in transmission and fluorescence, even with high self-absorption), The PCA analysis of the µ-XANES spectra acquired on the paint fragment shows that group 1 of compounds located in the interior of the section corresponds to Pb/Ca phosphates (Figure 3.16B). The fact that both P K- and Ca K-edges µ-XANES spectra were affected by self-absorption prevents us to confidently quantify the Pb substitution in the thin section [10]. However, by combining both Ca and P K-edges µ-XANES spectroscopy results we can confidently conclude that the Pb:Ca stoichiometry must be larger than 0.5 in the average group 1 spectra (Figure 3.16C). The group 2 Ca K-edge XANES spectra were found in the edge of the thin section (Figure 3.16A) and possibly corresponds to $CaCO_3$ compounds and different lead-calcium phosphate based phases. We do not discard that other phosphate compounds could be representative of the group 2 spectra as well, such as Cl containing phosphates.

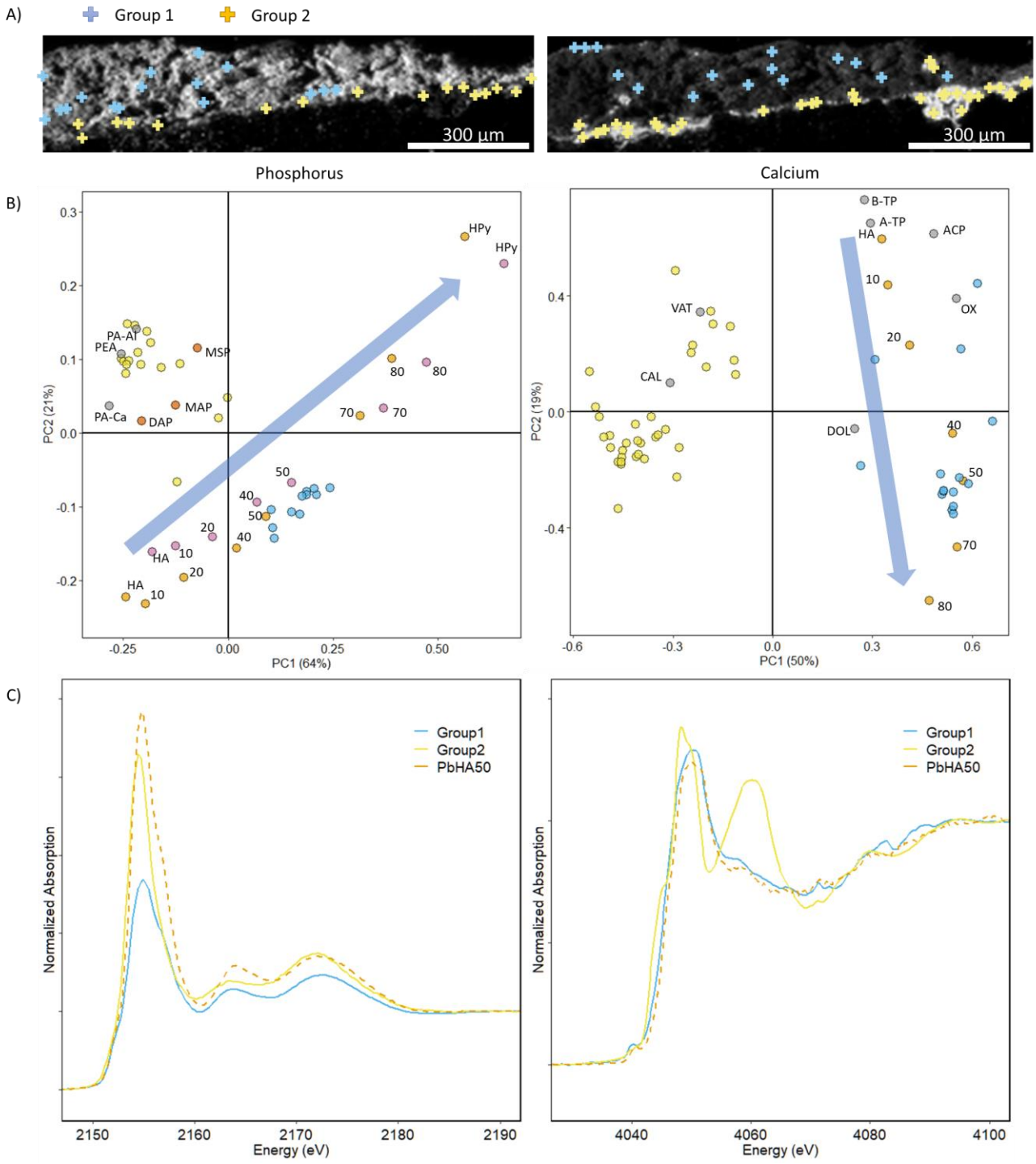

Figure 3.16 (A) µXRF map (left: Phosphorus, right: Calcium) and µXANES spectroscopy measurements (crosses) of thin section NJH-18. (B) PCA analysis at the P K-edge (left) and Ca K-edge (right) showcasing the distribution of the $PbHA_x$ compounds measured in transmission (for P K-edge XANES spectroscopy) and fluorescence (Ca and P K-edge XANES spectroscopy), the two distinct groups of XANES spectra in the thin section, and selected standards (HA: Hydroxyapatite, HPy: hydroxyyromorphite, MSP: Monosodium phosphate, MAP: Monoammonium phosphate, DAP: Diammonium phosphate, PA-Ca: Phytic acid Ca-salt, PA-Al: Phytic acid Al-salt, PEA: Phosphoethanolammine, CAL: Calcite, VAT: Vaterite, DOL: Dolomite, B-TP, Beta-tricalcium phosphate, A-TP: Alfa Tricalcium phosphate, ACP: Amorphous calcium phosphate, OX: Calcium oxalate). The direction of the arrow indicates an increasing Pb:Ca ratio in the standards. (C) Average XANES spectra of the PCA group 1 and 2 and the in house-synthesised compound PbHA-50.

In the more whitish Pb-P-Ca rich areas of the thin section, ID13 µ-XRD investigations confirmed the presence of calcite in the ground layer. The average pattern in the brown layer is characteristic of a lead-calcium phosphate compound (Figure 3.17; with its relative amount that gradually increases from the green, to the orange, to the red areas). The refinement of XRD peak positions gave the following unit cell: a = 9.817(1) Å, c = 7.176(1) Å. With the help of the linear regressions reported in Figure 3.4A these parameters would give a value of X_{Pb}, of 0.84 and 0.62, respectively. This apparent inconsistency can possibly be explained by the fact that the lead calcium phosphate may contain a mixture of hydroxide and chloride anions. An attempt to refine the Ca/Pb site occupancy factors provided a refined X_{Pb} value similar to that obtained from the linear regressions described above, while from peak profile parameters it was possible to estimate an average crystallite size of about 100 nm and a microstrain of 1.9 %.

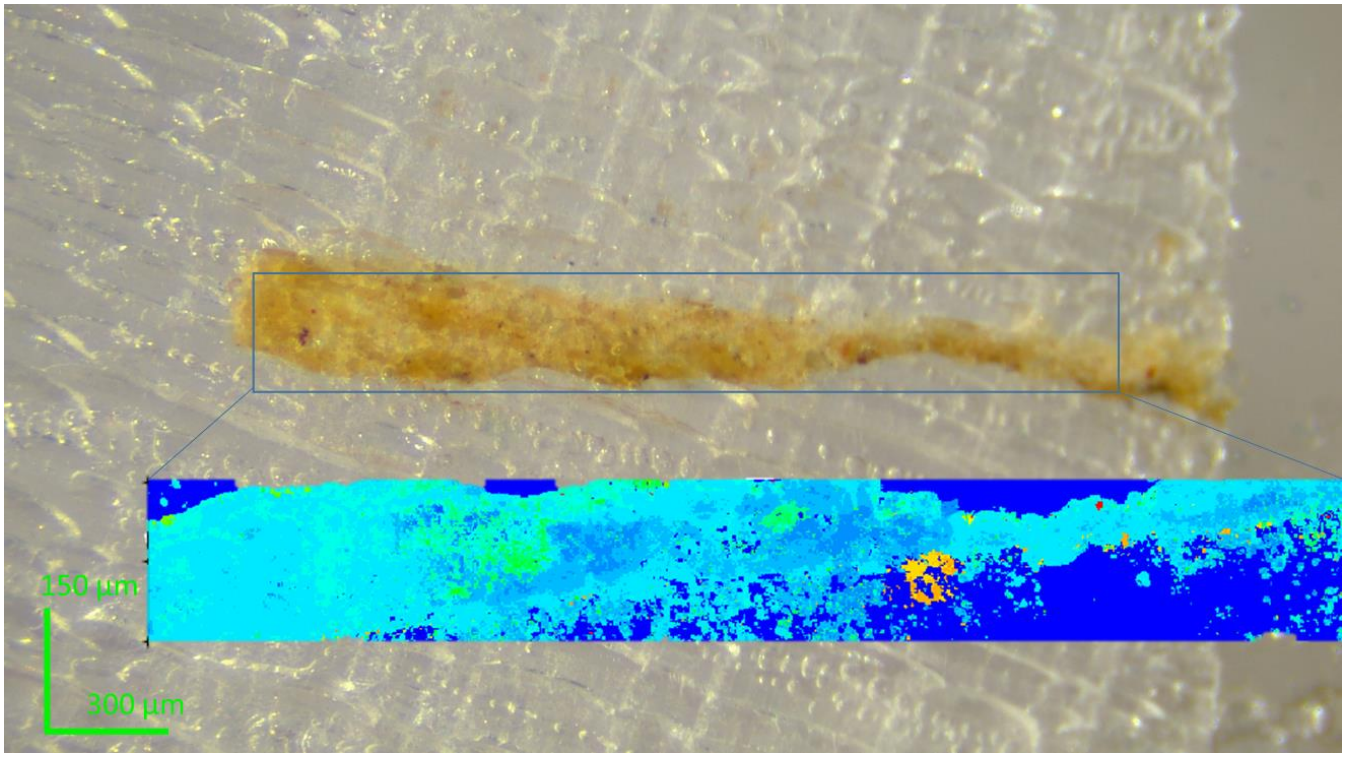

Figure 3.17 µXRD mapping of NJH-18 thin section showing the distribution of $(Pb_xCa_{1-x})_5(PO_4)_3OH$ (with $0.6<X_{Pb}<0.85$) (map size 90×1500 µm², pixel size 2 µm). The color grading goes from blue (absence of the ROI peak at ~18.7° 2θ) to red (maximum intensity of the ROI peak at ~18.7° 2θ).

In line with X-ray analysis, µ-FTIR mapping and single point µ-Raman measurements reveal the widespread presence of possible $(Pb_xCa_{1-x})_5(PO_4)_3OH$ solid solution having spectral features very close to that of the reference powder compound PbHA-70 [Figure 3.18; pts. 02_{IR} and 04_{Rm} – $\nu_1(PO_4^{3-})$ at 932 cm^{-1}]. In the whitish-reddish sample regions where also Fe was identified, a mixture of hematite (pt. 03_{Rm} - signals at 615, 414, 295 and 228 cm^{-1}) with variable abundances of a possible $PbHA_x$ compound (PbHA-70) and $CaCO_3$ was identified by Raman and µ-XRD. The latter analysis also showed the presence of a minor amount of quartz in these areas. Ca-rich grains mainly

composed of $CaCO_3$ (Figure 3.18, pts. 01_{IR} and 01_{Rm} - peaks at 1083 and 279 cm^{-1}) along with a few crystals of lead white (pt. 02_{Rm}, band at 1055 cm^{-1}) were found distributed within the stratigraphy of the sample.

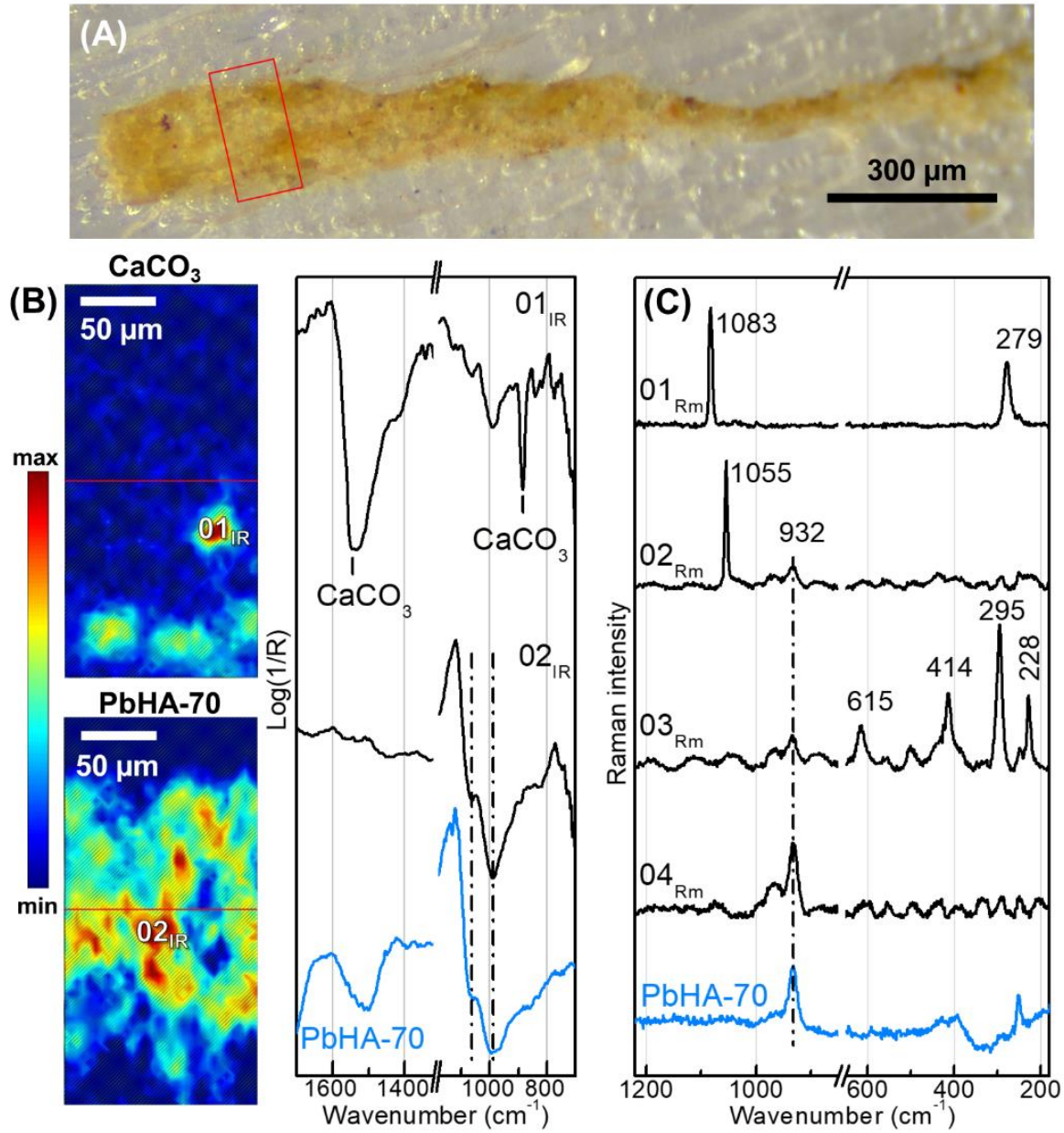

Figure 3.18 Vibrational spectroscopy measurements of thin section NJH-18: (A) Micrograph showing the region analysed by µ-FT-IR mapping and in blue the PbHA-70 powder reference; (B) µ-FT-IR distribution maps of $CaCO_3$ and $PbHA_x$ (left) with selection of the corresponding reflection mode FT-IR spectra extracted from the areas indicated in the maps (right); (C) µ-Raman spectra recorded from selected white and white-red spots, in blue the PbHA-70 powder reference.

Even if a phase compatible with PbHA-70 was identified on the historical NJH-18 sample, further investigations are required to verify the presence or not of chlorine-apatite phases. Cl was indeed detected by µ-XRF mapping, thus, at the moment, we cannot excludes the presence of this phase on the sample.

Overall, the applied multi-technique and multi-scale approach allows a comprehensive study and identification of $PbHA_x$ compounds, even in a more complex historical sample.

In particular, μ-XRD provide a precise phase determination, even in complex mixture, and the possibility to have a micro beam. On the other hand, it needs to be considered and evaluated the quality of patterns with portable instruments that are generally affected by a lower resolution.

P K- and Ca K-edges μ-XANES offers a high sensitivity in XRF mode (even if P is not the main element), by giving the possibility to detect both crystalline and amorphous phases, and to work with a sub-micrometric beam. Its main limitations rely on the fact that the technique is not able to make an accurate discrimination of different lead-calcium phosphate compounds on the basis of lead content. This might become even a more challenge aspect when also other P and/or Ca-containing phases are present in the analyzed sample.

Similarly to XRPD, vibrational spectroscopies allows of distinguishing $PbHA_x$ compounds with different lead content, both with bench-top and portable instrumentations.. On the contrary, FT-IR in reflectance mode is affected by spectral distortion and Raman may be affected by fluorescence and potential damages induced by the laser

REFERENCES

[1] Y. Zhu, B. Huang, Z. Zhu, H. Liu, Y. Huang, X. Zhao, M. Liang, Characterization, dissolution and solubility of the hydroxypyromorphite-hydroxyapatite solid solution [$(Pb_xCa_{1-x})_5(PO_4)_3OH$] at 25 °C and pH 2-9, Geochem Trans. 17 (2016) 1–18. https://doi.org/10.1186/s12932-016-0034-8.

[2] R.M. Wilson, J.C. Elliott, S.E.P. Dowker, Rietveld refinement of the crystallographic structure of human dental enamel apatites, 1999.

[3] M. Andres-Verges, F.J. Higes-Rolando, P.F. Gonzalez-Diaz, Infrared spectra of calcium-strontium phosphate apatites, J Solid State Chem. 43 (1982) 237–243. https://doi.org/https://doi.org/10.1016/0022-4596(82)90235-3.

[4] A. Bigi, A. Ripamonti, S. Brückner, M. Gazzano, N. Roveri, S.A. Thomas, Structure refinements of lead-substituted calcium hydroxyapatite by X-ray powder fitting, Acta Crystallographica Section B. 45 (1989) 247–251. https://doi.org/10.1107/S0108768189001928.

[5] M. Andres-Verges, F.J. Higes-Rolando, C. Valenzuela-Calahorro, P.F. Gonzalez-Diaz, On the structure of calcium-lead phosphate apatites, Spectrochim Acta A. 39 (1983) 1077–1082. https://doi.org/10.1016/0584-8539(83)80128-7.

[6] Hata M, Marumo F, Iwai S-I, Aoki H, Structure of a lead Apatite $Pb_9(PO_4)_6$, Acta Crystallographica Section B. B36 (1980) 2128–2130.

[7] R.D. Shannon, Revised Effective Ionic Radii and Systematic Studies of Interatomie Distances in Halides and Chaleogenides, 1976.

[8] J.D. Hopwood, G.R. Derrick, D.R. Brown, C.D. Newman, J. Haley, R. Kershaw, M. Collinge, The identification and synthesis of lead apatite minerals formed in lead water pipes, J Chem. 2016 (2016). https://doi.org/10.1155/2016/9074062.

[9] E.D. Ingall, J.A. Brandes, J.M. Diaz, M.D. de Jonge, D. Paterson, I. McNulty, W.C. Elliott, P. Northrup, Phosphorus K-edge XANES spectroscopy of mineral standards, J Synchrotron Radiat. 18 (2011) 189–197. https://doi.org/10.1107/S0909049510045322.

[10] L.C.C. Hurtarte, L.F. Souza-Filho, W.O. Santos, L. Vergütz, J. Prietzel, D. Hesterberg, Optimization of data processing minimizes impact of self-absorption on phosphorus speciation results by P K-edge XANES, Soil Syst. 3 (2019) 1–13. https://doi.org/10.3390/soilsystems3030061.

[11] V. Martin-Diaconescu, M. Gennari, B. Gerey, E. Tsui, J. Kanady, R. Tran, J. Pécaut, D. Maganas, V. Krewald, E. Gouré, C. Duboc, J. Yano, T. Agapie, M.N. Collomb, S. Debeer, Ca K-edge XAS as a probe of calcium centers in complex systems, Inorg Chem. 54 (2015) 1283–1292. https://doi.org/10.1021/ic501991e.

[12] A. Manceau, M. Merkulova, O. Mathon, P. Glatzel, M. Murdzek, V. Batanova, A. Simionovici, S.N. Steinmann, D. Paktunc, The Mode of Incorporation of As(-I) and Se(-I) in Natural Pyrite Revisited, ACS Earth Space Chem. 4 (2020) 379–390. https://doi.org/10.1021/acsearthspacechem.9b00301.

[13] Z. Mathe, O. McCubbin Stepanic, S. Peredkov, S. DeBeer, Phosphorus Kβ X-ray emission spectroscopy detects non-covalent interactions of phosphate biomoleculesin situ, Chem Sci. 12 (2021) 7888–7901. https://doi.org/10.1039/d1sc01266e.

[14] W.E. Klee, G. Engel, I.R. spectra of the phosphate ions in various apatites, Journal of Inorganic and Nuclear Chemistry. 32 (1970) 1837–1843. https://doi.org/10.1016/0022-1902(70)80590-5.

[15] S.J. Gadaleta, R. Mendelsohn, E.L. Paschalis, N.P. Camacho, F. Betts, A.L. Boskey, Fourier Transform Infrared Spectroscopy of Synthetic and Biological Apatites, Inorg Chem. 13 (1974) 194–207. https://doi.org/10.1007/978-1-4899-1400-2_23.

[16] B. Fowler, Infrared studied apatites I. Vibrational assignment for calcium, strontium and barium Hydroxyapatites utilizing isotopic substitution, 13 (1974) 194–207.

[17] H. Tsuda, J. Arends, Raman spectra of human dental calculus., J Dent Res. 72 (1993) 1609–1613. https://doi.org/10.1177/00220345930720121401.

[18] G.R. Sauer, W.B. Zunic, J.R. Durig, R.E. Wuthier, Fourier transform raman spectroscopy of synthetic and biological calcium phosphates, Calcif Tissue Int. 54 (1994) 414–420. https://doi.org/10.1007/BF00305529.

[19] W.P. Griffith, Raman studies on rock-forming minerals. Part II. Minerals containing MO_3, MO_4, and MO_6 groups, Journal of the Chemical Society A: Inorganic, Physical, Theoretical. (1970) 286–291.

[20] P.N. de Aza, C. Santos, A. Pazo, S. de Aza, R. Cuscó, L. Artús, Vibrational Properties of Calcium Phosphate Compounds. 1. Raman Spectrum of β-Tricalcium Phosphate, Chemistry of Materials. 9 (1997) 912–915. https://doi.org/10.1021/cm960425d.

[21] S. Koutsopoulos, Synthesis and characterization of hydroxyapatite crystals: A review study on the analytical methods, J Biomed Mater Res. 62 (2002) 600–612. https://doi.org/10.1002/jbm.10280.

[22] S.J. Joris, C.H. Amberg, The nature of deficiency in nonstoichiometric hydroxyapatites. I. Catalytic activity of calcium and strontium hydroxyapatites, Journal of Physical Chemistry. 75 (1971) 3167–3171. https://doi.org/10.1021/j100689a024.

[23] J.M. Stutman, J.D. Termine, A.S. Posner, Vibrational Spectra and Structure of the Phosphate Ion in Some Calcium Phosphates., Trans N Y Acad Sci. 27 (1965) 669–675. https://doi.org/10.1111/j.2164-0947.1965.tb02224.x.

[24] J. Arends, J. Christoffersen, M.R. Christoffersen, H. Eckert, B.O. Fowler, J.C. Heughebaert, G.H. Nancollas, J.P. Yesinowski, S.J. Zawacki, A calcium hydroxyapatite precipitated from an aqueous solution. An international multimethod analysis, J Cryst Growth. 84 (1987) 515–532. https://doi.org/10.1016/0022-0248(87)90284-3.

[25] D.C. O'Shea, M.L. Bartlett, R.A. Young, Compositional analysis of apatites with Laser-Raman spectroscopy: (OH,F,Cl)apatites, Arch Oral Biol. 19 (1974) 995–1006. https://doi.org/https://doi.org/10.1016/0003-9969(74)90086-7.

[26] C.B. Baddiel, E.E. Berry, Spectra structure correlations in hydroxy and fluorapatite, Spectrochimica Acta. 22 (1966) 1407–1416. https://doi.org/10.1016/0371-1951(66)80133-9.

[27] H. Liu, X. Cui, X. Lu, X. Liu, L. Zhang, T.S. Chan, Mechanism of Mn incorporation into hydroxyapatite: Insights from SR-XRD, Raman, XAS, and DFT calculation, Chem Geol. 579 (2021) 120354. https://doi.org/10.1016/j.chemgeo.2021.120354.

[28] A. Bigi, E. Boanini, C. Capuccini, M. Gazzano, Strontium-substituted hydroxyapatite nanocrystals, Inorganica Chim Acta. 360 (2007) 1009–1016. https://doi.org/10.1016/j.ica.2006.07.074.

[29] Y. Jiang, Z. Yuan, J. Huang, Substituted hydroxyapatite: a recent development, Materials Technology. 35 (2020) 785–796. https://doi.org/10.1080/10667857.2019.1664096.

[30] M. Li, X. Xiao, R. Liu, C. Chen, L. Huang, Structural characterization of zinc-substituted hydroxyapatite prepared by hydrothermal method, J Mater Sci Mater Med. 19 (2008) 797–803. https://doi.org/10.1007/s10856-007-3213-4.

[31] L. Bertrand, S. Schöeder, D. Anglos, M.B.H. Breese, K. Janssens, M. Moini, A. Simon, Mitigation strategies for radiation damage in the analysis of ancient materials, TrAC - Trends in Analytical Chemistry. 66 (2015) 128–145. https://doi.org/10.1016/j.trac.2014.10.005.

[32] L. Monico, K. Janssens, E. Hendriks, B.G. Brunetti, C. Miliani, Raman study of different crystalline forms of $PbCrO_4$ and $PbCr_{1-x}S_xO_4$ solid solutions for the noninvasive identification of Chrome yellows in paintings: A focus on works by vincent van Gogh, Journal of Raman Spectroscopy. 45 (2014) 1034–1045. https://doi.org/10.1002/jrs.4548.

[33] B.J. Reddy, R.L. Frost, S.J. Palmer, A near-infrared spectroscopic study of the phosphate mineral pyromorphite $Pb_5(PO_4)_3Cl$, Spectrochim Acta A Mol Biomol Spectrosc. 71 (2008) 430–435. https://doi.org/10.1016/j.saa.2007.12.030.

[34] M. Vagnini, C. Miliani, L. Cartechini, P. Rocchi, B.G. Brunetti, A. Sgamellotti, FT-NIR spectroscopy for non-invasive identification of natural polymers and resins in easel paintings, in: Anal Bioanal Chem, 2009: pp. 2107–2118. https://doi.org/10.1007/s00216-009-3145-6.

[35] F. Rosi, A. Daveri, P. Moretti, B.G. Brunetti, C. Miliani, Interpretation of mid and near-infrared reflection properties of synthetic polymer paints for the non-invasive assessment of binding media in twentieth-century pictorial artworks, Microchemical Journal. 124 (2016) 898–908. https://doi.org/10.1016/j.microc.2015.08.019.

[36] F. Rosi, L. Cartechini, D. Sali, C. Miliani, Recent trends in the application of fourier transform infrared (FT-IR) spectroscopy in Heritage Science: From micro: From non-invasive FT-IR, Physical Sciences Reviews. 4 (2019). https://doi.org/10.1515/psr-2018-0006.

[37] C. Invernizzi, T. Rovetta, M. Licchelli, M. Malagodi, Mid and near-infrared reflection spectral database of natural organic materials in the cultural heritage field, Int J Anal Chem. 2018 (2018). https://doi.org/10.1155/2018/7823248.

[38] V. Gonzalez, G. Wallez, T. Calligaro, M. Cotte, W. de Nolf, M. Eveno, E. Ravaud, M. Menu, Synchrotron-Based High Angle Resolution and High Lateral Resolution X-ray Diffraction: Revealing Lead White Pigment Qualities in Old Masters Paintings, Anal Chem. 89 (2017) 13203–13211. https://doi.org/10.1021/acs.analchem.7b02949.

CHAPTER 4

SCIENTIFIC DISSEMINATION and COMMUNICATION

4.1 Design and planning

In this chapter, it is crucial to recall the difference between dissemination, that is focused on spreading knowledge and results to enable their use by third parties (such as other researchers, industries, etc…,), and communication, which aim is to reach out to society, by informing and promoting the project and its results (for further details see Chapter 1, par. 1.2.4).

Traditionally, the scientific community was mainly focused on scientific dissemination with peer-to-peer interactions between researchers and the community of experts (peer-reviewed publications or congresses participation, etc..,). In recent years, the scientific community has placed an emphasis on good practice in research projects, particularly in communication. Even if this aspect still needs improvements, there are many ways in which the scientific community meets society starting from more traditional channels, such as science museums, books, and internet, to more innovative forms including science festivals, art exhibitions, performing arts, and the production of specific games with scientific content (boards or video games).

During this PhD thesis, dissemination was carried out *via* congress presentations, peer-reviewed papers (one published paper[1] , and one manuscript in preparation), and the thesis itself.
Nevertheless, the present Chapter is also centred on scientific communication for a non-specialist audience with an uncommon format, trying to highlight its relevance since this aspect of research is not still considered as it should be.

As previously described (Chapter 1, par. 1.2), scientific communication helps to carry a piece of knowledge from the researchers to an audience. It can be done through many different formats (text,

[1] Cotte, M.; Gonzalez, V.; Vanmeert, F.; Monico, L.; Dejoie, C.; Burghammer, M.; Huder, L.; de Nolf, W.; Fisher, S.; Fazlic, I.; Chauffeton, C.; Wallez, G.; Jiménez, N.; Albert-Tortosa, F.; Salvadó, N.; Possenti, E.; Colombo, C.; Ghirardello, M.; Comelli, D.; Avranovich Clerici, E.; Vivani, R.; Romani, A.; Costantino, C.; Janssens, K.; Taniguchi, Y.; McCarthy, J.; Reichert, H.; Susini, J. The "Historical Materials BAG": A New Facilitated Access to Synchrotron X-ray Diffraction Analyses for Cultural Heritage Materials at the European Synchrotron Radiation Facility. *Molecules* **2022**, *27*, 1997. https://doi.org/10.3390/molecules27061997

audio content, video content, live performance as Science theatre, etc...,) and in many different media (periodicals, blog articles, podcasts/radio, television, social media, etc...,).
Therefore, to assess people's interest in Heritage Science content and identify which kind of content they prefer most, in a first step, a submitted panel of persons were invited to fill in a survey.

4.1.1 Survey structure and results

The survey was mainly divided into the following three different sections:

1. The first section was focused on understanding if people are interested in scientific contents and how they interact with them;
2. The second section was focused on public knowledge about Heritage Science and its communication. Based on the view of a short Heritage Science communicative video (roughly 2 min) the public replies to a series of questions with a rank between 1 and 5 (1= not at all, 5= absolutely positive) on whether or not they knew the existence of Heritage Science as a field of study, if they ever viewed similar content before, and about their interest on learning or deepening their knowledge on Heritage Science topics, especially through video contents;
3. The third section was centred on audience profiling.

The survey reached a population of 266 people; the sampling was done within 2 degrees of separation from the author (author's socials contacts and their contacts) and the author tried to not involve many experts on Heritage Science, which could unbalance the results. The survey was completed in Italian to reach the largest possible crowd (Italian people are not famous for their knowledge on English language, unfortunately), so it can be applied to an Italian (or Italian speaker) setting but not directly shifted on a global scale. These pieces of information do not allow the survey statistically to be considered relevant because the sampling was not conducted randomly and may have been small. Even considering the survey limitation, it represents a relevant part of the public and has proven to be an excellent tool for analysing public interest and habits.

The survey in its entirety can be found at this link. However, for convenience, all the questions present in the survey are also reported in Table 4.1.

Table 4.1 summary of the survey, divided by questions and different types of replies.

Section	Questions	Type of reply
1	Are you interested in scientific communication content?	Multiple choice question (yes, no, it depends)
	Which media do you prefer to enjoy popular science content?	Multi select multi choice question (journals, blog and website, social media, radio/podcast)
	Are you subscribed/do you follow at any of the following science channels?	Multi select multi choice question (journal, newsletter, following research institutions on social media, following influencer on social media, any of the previous choices)
	What kind of content do you prefer to deepen your knowledge about scientific topics?	Multi select multi choice question (written texts, social post with images and texts, videos, podcasts)
2	Were you aware of this area of scientific research before watching the previous video?	ranking (1= not at all , 5= absolutely positive)
	Have you ever seen on other media similar contents on a similar topic?	ranking (1= not at all , 5= absolutely positive)
	Would you be interested in learning/deepening your knowledge on Heritage Science topics?	ranking (1= not at all , 5= absolutely positive)
	Would you watch other videos to learn/deepen your knowledge about Heritage Science topics?	ranking (1= not at all , 5= absolutely positive)
	Would you follow/subscribe to a Heritage Science communicative channel?	ranking (1= not at all , 5= absolutely positive)
3	What is your age?	Multiple choice question
	Which is your gender?	Multiple choice question
	What is your educational level?	Multiple choice question

Concerning the first section of the survey, results highlight that the public is interested in this kind of content (68.8%), and that the most regular access occurs via internet and social media (63.9%), where they follow research centres/institutions and influencers. Moreover, as shown in Figure 4.1, the outputs highlight that the public prefers video content to deepen scientific topics (69.9%).

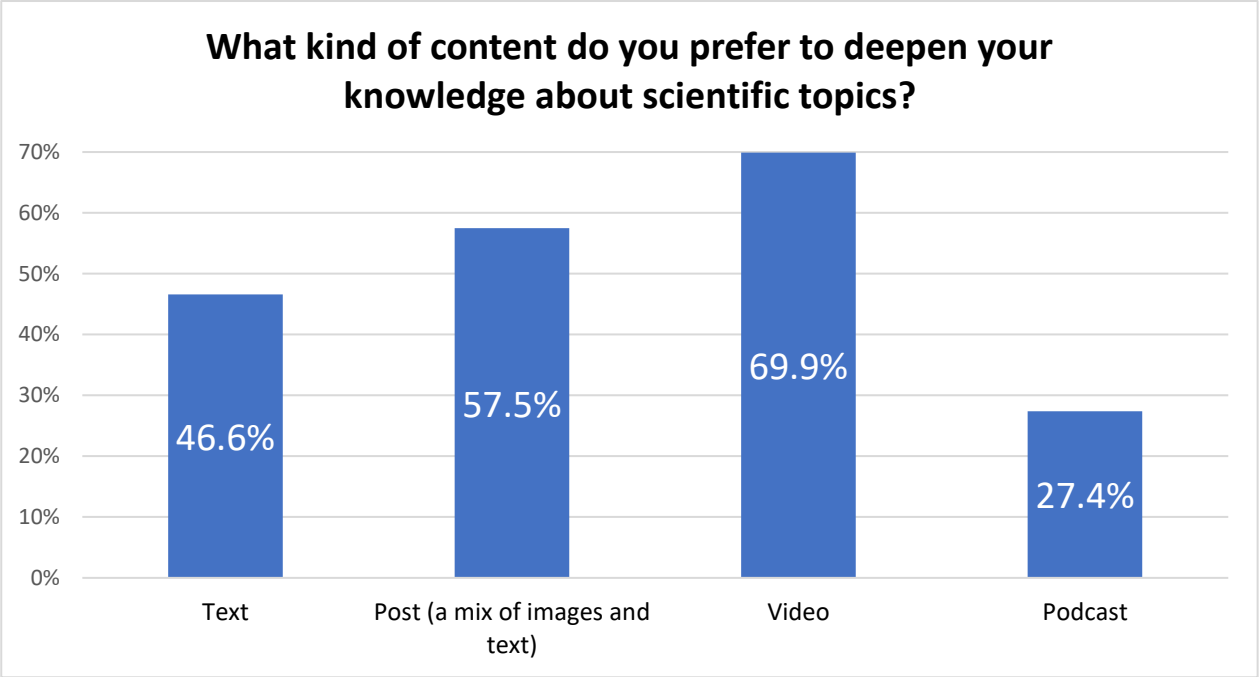

Figure 4.1 Graph from the survey results that shows audience preferences on the kind of content they prefer to deepen knowledge about scientific topics; multiple answers could be selected for this question.

This second section emphasises that the audience chiefly does not know about Heritage Science and that they are not usual to watch any video with a similar topic on other platforms. On the other hand, there is a high interest in learning and deepening Heritage Science topics, especially through video content (Figure 4.2).

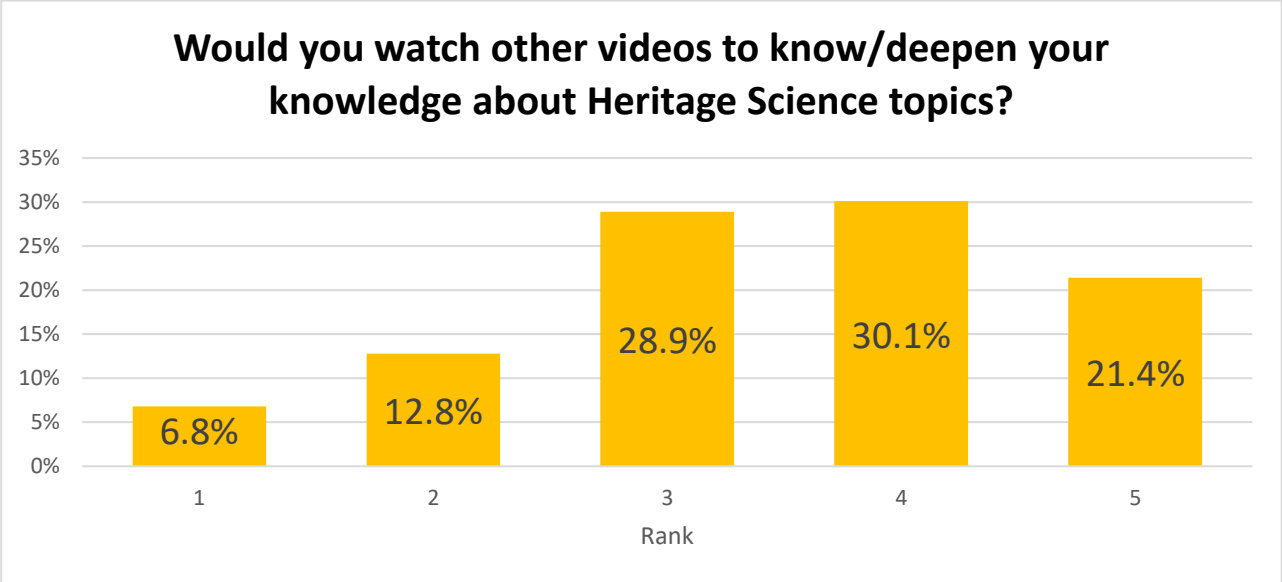

Figure 4.2 Public interest on watch Heritage Science video contents.

The third and last section (Figure 4.3) shows that participants are mostly under 40 (18.4% is under 25, 66.5% in the range of 26-40, 7.9% between 41-55 and 7.1% over 56), with higher participation of women (56%) and people with a medium-high educational level (high school diploma 25.6%, or university degree 62.4%).

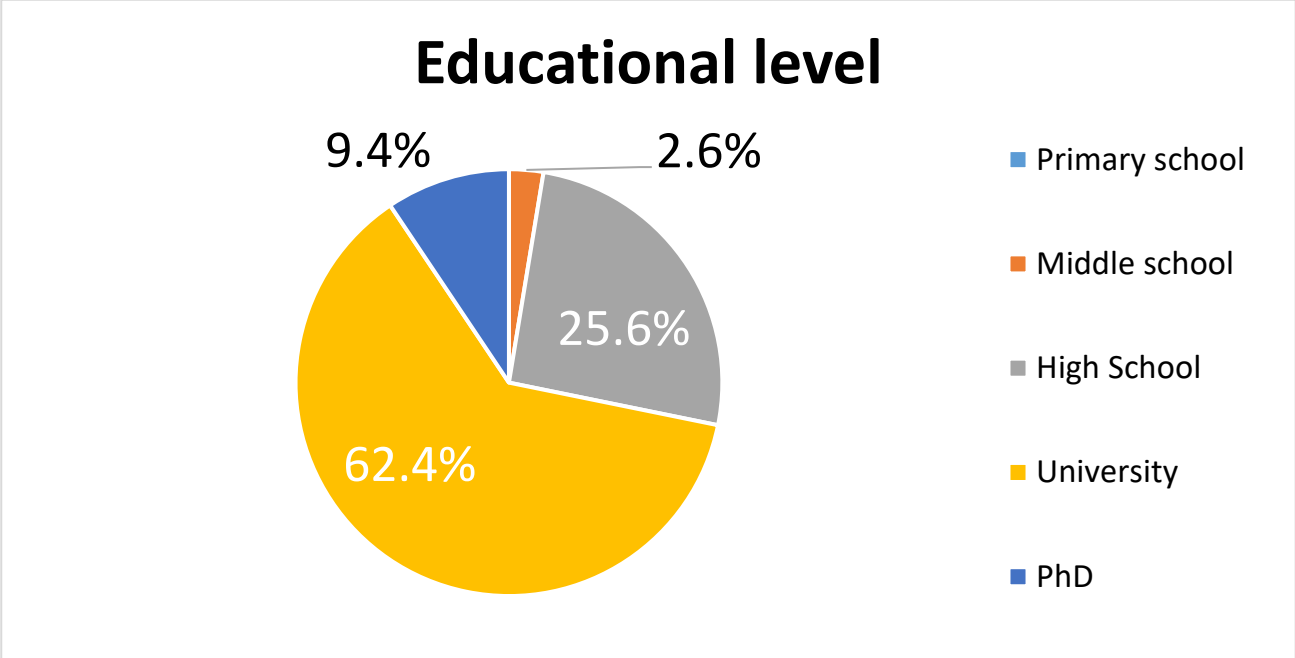

Figure 4.3 Audience profiling by their educational level.

Generally, the survey showcases a lack of connection between the Heritage Science expert community and the non-specialist audience, while it highlighted the positive public interest in Heritage Science content. If this data is incorporated concurrently, it is possible to conclude that the scientific dissemination and communication project of this PhD thesis may contribute to create a further opportunity to involve our society in research work and have feedback from them. Another relevant piece of information highlighted by the survey is that there is no correlation between age or educational level and interest in Heritage Science; the data suggest that these topics arouse great interest in the whole interviewed audience.

The few competitors (namely, other relevant actors who do Heritage Science communication) is still a positive aspect, since it allows it to be easily visible and reachable on the internet and social media by those users interested in the matter.

From all the obtained information, it was clear that the production of video content was the best way to spread this research to a large audience. In addition to the audience's interest in video content, this medium is ideal for storytelling because it allows for the simultaneous use of multiple forms of communication, such as visual, auditory, and kinetic elements (such as objects or persons in

movement), to convey a story. The video can create a more immersive and engaging experience for the viewer in comparison to other mediums, like text or audio alone. Additionally, the video can be edited and manipulated in various ways to convey a non-linear narrative and create, for example, a sense of pacing or tension. Furthermore, special effects allow the creation of animations that could help explain complex concepts.
In addition, the video gives the viewer a dive into the researcher's daily activities inside their labs with their instruments and materials.

4.2 Docuseries realisation

4.2.1 The concept

Based on the considerations above reported, it was decided to produce a docuseries (3 episodes of circa 10 min each, plus a trailer of circa 2 min).

The episodes have different topics that directly involve the present research work and generically Heritage Science and activities of the researcher. The audience was set to the non-specialist (ideally >16 years old, to communicate to somebody with some basic chemistry knowledge). It was decided to record videos in English with Italian subtitles, so the docuseries would be suitable for both Italian and international audiences.

The survey also indicates the better choice of where to spread the docuseries on social media. This decision was also validated not only because of the public's preferences but because they are easy to arrange, user-friendly, free, and can easily reach an international audience. Furthermore, billions of people daily use social media for entertainment and information. There is also a high interest in educational content, including scientific topics. Therefore, social media also gives the chance to engage and interact with the audience, thus improving awareness of scientific research, and scientific culture.

4.2.2 Production

The docuseries project is titled *Metamorphosis: an unusual art-compounds tale*; each episode has a subtitle that gives a clue about the topic. The title and subtitles must be charming to attract the public.
Below, each episode will be described with a scheme of its narrative structure, explaining the location and the topic in order to give a general idea of what is reproduced in the video, like a script or storyboard in cinema.

The narrative thread is the scientific part of my PhD research project, from how it was born (ESRF identification of lead-calcium phosphate on Egyptian papyri), to what was done during this PhD thesis and how the research can be applied, including some future perspectives. This last episode also focuses on more emotional aspects, for example, what pushed someone to become a Heritage scientist, tips for a young student interested in Heritage Science, and remembering happy memories related to the researcher's work. These emotional aspects are crucial for any narration because they help the viewer to empathise with what is happening on video. The connection with the audience is essential because it can help to maintain their interest in what they are watching.

4.2.3 Trailer

The trailer helps to have a brief overview of the project as it will help to introduce the audience to the treated topics. It is about 2 min, recorded with a double shot of me presenting the docuseries, mixed with some b-rolls (records at Perugia and ESRF, lab analysis, etc...). It ends by showing the title of the docuseries: *Chasing Pigments.*

4.2.2 Episode 1 – *Light the past*

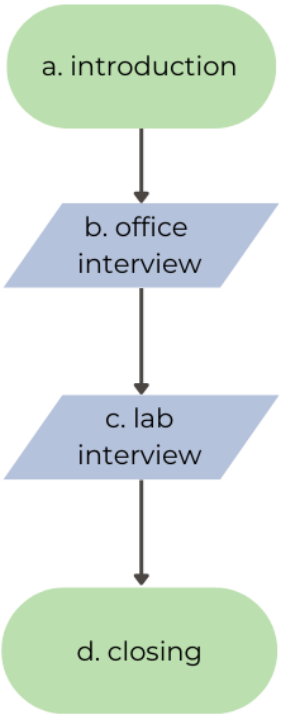

a. This first scene will introduce where the episode takes place, literally guiding the audience with multiple shots from the outside to the inside of the synchrotron facility. A voiceover will help to briefly explain what ESRF is.

b. The scene moves to a conference room where I am interviewing Dr. Marine Cotte, by introducing herself and her roles at ESRF to the audience. Following the conversation, the interview shifts to how she and her colleagues unexpectedly found lead apatite compounds on an artistic sample. This scene integrates with b-rolls of sample preparation, sample analysis, and other operations done in the synchrotron's hutch.

c. The second part of the interview takes place at the ID21 beamline, where Dr Cotte explains what a synchrotron is, how it works, and which are its peculiarities. It is discussed how synchrotron analyses can be applied to Heritage Science and which specific information can be obtained by researchers. In this scene, an animation will help to visualise the synchrotron explanation by Dr Cotte.

d. The last scene is a resume of what has been shown previously and a hint to the next episode. The shot takes place in the hall of the main building of ESRF. There is a movement from the inside to the outside, with a visual connection to the introduction shots.

4.2.3 Episode 2 – How I did it

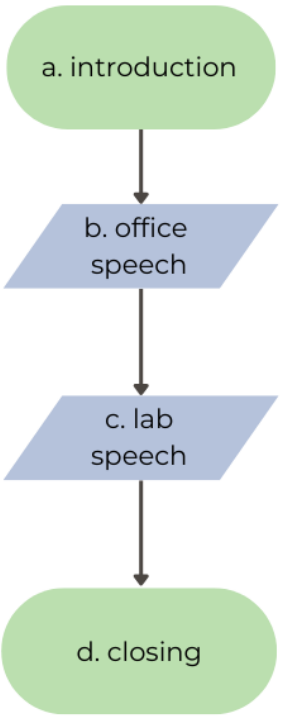

a. This second episode takes place in Perugia. First, it introduces the location with drone shots guiding the audience from the city centre to the entrances of the Chemistry, Biology, and Biotechnology Department of the University of Perugia. Then there is a cut to the lab where the episode's topics are introduced.

b. The scene moves to the PhD student's office. Here the fundamental role of literature study is described. More specifically, it is briefly explained where lead apatite compounds were found and by which techniques they were identified, the possible methods to synthesise reference materials and some of their properties. In this scene, there is an animation to help to understand one of such properties (i.e., the substitutional model).

c. Since the episode is moving to the experimental part of my PhD activities, the episode moves back to the lab. There, the synthesis of $PbHA_x$ compounds and their characterisation, the preparation of paint mock-ups, and the analysis of the historical sample have described. This record mixes my speech with b-rolls of the in-house synthesised powders, the mock-ups, and some samples analysis.

d. The episode closing takes place on a terrace of the Department, where I quickly summarise the episode's topics; in addition, I also hint about what the audience will see in the third episode.

Episode 3 – Looking forward

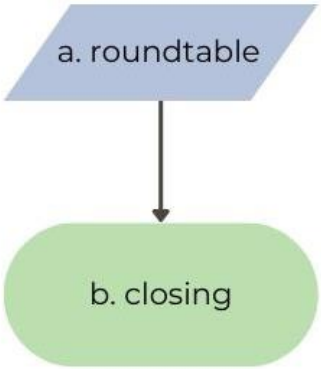

a. In this last episode, there is a roundtable with the author, Prof. Aldo Romani, and Dr. Letizia Monico, where, after their introduction, they will illustrate some of this research applications and how this research can evolve. Moreover, I explore some emotional aspects related to the research through questions to Aldo and Letizia, for example what pushed them to become researchers and a few tips to young people who want to approach Heritage Science. This scene was shot from four different points of view, using a camera for each, and a total shot with all the involved people.

b. The episode ending in this case is more focused on closing all the docuseries with a speech that can be a general overview and a summarisation of all aspects covered in all three episodes.

4.3 Agreement and spreading

After the production and post-production (video and audio editing, voice-over, colour correction, soundtrack, visual effects, subtitling), the docuseries needed to be published on social media. In order to give the best resonance to the project, a decision was made to ask the communication office of the Institutions related to this PhD thesis (Università degli Studi di Perugia, ESRF, CNR – SCITEC, and CNR-ISPC) about their interest to spread the docuseries via their social media and web-sites. This decision was taken because these Institutions have a reputable scientific background that is globally recognised and socially trusted, including on social media. Therefore, the project could exploit institutions' trust and visibility to spread through the internet.

Both CNR Institutes, SCITEC and ISPC, responded positively. The docuseries aligns with their objectives of valorising research through the transfer of knowledge to local, national, and international stakeholders, both specific (*intra pares*) and general (citizens). The docuseries will be used and spread on social media and websites used or owned by CNR SCITEC and ISPC institutions. In the case of the SCITEC, the communication office team leader suggests producing a document that formalises this agreement. It is crucial to highlight that the video will be published only after the review of the thesis and the publication of the manuscript in preparation because the scientific community must evaluate the quality of the work done before communicating it to the non-specialist audience. This ensures to prevent spreading to the public misleading results or other inaccurate information that might be present in this work .

Unfortunately, during this thesis, it was not feasible to include the observation and measurement of the audience feedback on the docuseries. This would have been an engaging topic because social media has powerful tools that permits to do this, including metrics of audience engagement (likes, comments, sharing), interaction with them (e.g., asking for tips to improve future projects), and profiling (gender, age, nationality, etc…). Furthermore, with social media metrics (also called analytics), it is possible to measure the interest of the public in the docuseries with data: duration of the view (do they watch the entire video?), which are the points of higher interest (was the video backward to rewatch a piece of it?), and traffics (how viewers found the docuseries?).

All this information gives precious feedback to the researcher or the communicator, by helping them to learn which are strengths and weak points that need to be improved in new projects. For this reason, all analytics data should be considered in every communication project. For reliable analysis of the social media analytics, it is necessary to wait several months after the docuseries publication (roughly between 1 and 6 months); this will allow the video to reach the widest possible audience, so an analysis of the most relevant dataset (after six months, social media algorithm surely does not promote the content anymore). After this period and the subsequent data analysis, it will be possible to consider the use of videos and related documents for a future scientific paper, where to analyse this format, its impact on the non-specialist audience, and the obtained feedback, discussing the pros and cons of this communicative approach.

Overall, the docuseries here proposed is, surely for the Italian context, one of the firsts cases through which spreading ongoing research for Heritage Science topics in innovative way; for this reason, it would be remarkably interesting to analyse and comment the public engagement of this new kind of spreading scientific results.

CONCLUSIONS AND PERSPECTIVES

This PhD thesis focused on the study of lead-calcium phosphate solid solutions, $(Pb_xCa_{1-x})_5(PO_4)_3OH$ (with $0 \leq x \leq 1$), by developing of a multi-technique and multi-scale approach for their identification and characterization in cultural heritage materials.

The investigation of a series of powders and paint mock-ups by a combination of vibrational spectroscopy methods (FT-IR and Raman) with X-ray based methods (XRPD; XRF and XANES) allowed to non-invasively and non-destructively define specific spectral "markers" that can be used for the discrimination of $(Pb_xCa_{1-x})_5(PO_4)_3OH$ compounds according to their Pb content. The outcomes so obtained, were then successfully exploited for revealing the presence of a lead-calcium phosphate compound in a historical fresco fragment.

Questions remain still open about the origin of lead-calcium phosphate solid solutions in cultural heritage objects. Further research will be therefore required to understand if these compounds were originally present in the artwork or if they are secondary products of its constitutive Pb-, P- containing materials. In addition, considering the widespread presence of chlorine, often associated with that of lead and phosphorous, in different kind of cultural heritage objects (included the paint fragment analysed in this thesis), it will be relevant setting-up also a systematic study of chloro-apatite compounds (such as pyromorphite and phosphohedyphane). Another aspect of future research is related to the assessment of XRPD portable devices to non-invasively discriminate among different $(Pb_xCa_{1-x})_5(PO_4)_3OH$ compounds in artworks. Deepening all such aspects will be fundamental to further deepen understanding of origin, use and application of lead-calcium phosphate in the heritage science context, thus optimizing the conservation and restoration strategies of artworks containing this class of materials.

The subsequent knowledge transfer to the non-specialist public have highlighted the high interests of the interviewed public on scientific content, and their rough knowledge on heritage science topics. The work developed in the framework of this thesis is a perfect starting point to improve scientific communication, by exploiting new ways and interactive media to make the community aware of the researchers' work. Moreover, the produced docuseries has shown how a research communication project can be planned and executed, has given the idea of how the communication activities cannot be neglected and should become a common practice in almost every research project.

The future perspective of the communication part, after the publication of the media, will be the measurement of public interest, interaction, and engagement on this content through the analytics study and the submission of another survey. Only with this further analysis, it will be possible to deeply understand the value of the docuseries and their effect on the audience as well as plan future

projects. Another relevant aspect that will need further investigation is the study of the audience. Since this work was limited to an Italian (or Italian-speaking) public, it will be interesting to expand that study to an international scale in order to obtain a global view of public habits and interest in Heritage Science contents.

Acknowledgements

I would like to acknowledge the Department of Chemistry, Biology and Biotechnology of Università degli Studi di Perugia, the Scientific Methodologies Applied to Archaeology and Art (S.M.A.Art) Excellence Centre, CNR-SCITEC and ESRF for having supported my PhD thesis. I would also like to acknowledge the CNR-SCITEC and CNR-ISPC institutions for their support on the communication part of this research. Thanks to Prof. Riccardo Vivani for his strong contribution to the analysis and interpretation of the XRPD data, to Dr Luis Carlos Colocho Hurtarte, Eduardo Villalobos and Christoph Sahle, at the ESRF, for the support in the collection, processing and simulation of the XANES data, and Dr Luc Megens for providing the historical sample NJH-18. I thank the Heritage BAG-ESRF (experiment HG-172) for the opportunity to carry out synchrotron analysis at ID13 and ID22, and Marine Cotte for access to in-house beamtime at ID21